Stellenbosch UNIVERSITY IYUNIVESITHI UNIVERSITEIT

Physical model tests on stability and overtopping of new concrete armour unit Cubilok™

by

Melissa Cairns

Thesis presented in fulfilment of the requirements for the degree of Master of Engineering in Civil Engineering in the Faculty of Engineering at Stellenbosch University

Supervisor: Dr Andre Theron

Co-supervisor: Mr Anton Holtzhausen

Co-supervisor: Mr Carl Wehlitz

December 2023

PLAGIARISM DECLARATION

By submitting this thesis electronically, I declare that the entirety of the work contained therein is my own, original work, that I am the sole author thereof (save to the extent explicitly otherwise stated), that reproduction and publication thereof by Stellenbosch University will not infringe any third party rights and that I have not previously in its entirety or in part submitted it for obtaining any qualification.

Student number: XXXXXXXX

Signature*:*

Initials and surname: MC CAIRNS

Datum / *Date:* December 2023

ABSTRACT

Artificial concrete armour units are employed to protect coastal structures and infrastructure such as rubble mound breakwaters, revetments, and artificial headlands. Several concrete armour unit types have been developed over the last few decades, where each specific unit has a unique shape and behavioural properties. As the need for breakwaters deployed in harsher wave climates and deeper waters increased, the need for larger armour units also grew. Where concrete armour units are required, generally, the best value is achieved with a single-layer option, provided that construction conditions allow for accurate placement of armour units. PRDW Consulting Port and Coastal Engineers are developing a new concrete armour unit called the Cubilok™. This unit is defined by four principal dimensions, which can be modified to obtain variations of the Cubilok™ shape. These parameters can also be used to alter the structural robustness of the unit, which is indicated by its slenderness ratio (H'). Two different unit shapes have been tested previously: single-layer (H' = 1.09) and double-layer (H' = 0.92). For this study, the shape previously tested as a single layer was modified by removing the tapered ends of the protuberance (or arms). These changes were made to reduce the settlement observed in previous research; however, it also resulted in a unit with higher structural robustness where H' equalled 0.6. This unit's viability as a single and double layer was investigated in this study.

The overall efficacy of an armour unit during wave attack is determined by the hydraulic stability. This study was the first attempt to understand the modified unit's hydraulic stability and recommended wave overtopping discharge. The primary objective of this research was to investigate the behaviour of the Cubilok at slopes of 1:1.5 and 1:1.33 (V:H), which involved testing various wave heights and periods. A 2D flume configuration was tested at the Council for Scientific and Industrial Research (CSIR) in Stellenbosch, South Africa. The configuration included, a sloping foreshore of 1:30, and a constant water level measured at the structure's toe. The wave conditions were measured with capacitance probes, and the overlay photography technique was utilised to capture and examine the armour layer reaction. Overtopping volumes were measured throughout testing and converted to l/s/m to indicate the average rate of overtopping discharge.

The test schedule included two test series to determine a suitable storm duration for the steeper slope of 1:1.33 (H:V). Packing densities of Ø = 0.63 and 0.65 were investigated for the storm duration tests. A repeatability test was also conducted for both slopes with the same wave condition. The findings showed an improvement in stability for the tighter packing density; therefore, the test programme continued with the packing density of Ø = 0.65.

According to the stability test results, the armour layer was influenced slightly more negatively by longer wave periods, with larger movements and earlier displacements. By the end of the study, 17 test series were completed, totalling 102 individual tests.

The stability number was found to increase with decreasing Iribarren parameters at the start of damage. The inconsistent results achieved at the start of damage yielded no conclusive influence of the varying slope gradients on the hydraulic stability. The average stability numbers achieved for the milder slope were often greater at failure. Throughout testing, the stability numbers ranged from N_S = 2.04 to 4.64. At the start of damage, the average stability number was N_S = 3.51, and at failure, it was N_S = 4.30. The research revealed that the Cubilok's performance notably improved on steeper slopes, indicating competitive potential against other single-layer units. Based on previous research, the Cubilok outperformed Accropode in terms of no damage and design stability at a 1:1.33 slope. However, on steeper slopes, Xbloc's design parameter exceeded Cubilok's by 7%.

The overtopping rate increased significantly for low wave steepness values (s_{op} =0.01). For low wave steepness values, the results indicated that the overtopping rate increases approximately twofold with an increase in wave height. Furthermore, compared to the CLASH results of other single-layer units, the measured rate of overtopping for the Cubilok slope was slightly greater. The increased overtopping rate was most apparent in test results with low wave steepness of s_{op} = 0.01, falling outside the CLASH range of s_{op} = 0.02, 0.035 and 0.05. It should be highlighted that this study was only a preliminary investigation into the behaviour of the modified Cubilok. The effect of the packing density and shape were compared in relation to the settlement of the unit. Further tests are recommended to address variability in test results.

OPSOMMING

Beton bewapeningseenhede word gebruik om kusstrukture en infrastruktuur soos ruklip-golfbrekers, seemure en kunsmatige landhoofde te beskerm. Verskeie tipes bewapeningseenhede is oor die afgelope paar dekades ontwikkel, waar elke spesifieke eenheid sy unieke vorm en gedragskenmerke het. Namate die behoefte aan golfbrekers in hoe-energie golfklimate en dieper waters toegeneem het, het die behoefte aan groter bewapeningseenhede ook gegroei. Waar betonpantser-eenhede benodig word, word oor die algemeen die beste waarde verkry met 'n enkellaag opsie, mits konstruksie omstandighede akkurate plasing van die bewapeningseenhede toelaat. PRDW Consulting Hawens en Kus Ingenieurs ontwikkel 'n nuwe betonpantser-eenheid genaamd die Cubilok™. Die vorm van hierdie eenheid word bepaal deur vier hoof afmetings, wat verander kan word om variasies van die Cubilok™ vorm te verkry. Hierdie parameters kan ook gebruik word om die strukturele robuustheid van die eenheid te verander, wat aangedui word deur sy slangkheidsgraad (H’). Twee verskillende panser vorms is voorheen getoets: enkellaag (H’ = 1.09) en dubbellag (H’ = 0.92). Vir hierdie studie is die vorm wat voorheen as 'n enkellaag getoets is, verander deur die afgeplatte punte van die uitsteeksel (of arms) te verwyder. Hierdie veranderinge is aangebring om die versakking wat in vorige navorsing waargeneem is, te verminder; dit het egter ook 'n eenheid met hoër strukturele robuustheid tot gevolg gehad, waar H’ gelyk was aan 0.6. Hierdie eenheid se vermoë as 'n enkellaag en dubbellaag is in hierdie studie ondersoek.

Die algehele effektiwiteit van 'n bewapeningseenhede tydens golfaanval word bepaal deur die hidrouliese stabiliteit. Hierdie studie was die eerste poging om die gewysigde eenheid se hidrouliese stabiliteit en aanbevole golfoorslag te verstaan. Die primêre doel van hierdie navorsing was om die gedrag van die Cubilok te ondersoek by hellings van 1:1.5 en 1:1.33 (V:H), wat behels het die toetsing van verskeie golfhoogtes en periodes. 'n 2D golfkanaal uitleg is getoets by die Wetenskaplike en Nywerheidsnavorsing Raad (WNNR) in Stellenbosch, Suid-Afrika. Die opstelling het 'n nabystrandse helling van 1:30 ingesluit, en 'n konstante watervlak gemeet by die golfmaker van die struktuur. Die golfkondisies is gemeet met kapasitansieprobes, en die oorlê fotografie tegniek is gebruik om die reaksie van die bewapeningslaag vas te vang en te ondersoek. Die oorslagvolumes is deurlopend gemeet gedurende toetsing en omgeskakel na l/s/m om die gemiddelde tempo van oorslag aan te dui.

Die toetsskedule het twee toetsreekse ingesluit om 'n geskikte stormduurte vir die steiler helling van 1:1.33 (H:V) te bepaal. Pakdigtheidswaardes van Ø = 0.63 en 0.65 is ondersoek vir die stormduurtetoetse. 'n Herhaalbaarheidstoets is ook vir beide hellinge met dieselfde golfkondisie uitgevoer. Die bevindinge het 'n verbetering in stabiliteit vir die groter pakdigtheid getoon; dus het die toetsprogram voortgegaan met die pakdigtheid van Ø = 0.65. Volgens die

stabiliteitstoetsresultate is die bewapeningslaag effens meer nadelig beïnvloed deur langer golfperiodes, met groter bewegings en vroeëre verskuiwings. Teen die einde van die studie is 17 toetsreekse voltooi, wat 'n totaal van 102 individuele toetse beloop het. Die stabiliteitsgetal is bevind om te verhoog met afnemende Iribarren waardes aan die begin van skade. Die onkonsekwente resultate wat aan die begin van skade behaal is, het geen oortuigende invloed van die wisselende hellingsgradiënte op die hidrouliese stabiliteit opgelewer nie. Die gemiddelde stabiliteitsgetalle wat vir die platter helling behaal is, was dikwels groter voor swigting. Gedurende toetsing het die stabiliteitsgetalle gewissel van N_S = 2.04 tot 4.64. Aan die begin van skade was die gemiddelde stabiliteitsgetal N_S = 3.51, en by swigting was dit N_S = 4.30. Die navorsing het aan die lig gebring dat die stabiliteit van die Cubilok merkbaar verbeter het op steil hellings, wat dui op mededingende potensiaal teenoor ander enkellaag eenhede. Gebaseer op vorige navorsing die Cubilok het die Accropode oortref wat betref geen beskadiging en ontwerpstabiliteit op 'n 1:1.33 helling. Nietemin, het die ontwerpparameter van die Xbloc op steiler hellings die Cubilok met 7% oorskry.

Die oorslagtempo het aansienlik toegeneem vir lae golfsteilheidswaardes (s_{op} = 0.01). Vir lae golfsteilheidswaardes dui die resultate daarop dat die oorslagtempo ongeveer tweemaal soveel toeneem met 'n toename in golfhoogte. Verder, in vergelyking met die CLASH resultate van ander enkellaag eenhede, was die gemete oorslagtempo vir die Cubilok helling effens groter. Die verhoogde oorslagtempo was mees opvallend in toetsresultate met 'n lae golfsteilheid van s_{op} = 0.01, wat buite die CLASH reeks van s_{op} = 0.02, 0.035 en 0.05 val. Dit moet beklemtoon word dat hierdie studie slegs 'n voorlopige ondersoek na die gedrag van die gewysigde Cubilok was. Die effek van die pakdigtheid en vorm is vergelyk met betrekking tot die stabiliteit van die eenheid. Verdere toetse word aanbeveel om die variasie in toetsresultate aan te spreek.

ACKNOWLEDGEMENTS

I would like to express my gratitude to my supervisors, Dr Andre Theron, Anton Holtzhausen (PRDW) and Carl Wehlitz (The CSIR), for their unwavering guidance, insightful feedback, and continuous support throughout the entire research process. Your expertise and dedication have been invaluable to me, and I am truly fortunate to have had the opportunity to learn from you all.

I extend my sincere appreciation to Michelle Davids and Lucille Ockhuizen for their invaluable contributions in fabricating the model units utilized in my testing. I am also grateful to PRDW for funding the operation. Furthermore, I would like to express my gratitude to the personnel of the CSIR laboratory, where my testing was conducted, and to the Stellenbosch Hydraulic Laboratory for generously providing the materials and test facilities. I wish to offer special recognition to Iliyaaz Williams (Stellenbosch) and Lukhanyo Somlota (CSIR), whose integral role in addressing daily challenges throughout my testing has been invaluable.

I am grateful to my friends and colleagues who provided encouragement, insightful discussions, and a positive atmosphere for intellectual exchange. You have been a source of inspiration and motivation. I would like to extend special recognition to Chris Momoh for reviewing my thesis and providing valuable comments and insights.

Finally, I am deeply indebted to my parents, Elmarie and Clive Cairns, and my brother, Adrian Cairns, for their unwavering support, love, and encouragement throughout my academic journey. Your belief in me has been the driving force behind my accomplishments.

TABLE OF CONTENTS

LIST OF FIGURES

LIST OF TABLES

1 INTRODUCTION

1.1 Background

Ports are required to adapt to keep up with the evolution of ships, which has seen a consistent increase in the size of ships throughout the previous century. Ports were previously intended for smaller ships with lesser draughts, and as ship size increased, so did the draught, requiring an increase in water depth within the port. Breakwaters play a crucial role in this adaptation process especially in deeper waters where greater waves are frequently present. Breakwaters are constructed to provide protection to ports and harbours by attenuating the waves before they reach the marine infrastructure.

Breakwaters built at greater depths are vulnerable to larger wave conditions, necessitating the use of larger armour rock . This is frequently restricted due to the size and quantity of rock available, as well as the quality of the rock. Concrete armour units may also be used in place of armour rock in situations where armour rock is not readily available or economically viable.

A compromise between structural strength and interlocking is invariably present when designing a new concrete armour unit. Large design waves along the South African coastline required the introduction of large and robust units, such as Antifer Cubes or Cubipods. The lack of significant interlocking between these units encouraged the creation of a new armour unit. The Cubilok ™ armour shape can easily be modified by changing its slenderness ratio, where a high slenderness ratio indicates the potential for improved interlocking capability, while a low slenderness ratio indicates a structurally robust unit. The envisaged application of the unit ranges from slenderer interlocking single-layer applications to larger, less slender double-layer applications that resemble cube-like units.

1.2 Objectives

The Cubilok™ (henceforth known as Cubilok) shape is defined by four principal dimensions. Previous testing has been conducted on the unit's original shape consisting of protuberances with tapered edges. To reduce the settlement of the original shape, the tapered edges are removed, resulting in a unit shape consisting of flat face protuberances. The primary goal is to develop the design characteristics of the Cubilok. As a result, the main objective of this study is to investigate the Cubilok's behaviour by considering the hydraulic stability and overtopping limits for the armour unit on a slope of 1:1.33 and 1:1.5. This study considers a variety of wave conditions and two packing densities. The findings of these experiments were compared to similar testing performed on commercially available concrete armour units. The process can be separated into three phases: academic research, laboratory research, and a real-world project.

The academic and laboratory research phases are addressed in this thesis and include:

- The investigation of potential solutions to the settlement problems experienced on steep slopes discovered in prior research on the original Cubilok shape.
- 2D-hydraulic model testing to determine the unit's hydraulic stability and allowable overtopping limits.
- A comparison of the modified Cubilok unit with other single-layer units.
- Evaluate the existing literature on the ecological enhancement of concrete armour units.
- Propose future model tests that may be considered to define the unit characteristics further.

1.3 Research questions

The following research questions were formulated to fulfil the research objectives:

- How does the Cubilok armour unit behave when subjected to different wave conditions, and does it demonstrate consistent and repeatable performance?
- How can understanding how different wave heights and wave steepnesses influence the unit's stability be achieved by systematically varying the test conditions?
- What impact does the slope and packing density exert on the stability of the unit?
- Can the failure mechanisms of the Cubilok be deduced by observing its performance during slope failure?
- How does the overtopping discharge vary in response to wave conditions and changes in slope?
- To what extent does the stability of Cubilok units differ from that of other commonly used single-layer units, considering both their stability and the associated relative damage number?

After thorough consideration of these inquiries, recommendations for future testing were made.

1.4 Scope

The research was limited in scope to encompass exclusively conventional rubble mound breakwaters, encompassing both single-layer and double-layer systems. As a result, the substantial literature review done as part of this research examined the essential design characteristics associated with conventional breakwater design. Moreover, the review thoroughly explored the interaction of concrete armour units and examined the various ways these structures obtain stability or fail. This study primarily focused on investigating the aspects that significantly affect the structural performance of the modified Cubilok unit to understand the unit strengths and limitations within the context of the tests conducted.

1.5 Limitations

In the context of hydraulic model testing, a cross-sectional representation of a typical breakwater is constructed and adjusted according to the study's requirements. Subsequently, comprehensive data collection is completed, including measuring critical parameters such as wave height and wave period. Detailed photographic documentation is also completed throughout the testing process. The collected data and photographs are analysed to derive insight into the unit's performance.

The study acknowledges certain limitations that warrant consideration. These limitations include the production of model units and utilising a 2-dimensional hydraulic model testing approach. The adaptation of the unit necessitated manufacturing new model units, a labour-intensive and financially demanding process, with financial backing and assistance provided by PRDW. The 2-dimensional model may be utilised to evaluate the hydraulic stability of a breakwater section; however, it falls short in accurately depicting real-world waves, lacking the capability to replicate oblique and diffracted waves. Moreover, it relies on an assumed average flow depth, neglecting the significance of varying bathymetry.

Furthermore, constraints relating to the testing procedure are evident. The study was constrained to the examination of only four-wave periods accompanied by six varying wave heights. This constraint arises from the significant time and financial investments required for the execution of a physical model study. Additionally, the availability of specific equipment fluctuated during the testing phase, introducing an additional layer of complexity. Additionally, it is crucial to acknowledge and address the effects and limitations related to laboratory and scale considerations. These factors must be taken into account to ensure the accurate interpretation and application of the study's findings.

1.6 Thesis outline

Chapter 2 includes a literature review on artificial concrete armour units, focusing on the units' modes of stability and failure. Chapter 3 provides an overview of the physical model methodologies and test program. Chapter 4 provides a summary of the results and discusses the observations made during the model testing process. Chapters 5 and 6 analyse the hydraulic stability and the overtopping respectively. Chapter 7 compares the results achieved in this study to the results obtained for other units. Chapter 8 provides a review of the ecological enhancement of concrete armour units. Chapter 9 discusses the conclusions as well as the recommendations for further testing.

2 LITERATURE REVIEW

2.1 Conventional rubble mound breakwater

A breakwater is a marine structure constructed with the purpose of sheltering vessels and port infrastructure from wave and current exposure. There are several types of breakwaters; however, the primary focus of this study is a conventional rubble mound breakwater illustrated in Figure 2-1 (CIRIA, 2007).

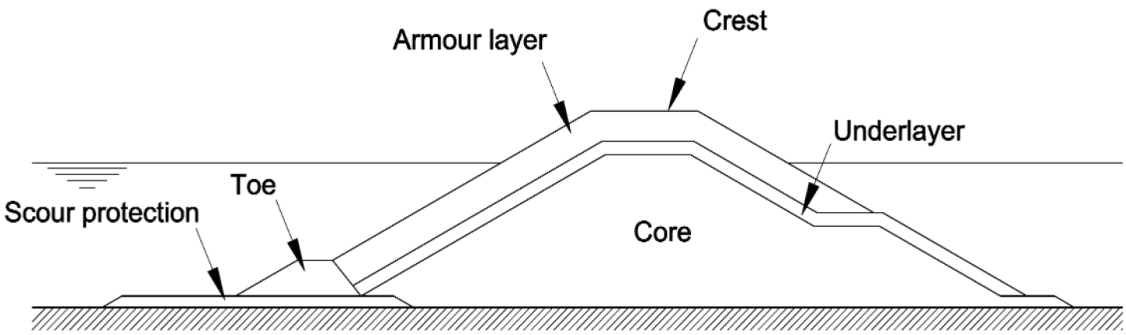

Figure 2-1: Cross-section for the various rubble mound types (CIRIA, 2007)

A conventional or typical rubble mound breakwater is comprised of several parts , including a core, an underlayer, an armour layer, and a toe. These structures typically have simple geometrical configurations with a trapezoidal shape and side slopes ranging from 1:1.33 to 1:2.

The armour layer consists of either large armour rock units or artificial concrete armour units. Concrete armour units offer a practical alternative in situations demanding the use of larger rocks for protecting marine structures, particularly when greater wave loads impact the breakwater (Bonfantini, 2014). This study focuses on concrete armour units and specifically the modified Cubilok unit.

2.2 Armour stability

2.2.1 Coastal parameters

Waves are the most important marine load to consider when constructing breakwaters since they have the greatest impact. Waves are also one of nature's most complex and varied phenomena; consequently, fully understanding their behaviour while designing and constructing coastal structures is challenging (Goda, 2000).

The wave conditions are categorised by the wave height recorded at the toe of the structure, the average or peak wave period, and the wave attack angle (β). Different wave measurements are employed in the analysis of waves, focusing on determining the wave height and period. The significant wave height can be determined by averaging the highest third of all waves ($H_S = H_{1/3}$) or by determining the wave height based on the wave spectrum ($H_S = H_{m0}$). The wave period, T_m or T_p, is determined using either a statistical or spectral analysis. The wave steepness (s_{op}) defined in Equation 1 describes the ratio of significant wave height to deep-water wavelength (CIRIA, 2007). Typical s_{op} values range from 0.02-0.06, with a wave steepness of 0.02 indicating long swell and values near 0.06 representing wind seas. Furthermore, the local water depth (h) is a crucial parameter to take into account when assessing the coastal environment.

$$s_{op} = \frac{\mathrm{H}_s}{\mathrm{L}_0} = \frac{2\pi \mathrm{H}_s}{\mathrm{g}{\mathrm{T}_P}^2} \tag{1}$$

where:

H_s	=	significant wave height	[m]
L_0	=	deep-water wavelength	[m]
g	=	gravitational acceleration	[m/s²]
T_P	=	peak wave period	[s]

The Rayleigh distribution may describe the wave height distribution in deep water. In such cases, one characteristic value, such as the significant wave height, can represent the entire distribution. In certain scenarios, such as in shallow and depth-limited waters, the occurrence of waves breaking cannot be sufficiently characterized by the Rayleigh distribution alone. Thus, it becomes critical to consider criteria beyond the significant wave height, such as the real distribution of wave heights (van der Meer, 2017).

The surf similarity parameter, or Iribarren parameter, described by Equation 2 helps understand the type of wave breaking (illustrated in Figure 2-2) on a structure's slope and the wave load sustained by the structure (CIRIA, 2007).

$$\xi = \tan\alpha/\sqrt{s} = \tan\alpha/\sqrt{2\pi \mathrm{H}/\mathrm{g}T^2} \tag{2}$$

where:

ξ	=	Surf similarity parameter, or Iribarren parameter	[m]
α	=	slope angle	[°]
s	=	wave steepness	[-]

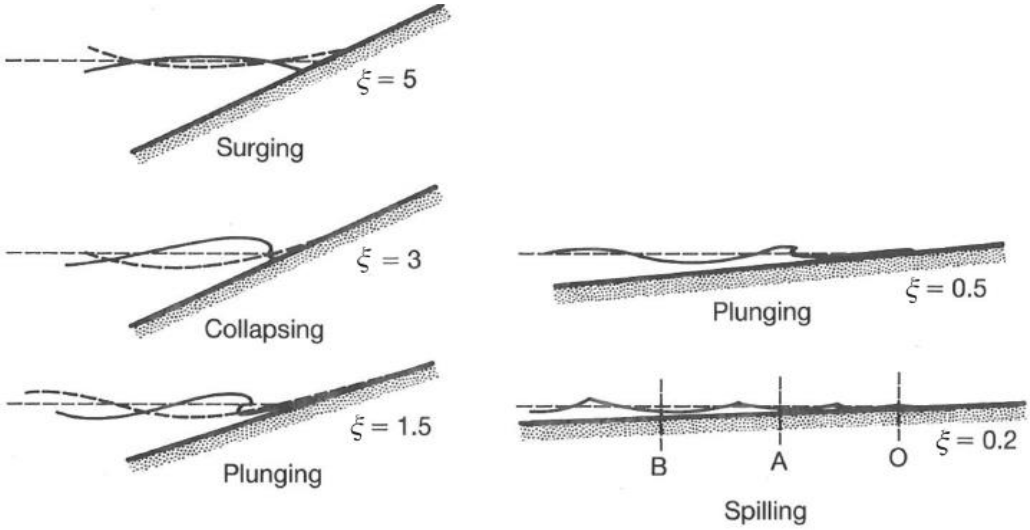

Figure 2-2: Breaker types (Battjes, 1974).

2.2.2 Damage definition

A breakwater is designed with multiple variables and with the worst-case storm scenario in mind. These variables include wave height and period, armour slope and density, core permeability, and storm duration. As a result, various authors developed many equations to anticipate the damage to the armour layer caused by wave attack and thus the required rock or armour size.

In the design process, the dimension of the equivalent cube, represented as D_n and commonly known as the nominal diameter, is utilized (CIRIA, 2007). The nominal diameter is calculated using Equation 3.

$$\mathrm{D}_n = \sqrt[3]{\frac{\mathrm{M}_a}{\rho_a}} \tag{3}$$

where:

D_n	=	nominal diameter	[m]
M_a	=	required median mass of armour unit	[kg]
ρ_a	=	density of concrete armour unit	[kg/m^3]

The level of damage, S_d, is determined by using the number of squares with a length of D_{n50}, which fits within the eroded zone. The influence of the slope is an important consideration when applying the damage level, S_d (van der Meer, 2017).

The degree of damage is determined by Equation 4:

$$\mathrm{S}_d = \frac{\mathrm{A_e}}{\mathrm{D}_n^2} \tag{4}$$

where:

S_d	=	damage level	[-]
$\mathrm{A_e}$	=	erosion area around still water level	[m²]
D_n	=	nominal diameter	[m]

The plot of the structural damage is represented graphically in Figure 2-3.

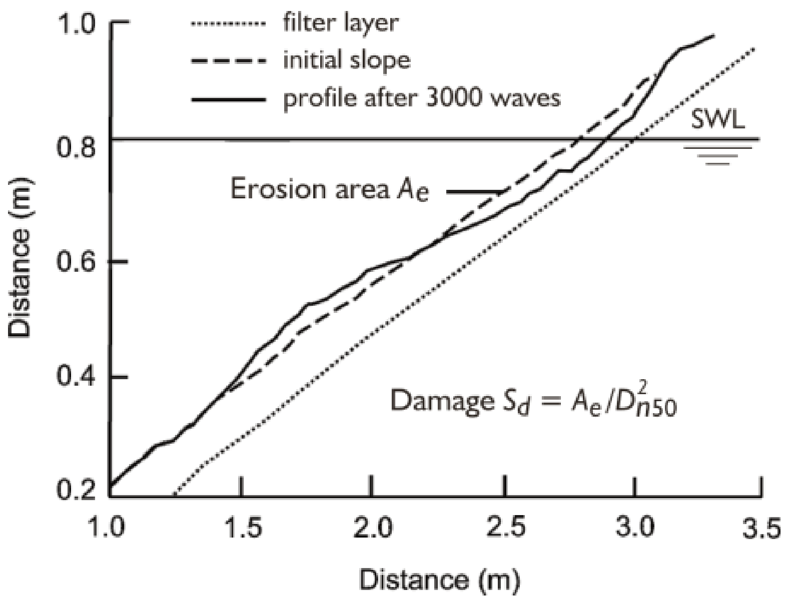

Figure 2-3: Damage S_d based on erosion area $\mathrm{A_e}$ (van der Meer, 2017)

Given the difficulties in determining a surface profile, the damage parameter S_d is less suited when complex concrete armour units are utilised. The damage may be expressed as the number of displaced armour units along a section width equal to the armour unit's nominal diameter, N_{od}, or as a percentage of the total dislodgements, N_d (%) (CIRIA, 2007).

The damage number, N_{od} is expressed by Equation 5:

$$\mathrm{N}_{od} = \frac{\textit{number of units displaced out of armour layer}}{\text{width of the tested section}/D_n} \tag{5}$$

The total damage, $N_{d\%}$ is expressed by Equation 6:

$$N_{d\%} = \frac{number\ of\ units\ displaced\ out\ of\ armour\ layer}{total\ number\ of\ units\ within\ reference\ area} \tag{6}$$

2.2.3 Hudson formula

The relative buoyant density is defined as the density of the unit relative to the density of water described by Equation 7:

$$\Delta = \frac{\rho_a}{\rho_w} - 1 \tag{7}$$

where:

ρ_a	=	density of concrete armour unit	[kg/m^3]
ρ_w	=	density of water	[kg/m^3]

The Hudson formula, defined in Equation 8, was derived from model studies involving non-overtopped rock structures featuring a permeable core and regular waves. This formula establishes a relationship between the wave height at the structure's toe, the median mass of an armour unit, and other relevant parameters (CIRIA, 2007).

$$M_a = \frac{\rho_a H^3}{K_d \Delta^3 \cot\alpha} \tag{8}$$

where:

M_a	=	required median mass of armour unit	[kg]
ρ_a	=	density of concrete armour unit	[kg/m^3]
H	=	design wave height, typically taken as H_s	[m]
K_d	=	stability coefficient	[-]
α	=	structure slope angle	[°]

The Hudson stability coefficient, K_d , is used to determine the suggested design values which accounts for a certain percentage of damage to the structure. Example K_d values are provided in Table 2-1.

Table 2-1: Hudson stability coefficients (Muttray & Reedijk, 2008; CLI, n.d.; DMC, 2003b).

Armour unit	Slope (V:H)	Hudson stability coefficient (K_d)	
		Trunk	Roundhead
Cube	1:1.33 – 1:1.5	6.5-7.5	5
Tetrapod	1:2	7-8	4.5-5.5
Dolos	1:2	16-32	8-16
Accropode	1:1.33 – 1:1.5	15	11.5
Core-Loc	1:1.33 – 1:1.5	16	13
Xbloc	1:1.33 – 1:1.5	16	-

The stability number is a significant design parameter, describing the relationship between the wave conditions and other relevant parameters, including the armour unit size and density. The rearranged Hudson formula with the stability number, N_S, indicated on the left-hand side, is illustrated in Equation 9:

$$N_s = \frac{H}{\Delta D_n} = (K_d \cot\alpha)^{1/3} \tag{9}$$

The Hudson formula's key strengths are its simplicity and the wide range of K_d values calculated for various armour units. The formula has several shortcomings including the fact that it does not account for the wave period or storm duration and fails to assess the severity of the damage (CIRIA, 2007).

2.2.4 Van der Meer formulae

Van der Meer (1988a) established formulae to evaluate the stability of armour rock on uniform slopes with crest levels greater than the maximum run-up for deep water conditions. The number of waves, N, describes the duration required to achieve an equilibrium profile. An additional number of waves may be investigated; however, the maximum number used is N = 7500 in Van der Meer's equations for rock stability (CIRIA, 2007).

Plunging and surging waves are characterised differently than breaking and non-breaking waves. A breaking wave is the type of breaking induced by the foreshore directly in front of the structure, as opposed to the type of breaking generated by the structure's slope (van der Meer, 1998). A critical value of ξ_{cr} can be used to determine the transition from plunging to surging waves as indicated in Equation 10:

$$\xi_{cr} = \left[\, 6.2\mathrm{P}^{0.31}\sqrt{\tan\alpha}\,\right]^{\frac{1}{\mathrm{P}+0.5}} \tag{10}$$

Two formulas were established for plunging and surging waves, respectively, and they are currently recognized as the Van der Meer formulas.

The Van der Meer formulae described in Equations 11 and 12 have been derived for plunging and surging wave conditions, respectively (van der Meer, 2017).

For plunging waves ($\xi_m < \xi_{cr}$):

$$\frac{\mathrm{H}}{\Delta \mathrm{D}_n} = 6.2\mathrm{P}^{0.18}\left(\frac{\mathrm{S}_d}{\sqrt{\mathrm{N}}}\right)^{0.2} \xi_{\mathrm{m}}^{-0.5} \tag{11}$$

For surging waves ($\xi_m \geq \xi_{cr}$):

$$\frac{\mathrm{H}}{\Delta \mathrm{D}_n} = 1.0\mathrm{P}^{-0.13}\left(\frac{\mathrm{S}_d}{\sqrt{\mathrm{N}}}\right)^{0.2} \sqrt{\cot\alpha}\; \xi_{\mathrm{m}}^{\mathrm{P}} \tag{12}$$

where:

P = notional permeability factor

S_d = damage level

N = number of waves (storm duration)

Figure 2-4 displays various notional permeability factor values, which depend on the specific structural configuration.

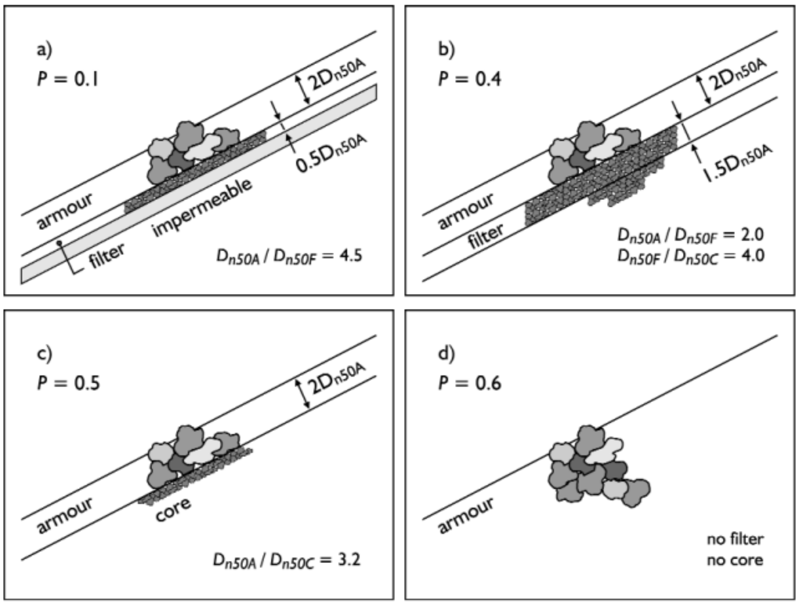

Figure 2-4: Notional permeability factor, P (CIRIA, 2007)

The wave height distribution diverges from the Rayleigh distribution in shallow water conditions. Van der Meer (1988b) conducted additional tests on a 1:30 (V:H) slope and discovered that in depth-limited situations, the stability of the armour layer is more accurately characterized by the wave height exceeded by 2% of the waves, $H_{2\%}$, rather than H_S. The wave height determined using the Rayleigh distribution can be described by the ratio of the two percent wave height over the significant wave height, as indicated in Equation 13.

$$\frac{H_{2\%}}{H_s} = 1.4 \, for \; deep \; water \; conditions \tag{13}$$

The Van der Meer formulae described in Equations 14 and 15 have been formulated to consider the influence of depth-induced wave breaking (van der Meer, 2017).

For plunging waves ($\xi_m < \xi_{cr}$):

$$\frac{H_{2\%}}{\Delta D_n} = 8.7P^{0.18} \left(\frac{S_d}{\sqrt{N}}\right)^{0.2} \xi_m^{-0.5} \tag{14}$$

For surging waves ($\xi_m \geq \xi_{cr}$):

$$\frac{H_{2\%}}{\Delta D_n} = 1.4P^{-0.13} \left(\frac{S_d}{\sqrt{N}}\right)^{0.2} \sqrt{\cot\alpha} \, \xi_m^{P} \tag{15}$$

2.2.5 Wave spectrum

The Pierson-Moskowitz, or PM, spectrum was developed in the mid-1960s and is based on ocean wave data gathered by ocean station vessels in the North Atlantic. However, this spectrum is not applicable for fetch limited seas. The Joint North Sea Wave Project, or JONSWAP, spectrum results from research on the wave energy spectrum based on North Sea data. The JONSWAP spectrum accounts for fetch and wind speed in formulating the equation. The study considered random wave conditions modelled using the standard JONSWAP spectral shape with a fixed peak-enhancement factor of ϒ=3.3 (Chadwick, et al., 2013).

2.3 History of concrete armour units

A Concrete Armour Unit, or CAU, can be identified using several parameters, including the unit's trademark name, volume, and dimensions. Furthermore, the royalties (if applicable), and the minimum class requirement that the concrete should meet are also useful when describing a unit.

The Cube (a concrete block) was the first concrete armour unit to replace armour rock. The unit was typically placed in a double layer. This option was chosen due to its great structural strength and ease of fabrication; however, the shape has a high concrete consumption. The Cube was comparable to armour rock because its hydraulic stability was provided mainly by the unit's weight (Bonfantini, 2014). Cubipods and Antifer Cubes represent two concrete armour units derived from the foundational concrete cube design. These units modify the basic cube structure by incorporating protrusions and creating grooves. While robust, they exhibit a limitation regarding interlocking capabilities and primarily rely on their weight as a stabilisation technique.

The Tetrapod was the first interlocking concrete armour unit created by the Laboratory Dauphinios d'Hydraulique (predecessor of Sogreah) in 1950. The Tetrapod outperforms the Cube in two ways: it uses less concrete and has improved interlocking capabilities. Between 1950 and 1980, a wide range of concrete armour units were created, usually randomly or uniformly placed in double layers (Oever, 2006).

The armour layer of a breakwater is constructed using either large armour rocks from a local quarry or CAUs; the latter may be placed in a uniform or random pattern. Table 2-2 includes details on a selection of CAUs, including the armour unit name, origin, year of development, and unit configuration.

Table 2-2: Overview of concrete armour units (Burcharth, 1993; DMC, 2003a).

Armour unit	Origin	Year	Shape	Armour unit	Origin	Year	Shape
Cube	-	-	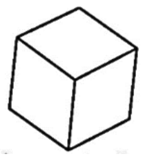	Accropode	FRA	1980	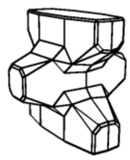
Tetrapod	FRA	1950	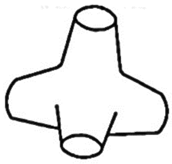	Shed	UK	1982	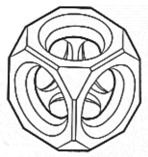
Modified Cube	USA	1959	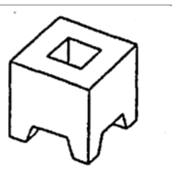	Haro	BEL	1984	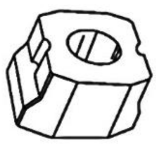

Stabit	UK	1961		Core-LocTM	USA	1996	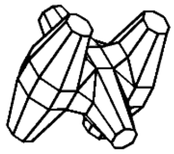
Akmon	NL	1962	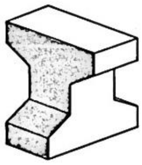	A-Jack	USA	1998	
Tripod	NL	1962	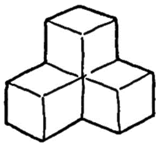	Diahitis	IRL	1998	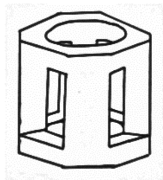
Dolos	RSA	1963	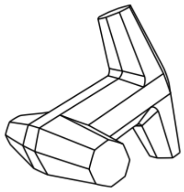	Accropode II	FRA	1999	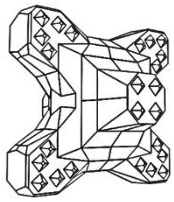
Cob	UK	1969	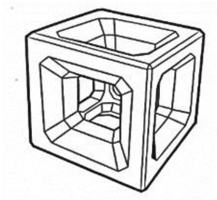	XblocTM	NL	2003	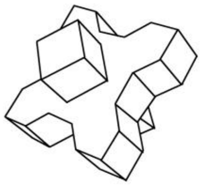
Antifer Cube	FRA	1973		Cubipod	ESP	2005	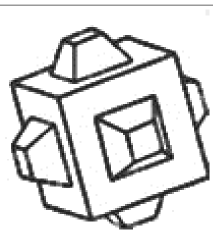
Seabee	AUS	1978	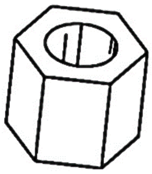	Crablock	UAE	-	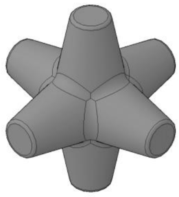

The armour units highlighted in Table 2-2 may be further categorised according to their shape, placement pattern, and stability factor. It is important to note that randomly placed units have a predetermined position. This statement may appear contradictory; however, it refers to the appearance of the units once placed and has nothing to do with the actual placement of the unit.

Hollow block configurations with simple designs like the Seabee and Diahitis or more complex designs like the Cob and Shed are commonly used for uniform placement. This placement pattern typically comprises a single layer with friction providing stability between adjacent units.

After 1950, armour unit development progressed from simple designs with limited interlocking, such as the Akmon and Tetrapod, to more complex shapes with good interlocking, such as the Dolos and Stabit. CAUs' interlocking capabilities are greatly enhanced by optimising their configuration to maximise slenderness.

The CAUs were often placed in a double layer to account for the uncertainty in the structural integrity and hydraulic stability. After the 1978 disastrous breakwater failure in Sines, Portugal, the safety of CAUs in breakwaters was reassessed. Since the 1980s, increased safety margins have been introduced for units placed in a single layer, influencing the design and structural strength of the units (DMC, 2008).

2.4 The Cubilok

PRDW Consulting Port and Coastal Engineers are currently developing a new concrete armour unit, referred to as the Cubilok. The Cubilok is characterized by four fundamental dimensions, which can be customized to generate diverse configurations of the unit shape.

2.4.1 History of the Cubilok

The trade-off between structural strength and the degree of interlocking is common among all concrete armour units. For instance, the waist-to-height ratio of the Dolos may be manipulated to increase the required structural strength, reducing the interlocking capability and the hydraulic stability (PRDW, 2019).

Several considerations contributed to the design of the new unit configuration, including existing units' cube-like geometries that lack interlocking in double layers and the Dolos armour unit's upper mass restriction of 30 tons (PRDW, 2019).

The inspiration for designing a new armour unit was created because of the lack of significant interlocking between existing bulky armour units, such as Antifer Cubes or Cubipods. The Cubilok design incorporated various design principles, including a flexible shape to adapt the structural strength and interlocking to suit the design criteria for specific sites. The armour unit's robust structure is also meant to resemble the strength of a concrete cube. The armour unit is also designed to be cast, handled, and placed easily on-site. An armour unit's interlocking ability depends on protuberances, commonly referred to as arms or legs (PRDW, 2019).

2.4.2 *Cubilok unit characteristics*

Figure 2-5 illustrates the alteration in the shape from the original to the modified shape, which is the basis of this study. The modified Cubilok is referred to as the Cubilok in this study for simplicity.

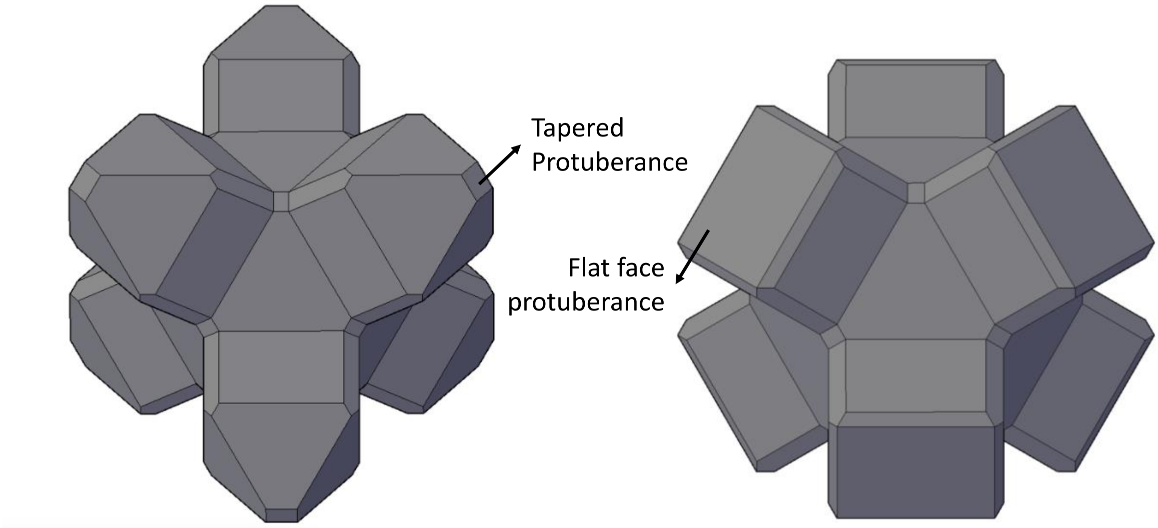

Original Cubilok Modified Cubilok

Figure 2-5: Slenderness ratios for the modified and original Cubilok.

A different configuration was considered to minimise the potential settlement experienced in previous hydraulic testing done by Wehlitz (2020). This configuration removes the tapered protuberance of the original experimental unit. The idea is that the unit's robustness and flat face would assist in the interaction with the underlayer and increase the structural integrity.

The Cubilok armour unit was developed to provide equivalent structural performance regardless of size. The influence of slenderness on unit stresses was determined using finite element modelling of various slenderness ratios. Excessive settlement of the original Cubilok shape was observed during the research done by Wehlitz & Schoonees (2023), which led to rethinking the design of the unit shape. The slenderness ratio, illustrated in Figure 2-6, is described by Equation 16 as a ratio of the height of a protuberance and the square root of its base area. The original and modified Cubilok has a slenderness ratio of H' = 1.09 and 0.583, respectively.

$$H' = \frac{H}{\sqrt{A}} \tag{16}$$

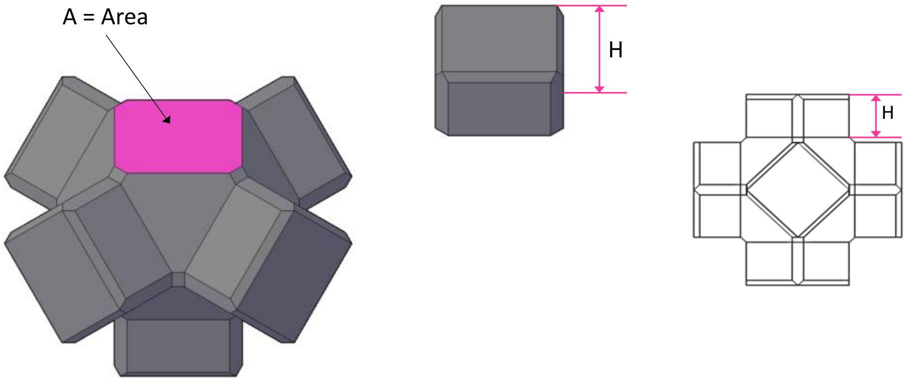

Figure 2-6: Visual representation of the slenderness ratio.

2.5 Unit interaction

The scarcity of rock at higher gradations drives the need for concrete blocks. Concrete usage is reduced by generating various configurations, increasing the potential interlocking. The hydraulic stability of the unit is achieved through various approaches; this includes utilising the units' weight as a means of stabilisation, ensuring significant interlocking of the units, and resistance achieved through friction between units (CIRIA, 2007). Table 2-3 categorises the CAUs depicted in Table 2-2 based on the parameters identified.

Table 2-3: Armour units classified by placement pattern, layer characteristics, shape, and stability factor - modified using multiple references (CIRIA, 2007; Salauddin, 2018)

Placement Pattern	Number of layers	Shape	Stability factor (main contribution)		
			Own weight	**Interlocking**	**Friction**
Random	Double Layer	Massive (Blocky)	Cube, Antifer Cube, Modified Cube		
		Bulky	Stabit, Akmon, Tripod		
		Slender		Tetrapod, Dolos	
	Single Layer	Massive (Blocky)	Cube		
		Bulky		Stabit, Accropode, Accropode II, Xbloc, Crablock	
		Slender		A-Jack, Core-Loc™	

Placement Pattern	Number of layers	Shape	Stability factor (main contribution)		
			Own weight	**Interlocking**	**Friction**
Uniform	Single Layer	Bulky		Crablock	Seabee, Haro, Diahitis
		Slender			Cob, Shed, Tribar

Note: The Haro may be placed in a double layer.

The motivation for developing highly interlocking units (such as the Tetrapod and Dolos) is the increased stability factor for K_d compared to rock gradings in a similar weight range. The use of slender interlocking units is limited in size as a result of breakage. This limitation has necessitated the development of more robust armour units.

It is important to understand how the interlocking capability of a concrete armour unit relates to slope stability. The point force as a result of contact between units (F) is generated through a combination of gravitational force and the flow force on the units further up the slope. Mild and steep slopes have different proportions of these forces acting on the units. The flow force would be dominant for mild slopes, whereas the gravitational force would be dominant for steep slopes. Figure 2-7 illustrates the effect of interlocking resulting from contact forces that complex concrete armour units generate (Burcharth, 1993).

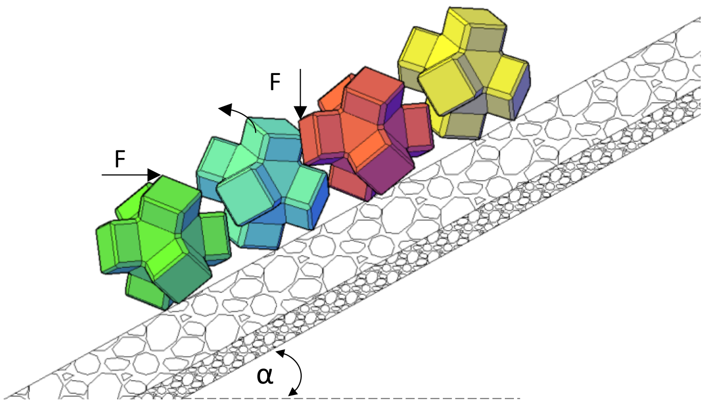

Figure 2-7: Interlocking forces applied on CAU, adapted from Burcharth (1993).

Figure 2-8 illustrates the variation in stability between complex interlocking units and rock or cube-like units. The contribution of the gravitational force is similar in both graphs; however, the contribution from interlocking and friction increases the total stability of the complex units compared to the cube-like and rock units.

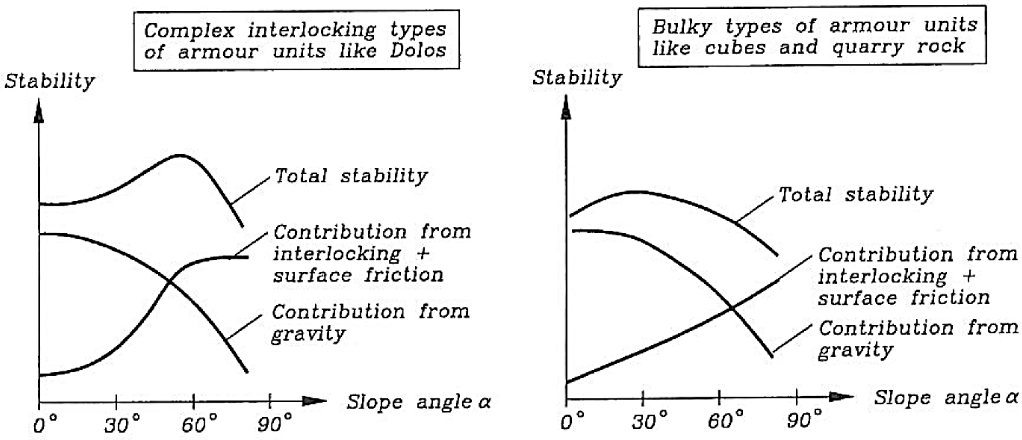

Figure 2-8: The stability as a function of the resistance mechanisms (Burcharth, 1993)

According to Wehlitz (2020), aside from the stability generated through unit-to-unit interaction, the interaction between the unit and the underlayer must be considered. This interaction may be demonstrated using the stability parameter, K_d, which accounts for the slope and its contribution to stability.

$$From\ Section\ 2.2.3\text{: } N_S = (\mathrm{K}_d \cot\alpha)^{1/3}$$

$$Slope\ 1\text{: }4/3 \rightarrow \cot\alpha = 0.0271$$

$$Slope\ 1\text{: }1.5 \rightarrow \cot\alpha = 0.0297$$

As seen in the equations above, the contribution to stability is greater for the milder slope than for the steeper slope. The contribution of the unit weight on the surface would increase for milder slopes. In contrast, the gravitational force is increased for unit-to-unit interaction on steeper slopes, which may influence the unit interlocking capability.

2.6 Wave loads

Determining the wave load affecting each unit on the slope through theory or hydraulic model testing is highly difficult due to increasing model complexity and parameter requirements. Thus, the relationship between the structural response and the wave conditions are determined experimentally (CEM, 2006).

The wave load may be described by the various wave forces generated by the incident wave. The resistance of a granular unit’s movement is complex, and Figure 2-9 assists in understanding these forces and their impact on the unit (Schiereck & Verhagen, 2012).

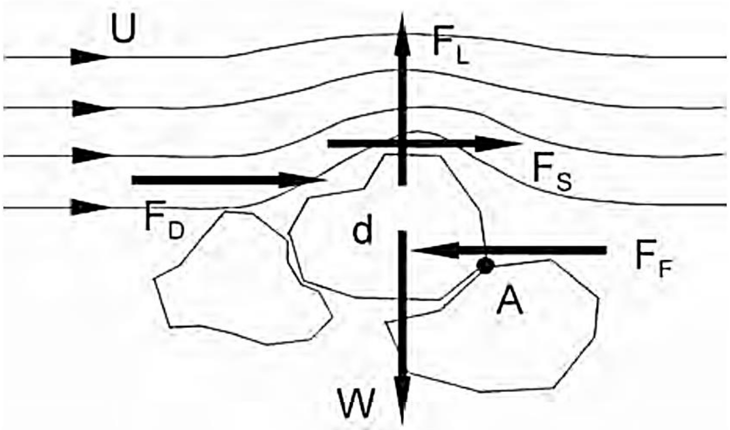

U = Flow velocity
F_D = Drag force
F_S = Shear force
F_L = Lift force
F_F = Frictional force
W = Submerged weight
A = Exposed surface area
d = Rock diameter

Figure 2-9: Forces acting on a granular unit in flow, modified from Schiereck & Verhagen (2012).

The various forces acting on an element in permanent (unidirectional) flow are expressed in Equation 17:

$$F_D = \frac{1}{2} C_D \rho_w u^2 A_D$$

$$F_S = \frac{1}{2} C_F \rho_w u^2 A_S \qquad (17)$$

$$F_L = \frac{1}{2} C_L \rho_w u^2 A_L$$

The coefficients C_i in the above formulae represent the proportionality, while A is representative of the surface area that is exposed. The parameter, ρ_w, describes the density of water, and the parameter u describes the flow velocity (Schiereck & Verhagen, 2012).

The force and counterforce are essential to understanding how the equilibrium of a unit is maintained. When the force acting on the granular unit exceeds the equilibrium point, the unit shifts out of its original placement or is dislodged from the slope entirely. The submerged weight, *W*, of the unit, counters the lift force. The shear and drag forces are countered by either the moment acting at point *A,* as illustrated in Figure 2-9, or by the frictional force, F_F. For further information on other relevant parameters refer to Schiereck & Verhagen (2012).

The porosity determined in armour layers, known as volumetric porosity (n_v) and sometimes referred to as void porosity, is primarily governed by factors such as the shape of the armour unit, the packing density, and their placement arrangement (CIRIA, 2007). The porosity of the armour layer has a significant impact on the hydraulic characteristics of the structure. The armour layer's porosity significantly impacts the structure's hydraulic properties, influencing wave reflection, run-up, overtopping, hydraulic stability, and the material requirements for construction. Furthermore, porous structures allow waves to dissipate, reducing the force on the structure and minimising the reflected wave.

2.7 Overtopping

2.7.1 Overtopping discharge

Coastal structures are used to protect the coastline, infrastructure or maritime transport against wave attacks and flooding. Many parameters influence the overtopping rate, making the process of predicting overtopping complex. The flow parameters used in this study to describe the overtopping are the mean overtopping discharge, q, and the maximum overtopping volume, V_{max} (EurOtop, 2018). The overtopping rate can be determined using Equation 18.

$$\frac{q}{\sqrt{g \times H_{m0}^{3}}} = 0.09 \times \exp[-(1.5\frac{R_c}{H_{m0} \times \gamma_f \times \gamma_\beta})^{1.3}] \quad (18)$$

where:

q	=	Wave overtopping discharge	[m/s^3]
H_{m0}	=	Wave height calculated from the spectrum	[m]
g	=	Gravitational acceleration $\cong 9.81$	[m/s^2]
R_c	=	Crest height	[m]
γ_f	=	Roughness influence factor	[m]
γ_β	=	Oblique waves influence factor	[m]

The overtopping rate, as defined in the equation mentioned above, quantifies the volume of water passing over the structure, but it falls short of capturing the irregularity in wave overtopping. Since waves exhibit irregularities, describing the overtopping rate as an average does not adequately represent the volume passing over the structure at any given time.

It is possible to describe this irregular process if the storm duration, the number of overtopping waves, and the overtopping discharge are known (EurOtop, 2018).

2.7.2 Percentage of wave overtopping

The 2% mean wave run-up for rough slopes is defined by Equation 19 (Schüttrumpf, et al., 2009). A maximum value of $R_{u,2\%}/H_{m0} = 1.97$ is possible when considering a permeable structure core.

$$\frac{R_{u,2\%}}{H_{m0}} = 1.65 \times \gamma_b \times \gamma_f \times \gamma_\beta \times \xi_{m-1,0} \tag{19}$$

There are two methods to calculate the percentage of a wave overtopping described by Equations 20 and 21. With the correct roughness factor Equation 19 could provide an accurate wave run-up required to determine the overtopping rate. The roughness influence has not yet been defined for the Cubilok unit; therefore, Equation 20 will be used in the overtopping analysis.

$$P_{ov} = \mathrm{N_{ow}}/\mathrm{N_w} = \exp[-(\sqrt{-\ln 0.02}\frac{R_c}{R_{u,2\%}})^{\,2}] \tag{20}$$

Figure 2-10 contains a wide range of wave overtopping percentages, ranging from no overtopping to complete overtopping of this structure.

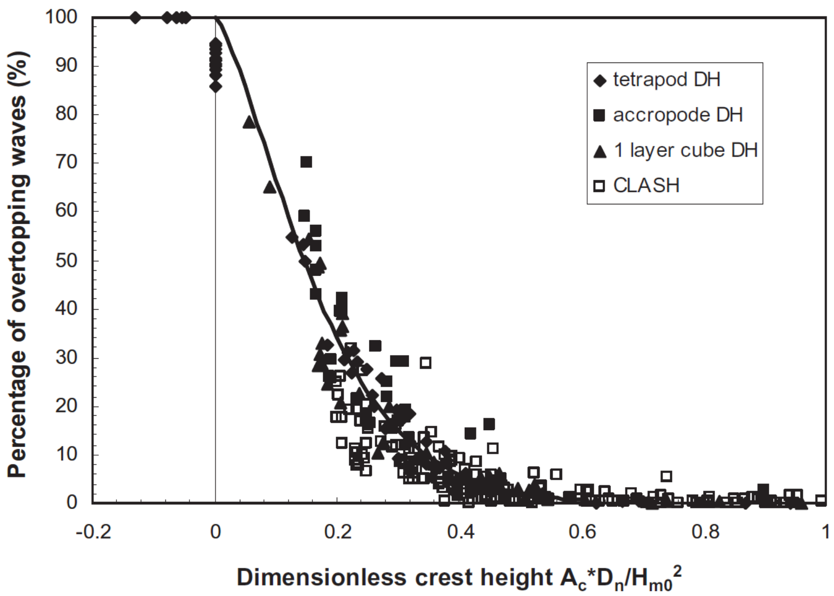

Figure 2-10: Percentage of wave overtopping relative to the dimensionless crest height (Schüttrumpf, et al., 2009).

The CLASH database (2004) included a maximum wave overtopping percentage of approximately 30%. A greater percentage would produce overtopping volumes too large to measure, increasing the effect of wave transmission. A Weibull curve is fitted on the data by assuming 100% overtopping at a zero freeboard. Equation 21 may be used to predict the number of overtopping waves or to determine the crest level for a given overtopping tolerance.

$$P_{ov} = \mathrm{N_{ow}}/\mathrm{N_w} = \exp[-(\frac{R_c \times D_n}{0.19 \times H_{m0}^2})^{\,1.4}] \tag{21}$$

where:

P_{ov}	=	Wave overtopping discharge	[m/s^3]
$\mathrm{N_{ow}}$	=	Number of overtopping waves	[waves]
$\mathrm{N_w}$	=	Number of waves (=1000)	[waves]

2.8 Failure modes

2.8.1 Breakwater failure modes

Breakwaters fail for a multitude of reasons, including but not limited to inadequate design, load exceedance, construction, and deterioration failure. Design failure occurs when the structure cannot withstand the load applied because of an inadequate preliminary design, and load exceedance failure occurs when the design conditions are exceeded. Construction failure may occur because of poor construction or sub-standard materials used for construction. Finally, deterioration failure occurs as a result of insufficient maintenance (CEM, 2006). Several failure modes that occur in a conventional rubble-mound breakwater are illustrated in Figure 2-11.

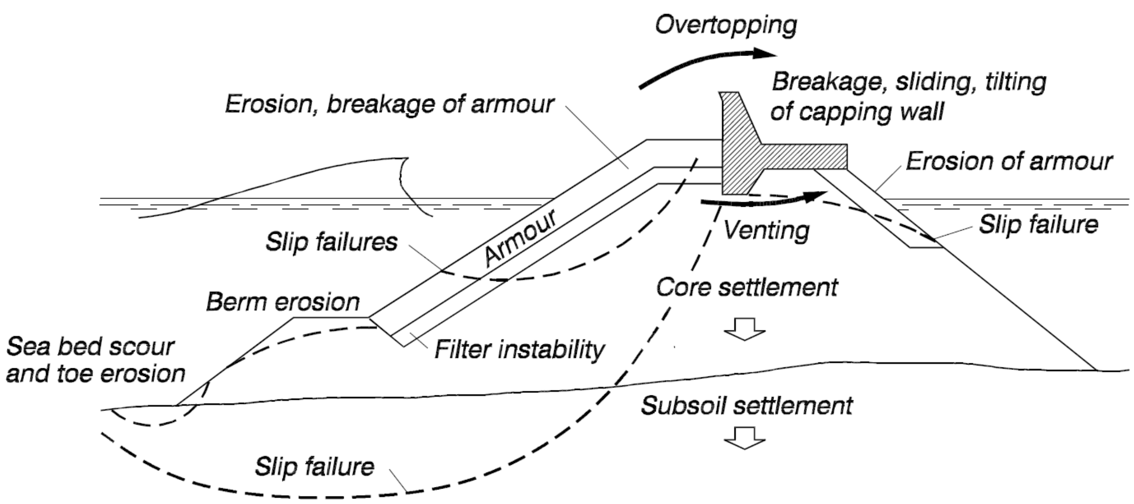

Figure 2-11: Failure modes for rubble-mound breakwater (CEM, 2006).

2.8.2 Concrete armour unit failure modes

There are various causes of concrete armour unit failure; wave-induced rocking is the more common form of unit breakage. Additionally, units are subjected to static loads and loads during construction, which may result in damage to the unit. Several techniques to stabilise an armour unit include utilising the unit's weight, potential interlocking capabilities, and friction between units (detailed in Table 2-3). Unit fractures or breakages reduce the structural strength of the armour unit. Additionally, displaced fragments of broken armour units, propelled by wave action, can compound the damage when they are subsequently carried back onto the structure (CIRIA, 2007).

Finite element stress modelling (or FEM) and drop testing of armour units may be used to gather critical information about an armour unit's structural integrity. In addition, special consideration should be given to the performance of in-service armour units. Unit breaking often occurs due to decreased structural strength as the unit size increases. Thus, the unit's applicability range should be carefully examined during the design phase, as utilising a unit outside of its applicability range could result in the structure failing prematurely due to unit breakage (CIRIA, 2007).

2.9 Physical Modelling

A crucial requirement in a model test is that the physical model behaves similarly to the prototype. The model must be similar to the prototype in the three basic categories of geometric shape, kinematics, and dynamic forces occurring in both the model and prototype (Goda, 2000).

The geometric shape similarity refers to the scaling down of the specific prototype dimensions to the model dimensions. According to kinematic similarity, the velocity and acceleration of different bodies and the fluid between the prototype and the physical model must be proportionate. Dynamic similarity states that an identical scale ratio is required when recreating the dynamic forces in the physical model as in the prototype (Goda, 2000).

The waves and currents in the coastal zone are explained by coastal hydrodynamics. Waves are classified into two types: short waves and long waves. A short-wave model examines wind waves and the impacts of swell in the coastal zone. These models may represent hypothetical or prototype coastal structures to gain an insight into how the model functions or establish engineering design guidelines (Hughes, 1993).

Dalrymple (1985) discusses two distinct benefits. The first is that the physical model incorporates the suitable equations regulating the process, eliminating the need for simplified analytical or numerical assumptions. The second benefit is that the model's modest size allows for simpler data collection throughout the modelling period at a lower cost. Furthermore, receiving visual feedback from the model provides an invaluable opportunity.

2.9.1 Distortion in Hydraulic Modelling

An undistorted model has an identical geometric scale in the horizontal and vertical orientations. A distorted model is one in which the geometric scales in the horizontal and vertical orientations differ. In coastal engineering projects, distorted physical models are used to reduce the horizontal area required for the model while simultaneously elevating the slopes within it. For instance, a distorted model may include scaling down a breakwater section in a 2-D wave flume, with the flume width geometrically distorted to accommodate multiple rows of armour units. There are numerous advantages to employing distorted models, including, but not limited to, reduced spatial demands for the model, exaggerated slopes resulting in easier measurements, and lower operational expenses due to the usage of scaled-down models. Among the disadvantages of distorted models are the potential for inaccuracies in replicating the refraction and diffraction and the possibility of unanticipated scale effects impacting the model results (Hughes, 1993).

2.9.2 Froude criterion

In hydraulic model testing, the governing forces are inertia and gravitational forces, where a water's surface tension and viscosities generally play minor roles. The Froude law states that the scale of the velocity and time is equivalent to the square root of the length scale (Goda, 2000). The Froude number, which is expressed by Equation 22, reflects the relative influence of inertial and gravitational forces on a fluid particle (Hughes, 1993):

$$Froude\ number = \sqrt{\frac{inertia\ force}{gravitational\ force}} = \sqrt{\frac{\rho L^2 V^2}{\rho L^3 g}} = \frac{V}{\sqrt{gL}} \tag{22}$$

Similitude is maintained when the Froude number in the model and prototype is the same, as expressed by Equation 23:

$$\left(\frac{V}{\sqrt{gL}}\right)_{prototype} = \left(\frac{V}{\sqrt{gL}}\right)_{model} \tag{23}$$

where:

V	=	Velocity	[m/s]
g	=	Gravitational acceleration	[m/s^2]
L	=	Length	[m]

Scaling hydraulic models based on the Froude model law is common practice in coastal engineering. Wave heights, wave durations, and the model size can be accurately replicated in a scaled-down laboratory environment by maintaining the same Froude number. As a result, while designing a scaled coastal model, this law is often used as the primary criterion (Hughes, 1993). Table 2-4 provides the model scales achieved using Froude's law.

Table 2-4: Scale parameters according to Froude (Goda, 2000).

Parameter	Scalar	Unit	Froude scale
Wave height, water level	Distance	m	N
Wave period, test duration	Time	s	$N^{0.5}$
Rock and sediment mass	Mass	kg	N^3
Scour area	Area	m^2	N^2
Rock and sediment volume	Volume	m^3	N^3
Overtopping	Discharge	m^3/s	$N^{3/2}$

2.9.3 Reynolds criterion

The ratio of the inertial force to the viscous force is important to consider when the viscous forces are dominant. The Reynolds number, which is expressed by Equation 24, reflects the relative influence of inertial and viscous forces on a fluid particle (Hughes, 1993):

$$Reynolds\ number = \frac{inertia\ force}{gravitational\ force} = \frac{\rho L^2 V^2}{\mu V L} = \frac{\rho L V}{\mu} \tag{24}$$

Similitude is obtained when the Reynolds number in the model and prototype is the same, as expressed by Equation 25:

$$\left(\frac{\rho L V}{\mu}\right)_{prototype} = \left(\frac{\rho L V}{\mu}\right)_{model} \tag{25}$$

where:

ρ	=	fluid density	[kg/m^3]
L	=	Length	[m]
V	=	Velocity	[m/s]
μ	=	dynamic viscosity	[kg m^{-1} s^{-1}]

The Reynolds scale law is used to describe flows that are primarily dominated by viscous forces. Scenarios warranting the application of Reynolds scaling include instances involving the assessment of forces on cylinders experiencing laminar flow and challenges arising from laminar boundary layers (Hughes, 1993).

2.9.4 Physical model uncertainties

There are several uncertainties regarding the input parameters used when conducting physical models. These uncertainties include fundamental, data, and model uncertainties and human errors. The unpredictability of natural physical processes and the inability to recreate these processes in model scale are referred to as fundamental and model uncertainties. Data uncertainties include errors when taking measurements, while human errors result from human involvement (EurOtop, 2018).

Scaling effects develop as a consequence of an inaccurate recreation of the prototype structure in modelling scale. The breakwater core's influence on the structure's permeability is a well-known scaling effect. Geometrically scaling the core would reduce the material, resulting in a nearly impermeable core, influencing the stability, wave run-up, and overtopping rate (Burcharth, et al., 1999). In contrast, the methodology proposed by Burcharth et al. (1999) modifies the scaling by considering the material's characteristic pore velocity.

The laboratory effects in hydraulic models result from the physical limitations posed by flow boundaries, the influences introduced through mechanical wave generation techniques, and simplifying prototype wave conditions (i.e., the inability to account for oblique waves). Natural wave reflection occurs at sea; however, in the wave flume, due to the lack of continuous ocean area, waves are reflected back to the structure. Active wave absorption at the wave board is one method for dealing with this lab-induced effect (Hughes, 1993).

The scale effects in hydrodynamic models are mainly the outcome of the assumption that gravity is the force that dominates and balances the inertial forces present. This assumption inaccurately extends to other relevant forces, such as viscosity, surface tension, and elasticity, assuming that these forces have a minor influence. As a consequence of the model's viscous effects, the wave reflection coefficient for riprap in scaled-down models is greater than what is observed in the prototype. As a result, the model behaves as though it experienced a lower porosity than it would in a prototype (Hughes, 1993).

Other notable scale effects include variations in density between fresh and saltwater and inconsistencies replicating model unit strength. CAUs, for example, are frequently scaled based on mass density, allowing model units to withstand greater levels of stress (Hughes, 1993). In future, further research could result in a better understanding of the scaling effects and improve upon the techniques and equipment utilised in physical modelling.

3 RESEARCH METHODOLOGY

The hydraulic stability of Cubilok armour units was investigated in this study using small-scale hydraulic model testing.

3.1 Physical model set-up

3.1.1 Testing equipment

The 2-D laboratory experiments were conducted in a wave flume at the Council for Scientific and Industrial Research (CSIR) in Stellenbosch. High-definition photographs were taken from the fixed camera position to determine the displacement and extraction of units on the slope.

3.1.1.1 Flume

The glass flume is 30 m long, 0.75 m wide, and 1 m deep (shown in Figure 3-1).

Figure 3-1: Glass flume.

At the time of testing, the flume had a 1:200 slope already constructed. The new slope of 1:30, selected based on previous testing conducted by Wehlitz (2020), was constructed above the existing slope, as shown in Figure 3-2.

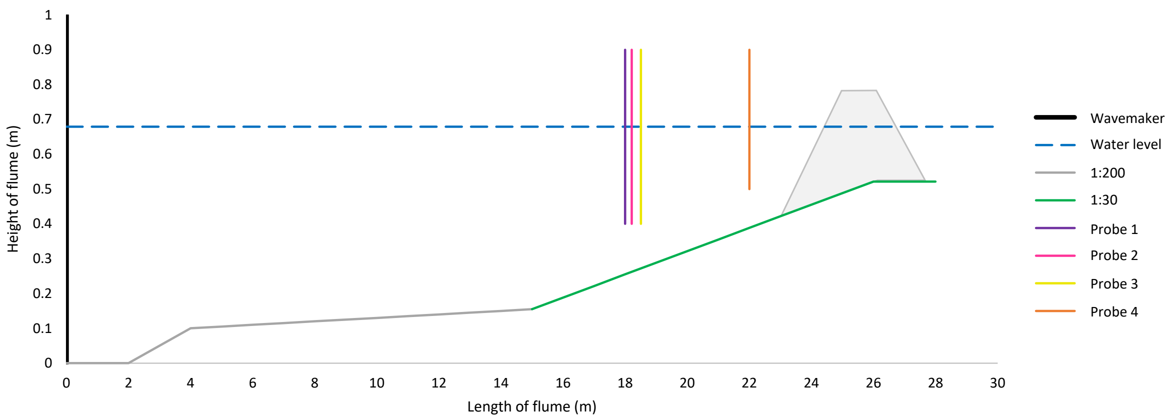

Figure 3-2: Slope and probe placement.

3.1.1.2 Wavemaker

The wavemaker can generate irregular waves that follow various spectra, including JONSWAP or Pierson-Moskowitz. The JONSWAP spectrum was used in this study as this spectrum is characteristic of the South African coastline (HR Wallingford, 2010).

3.1.1.3 Probe placement

The probe spacing locations were determined using the Mansard and Funke (1980) illustrated in Figure 3-3. The first probe was placed one wavelength away from the structure, and all distances are determined relative to Probe 1, as illustrated in Equations 26 – 28.

$$\text{Distance from Probe 1 to Reflecting structure: } X_{R1} = L_P \tag{26}$$

$$\text{Distance from Probe 1 to Probe 2: } X_{12} = \frac{L_P}{10} \tag{27}$$

$$\text{Distance from Probe 1 to Probe 3: } \frac{L_P}{6} < X_{13} < \frac{L_P}{3} \tag{28}$$

$$X_{13} \neq \frac{L_P}{5} \qquad AND \qquad X_{13} \neq \frac{3L_P}{10}$$

where: L_p = one wavelength from the structure to probe 1.

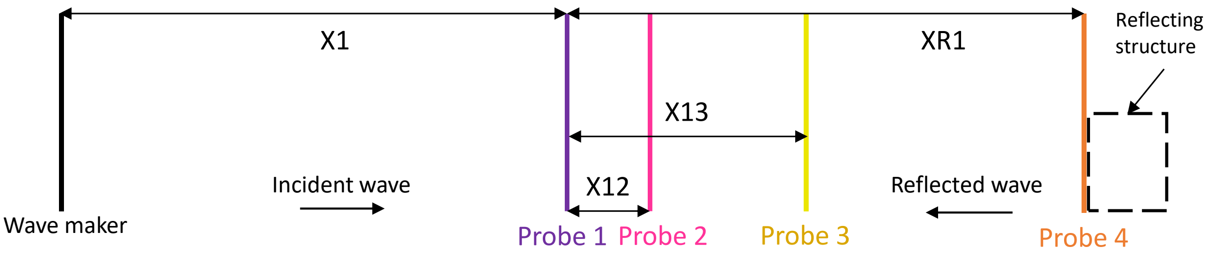

Figure 3-3: Probe spacing (Mansard & Funke, 1980).

The probe spacing results for several wave periods are indicated in Table 3-1.

Table 3-1: Probe spacing for various cases.

Case	T_P (s)	X12 (m)	X13 (m)
1	1.23	0.181	0.481
2	1.38	0.209	0.509
3	1.55	0.241	0.541
4	1.73	0.273	0.673
5	1.94	0.311	0.711
6	2.17	0.352	0.752
7	2.72	0.448	0.948

3.1.1.4 Overtopping equipment

The overtopping configuration comprises a simplistic arrangement depicted in Figure 3-4. A chute connects to a stationary overtopping container housing a submerged pump. This submerged pump facilitates the controlled transfer of water to a designated 50-litre container, as necessitated by the experimental conditions. After each transfer, the container is emptied, and a count of the containers is noted to establish the overtopping volume. Additionally, the remaining water within the overtopping container, housing the submerged pump, is determined using a water level gauge and combined with the overtopping volume.

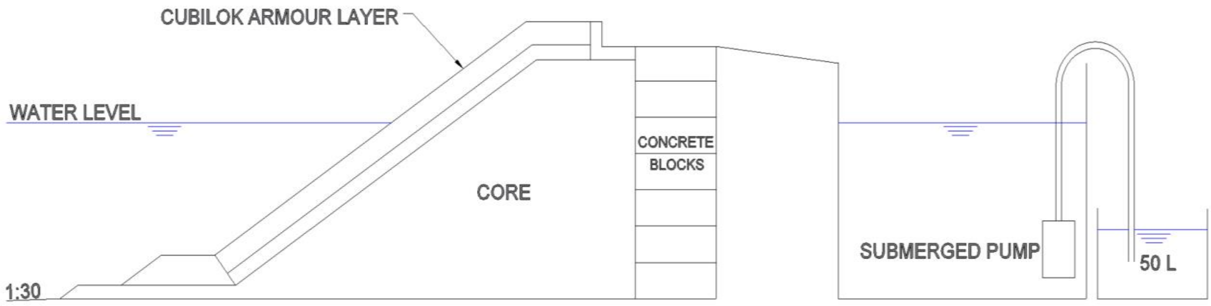

Figure 3-4: Overtopping set-up.

3.1.2 Test parameters

The water depth remained at a constant level of 0.291 m throughout the duration of testing. The number of waves remains constant at 1000 per test condition as determined by the initial testing conducted and elaborated upon in Section 4.2.3.

Six wave heights, wave periods, and test durations were calibrated before the rubble mound breakwater section was constructed in the flume. Furthermore, two packing densities were tested initially, and the packing density of $\emptyset = 0.65$ was decided on for further testing as it resulted in a significant reduction in settlement, which is discussed further in Section 5.2.

3.1.3 Model scale

Considering a model scale of N = 60, the model unit weight of 46.6 g corresponds to approximately 10 tonnes for a real-world prototype unit. The varied parameters are provided in the model and prototype scale in Table 3-2.

Table 3-2: Varied test parameters.

Parameter	Scalar	Unit	Froude scale	Model	Prototype
Water level	Distance	m	N	0.291	17.5
Wave height	Distance	m	N	0.100	6.0
				0.112	6.7
				0.125	7.5
				0.140	8.4
				0.157	9.4
				0.176	10.6
Wave period	Time	s	$N^{0.5}$	1.38	10.7
				1.55	12.0
				1.73	13.4
				2.72	21.1

3.1.4 *Material selection*

Concrete armour units typically require a specific underlayer size to ensure satisfactory load transfer, appropriate permeability, and resistance of the finer materials movement outward. Considering the reduced permeability that leads to decreased armour stability, it was critical that the underlayer material was big enough and the grading fell within a specified range (CIRIA, 2007).

This study made use of an underlayer of one-tenth of the concrete armour unit weight for the model breakwater following the Rock Manual (2007). The recommended underlayer sizes for single-layer interlocking and double-layer armouring are presented in Table 3-3.

Table 3-3: Armour size for underlayer with CAUs (CIRIA, 2007).

Type of armouring	Mass of underlayer ($\mathbf{M_u}$); Mass of armour unit ($\mathbf{M_a}$)		
Single-layer interlocking units	$M_{50,u} = 0.1M_a$	$M_{min,u} = 0.07M_a$	$M_{max,u} = 0.14M_a$
Double layer armouring	$M_{50,u} = 0.1M_a$	$M_{min,u} = 0.05M_a$	$M_{max,u} = 0.15M_a$

In conjunction with PRDW, the modified Cubilok units were fabricated and employed in the model testing that was carried out for this study. The average unit weighs 46.6 g and has a nominal diameter of 27 mm. Additional unit characteristics are provided in Table 3-4.

Table 3-4: Armour unit properties for the Cubilok.

Description	Material type	Material density	Nominal Mass (M_{50})	Nominal diameter (D_{50})
Armour layer	Resin mix	2360 kg/m^3	46.6 g	27 mm
Underlayer	Rock	2650 kg/m^3	4.1 g	11.5 mm
Core	Rock	2650 kg/m^3	1.0 g	7.2 mm
Toe	Rock	2650 kg/m^3	41 g	25 mm

3.1.5 Model configuration

The hydraulic test was specifically planned for a comparative analysis with a test series involving a single-layer Xbloc, illustrated in Figure 3-5. The cross-section design was influenced by previous testing of the original Cubilok unit (PRDW, 2019), which was based on the Xbloc cross-section (DMC, 2003b). The unit tested in the Xbloc study had a mass of 121 g, whereas the Cubilok tested in this study had a median mass of 46.6 g. The cross-section in Figure 3-5 was scaled to create a comparable Cubilok test section.

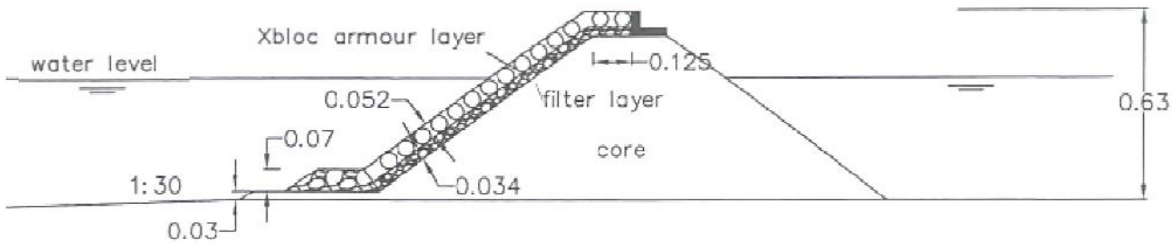

Figure 3-5: Xbloc^{TM} test section (DMC, 2003b).

The test structure consists of either a single or double-layer Cubilok armour layer, an underlayer, a rock toe, a permeable core, and a fixed L-shape capping on the crest. Test Series A has a steep slope of 1: 1.33, and Test Series B has a milder slope of 1: 1.5. For the milder slope, the number of rows increased from 26 to 28 rows. Test series C represents the double layer tests conducted in this study. The underlayer was shifted downward to maintain the crest level for Series C, reducing the overall core volume.

The nominal diameter of the Cubilok based on the median mass and density, determined from the manufactured units, is calculated using Equation 3 from Section 2.2.2.

$$D_n = \sqrt[3]{\frac{0.0466}{2364}} = 0.2701\ m \approx 27\ mm$$

The armour layer and underlayer thickness are determined using the Equation 29:

$$t = nk_t D_n \tag{29}$$

where:

n	=	number of layers
k_t	=	layer thickness coefficient
D_n	=	nominal diameter

To obtain the median target mass for the underlayer a grading of 13.2–19mm is utilised. Appendix B contains the grading curve for the underlayer.

The core material of a conventional rubble-mound breakwater often consists of quarry run which includes a wide range of particle sizes. The core was scaled using the approach developed by Burcharth et al. (1999), yielding a nominal weight of 0.91 g. Based on the available material, a core grading of 1 g is obtained using a mixture of six parts 5– 12mm to one-part 14mm.

According to the Rock Manual (2007), a minimum of three artificial units is recommended to obtain an adequate breakwater crest width (B). If extensive overtopping is foreseen, this is an essential requirement. Furthermore, the minimum width which is defined in Equation 30, ensures safe placement and a suitable amount of interlocking.

$$B \geq 3D_n \tag{30}$$

The toe was an important consideration as it forms the base of the structure's stability, and if the toe fails, the entire structure may fail prematurely. Conventional breakwaters should allow for at least three armour units for the width of the toe, as indicated in Equation 31 (CIRIA, 2007).

$$B_t \geq 3D_n \tag{31}$$

The nominal diameter of the toe rock is determined using the Equation 32:

$$\frac{H}{\Delta D_{n50}} = 2 + 6.2\left(\frac{h_t}{h}\right)^{2.7} N_{od}^{0.15} \tag{32}$$

where:

D_{n50}	=	required median mass of rock	m

h_t	=	highest depth of toe	m
h	=	bottom depth of foreshore at toe of structure	m

A damage number N_{od} of 0.5, which corresponds to the start of damage, is selected. The second largest wave height (9.4 m) and period (16.8 s) were selected to determine an appropriate toe rock size, as this condition was considered adequately conservative. An additional 10% was included to ensure that the toe has no significant impact on the structure, resulting in the adjusted rock size shown in Table 3-5. The model's toe is overdesigned in an effort to ensure the reliability of the test stability results. As a result, the contribution of the toe to the study's findings is minimal and does not significantly affect the overall outcome.

Table 3-5: Toe details.

Description	$\mathbf{D}_{n50}\ (m)$	$\mathbf{M}_{50}\ (g)$	$\mathbf{B}_t$
Calculated toe	0.023	31	$4 * D_n$
Adjusted toe	0.025	41	$4 * D_n$

Figure 3-6 provides a cross-sectional drawing of the single-layer system. It was decided to decrease the core level to accommodate a double armour layer and maintain a consistent crest level.

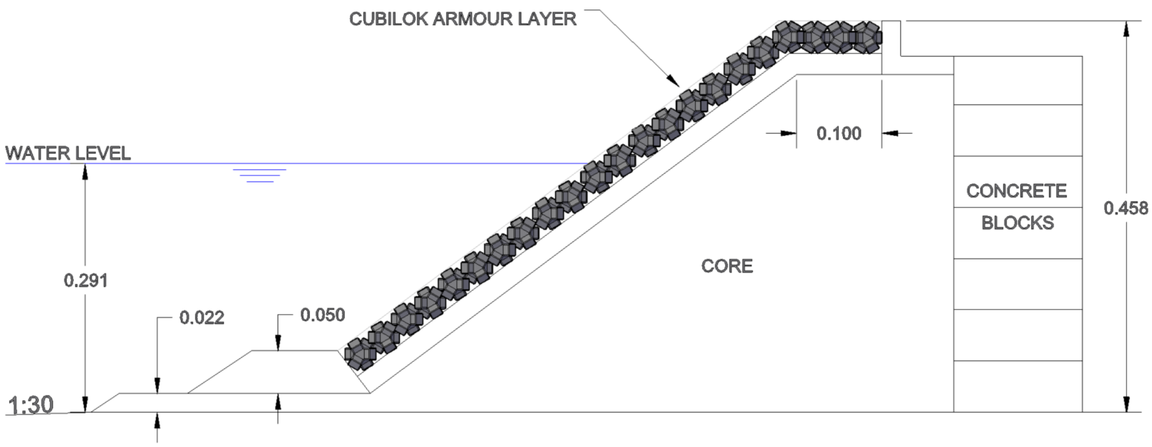

Figure 3-6: Test section for the unit in a single layer at a 1:1.33 and 1:1.5 slope.

3.1.6 *Unit placement*

The placement of the units has several contributing factors, including the placement pattern packing density and unit orientation. The symmetrical shape of the unit allows for fewer unique orientations and ensures ease when packing; see Section 7.1.

For single-layer units, the placement of the armour units was critical as it influenced the interlocking capability between units and the interaction with the underlayer. Since this was the first model testing done for the modified Cubilok, there were limited guidelines available regarding the placement of the unit, however certain parameters, such as the packing density were selected based on the outcome of the study done by Wehlitz (2020). The number of wave series was intended to determine the damage progression for the two packing densities investigated. The results of the tests were then analysed to determine which packing densities were used for the rest of the test series.

Concrete armour units are usually placed on a predefined grid where the location of each unit is known in relation to the surrounding units. The staggered grid placement pattern was used for all the tests conducted in this study and was based on the centre-to-centre distance of the armour unit used when packing, as illustrated in Figure 3-7 (CIRIA, 2007).

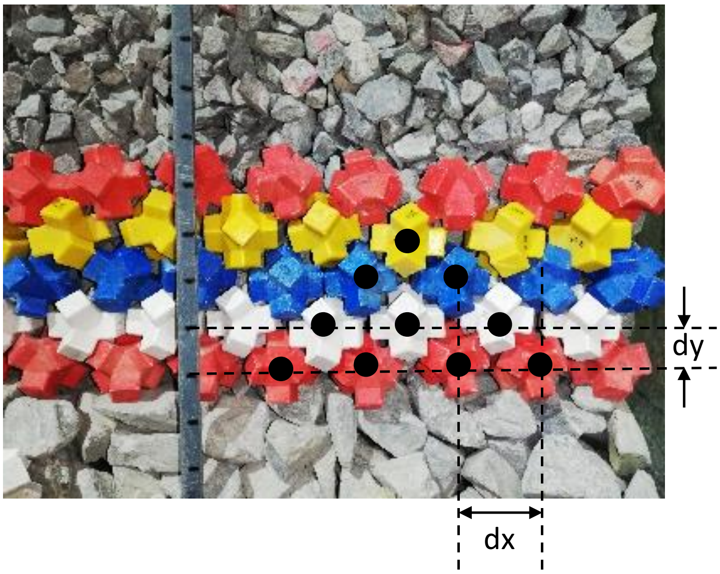

Figure 3-7: Staggered grid placement.

All of the slopes packed for testing were packed using a random orientation. The horizontal distance between units, $\mathrm{d_x}$, determines the number of units in the first row. The upslope distance, $\mathrm{d_y}$, and horizontal distance $\mathrm{d_x}$ was calculated using Equation 33 (PRDW, 2019):

$$\frac{1}{\emptyset} = \left(\frac{\mathrm{d_x}}{\mathrm{D_n}}\right)\left(\frac{\mathrm{d_y}}{\mathrm{D_n}}\right) \tag{33}$$

Estimated values for upslope and horizontal distances are provided in Table 3-6 relative to the assumed packing density.

Table 3-6: Packing density.

CAU	d_x/D_n	d_y/D_n	$\emptyset$
Single-layer Cubilok	1.780	0.890	0.63
	1.730	0.890	0.65
Double-layer Cubilok	1.850	0.925	1.17
	1.850	0.890	1.21
	1.730	0.890	1.30

Since interlocking contributes to the majority of the hydraulic stability, the unit placement pattern is critical to ensuring the structural integrity of the armour layer. The horizontal and upslope distances define the staggered grid placement pattern. Figure 3-8 provides an overview of various Cubilok configurations and their respective packing densities, illustrating what is theoretically achievable with various placement patterns. The yellow and green units represent uniform arrangement within a rectangular and diamond-shaped grid, respectively, while the blue units denote the loosest packing achieved with contact between adjacent units.

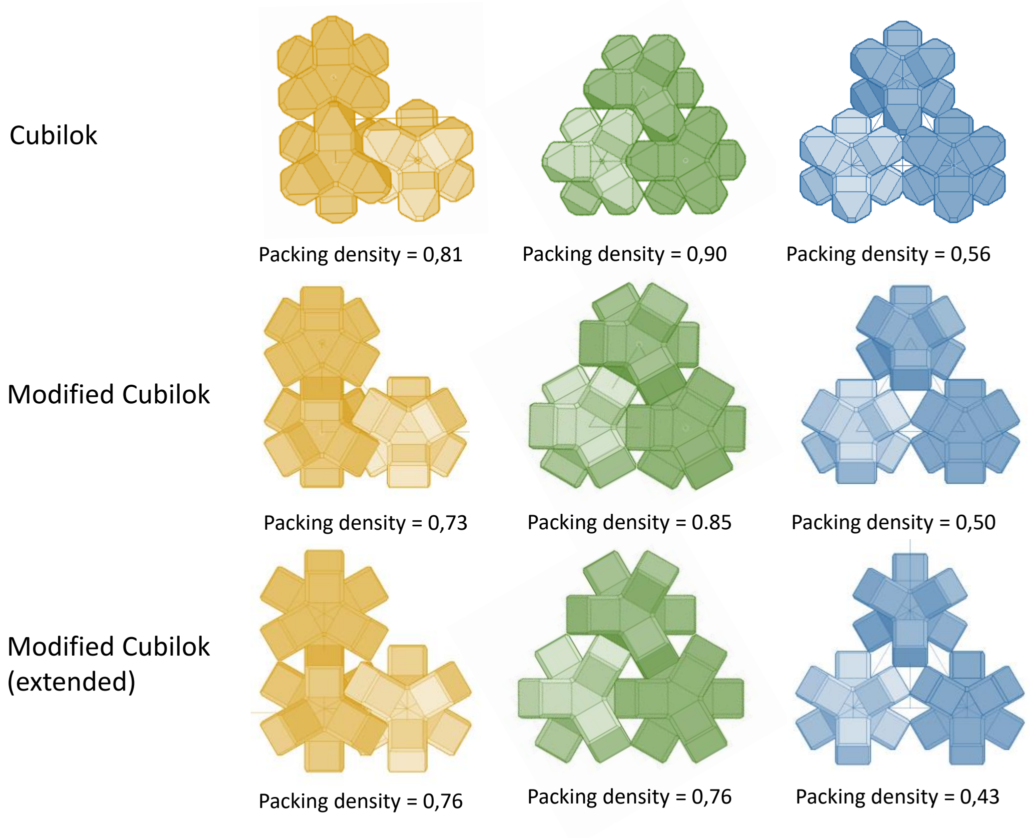

Figure 3-8: Packing densities for various Cubilok configurations.

3.2 Test program

Each test series comprises six tests with varying wave heights and a constant wave period. In order to make the test series identifiable, the following format indicated in the example was used for each test. As seen in the example, this slope corresponds to the first letter utilised in the example, and the number following the letter indicates the wave period used. The rest of the parameters define the test series and test number.

Example:

A1_01_001

A → Slope 1:4/3
1 → T_P =2.72 s

First test series

First test in test series

Test series C has a slight variation as the letter no longer indicates a slope change but rather a differentiation between the single- and double-layer testing. The labelling system used in the example was only valid for the test series included in the stability and overtopping analysis. Two test series were excluded from this analysis. These include the number of waves test series done at two specific packing densities at the beginning of the test schedule. This was done to determine an appropriate value for the number of waves and, thus, the duration of each test.

As the Cubilok was still in its developmental stage, the test schedule developed for this study aims to define unit characteristics. The effects of the various wave heights were analysed by grouping tests with the same wave periods.

Table 3-7: Test programme of the completed tests.

Test series	**Test No.**	**Ø**	**cotα**	**T_P (s)**	**H_i (m)**	**s_{op}**	**N_S**	**K_D**	**Number of waves**
N_63	1-8	0.63	1.33	1.545	0.140	0.038	3.80	41.1	500
N_65	9-22	0.65	1.33	1.545	0.140	0.038	3.80	41.1	500
A1	23-25	0.65	1.33	2.724	0.100-0.125	0.009-0.011	2.71-3.40	15.0-29.6	1000
A2_1	26-30	0.65	1.33	1.380	0.100-0.157	0.034-0.053	2.71-4.27	15.0-58.4	1000
A2_2	31-34	0.65	1.33	1.380	0.100-0.140	0.034-0.047	2.71-3.81	15.0-41.6	1000

Test series	Test No.	∅	cotα	T_P (s)	H_i (m)	s_{op}	N_S	K_D	Number of waves
A2_3	35-40	0.65	1.33	1.380	0.100-0.176	0.034-0.059	2.71-4.78	15.0-82.1	1000
A2_4	41-46	0.65	1.33	1.380	0.100-0.176	0.034-0.059	2.71-4.78	15.0-82.1	1000
A3	47-52	0.65	1.33	1.731	0.100-0.176	0.021-0.038	2.71-4.78	15.0-82.1	1000
B1	53-55	0.65	1.5	2.724	0.100-0.125	0.009-0.011	2.71-3.40	13.3-26.3	1000
B2_1	56-61	0.65	1.5	1.380	0.100-0.176	0.034-0.059	2.71-4.78	13.3-72.9	1000
B2_2	62-67	0.65	1.5	1.380	0.100-0.176	0.034-0.059	2.71-4.78	13.3-72.9	1000
B2_3	68-73	0.65	1.5	1.380	0.100-0.176	0.034-0.059	2.71-4.78	13.3-72.9	1000
B3_1	74-79	0.65	1.5	1.731	0.100-0.176	0.021-0.038	2.71-4.78	13.3-72.9	1000
B3_2	80-85	0.65	1.5	1.731	0.100-0.176	0.021-0.038	2.71-4.78	13.3-72.9	1000
C2_1	86-90	1.17	1.5	1.380	0.100-0.157	0.034-0.053	2.71-4.27	13.3-51.9	1000
C2_2	91-96	1.21	1.5	1.380	0.100-0.176	0.034-0.059	2.71-4.78	13.3-72.9	1000
C2_3	97-102	1.30	1.5	1.380	0.100-0.176	0.034-0.059	2.71-4.78	13.3-72.9	1000
D3_1	103-108	0.65	1.33	1.731	0.100-0.176	0.021-0.038	2.40-4.20	10.3-56.3	1000
D3_2	109-114	0.65	1.5	1.731	0.100-0.176	0.021-0.038	2.40-4.20	9.1-49.9	1000

3.3 Model checks and quality control

Various checks were completed before the start of each test series to ensure the equipment was in working order. These checks include ensuring water depth was at the correct level before the beginning of each test and ensuring the probe placement was correct according to the wave period. The probes were calibrated before each test series to ensure that they were in proper working condition (i.e., within a specified error margin) and then re-zeroed every few hours to ensure accurate readings. An excerpt of the data sheet generated using the probes may be found in Appendix C.

To ensure the photographs taken in the test series were comparable, the position and angle of the camera was consistent throughout the test series. This was achieved by correctly placing a tripod in a predetermined location, ensuring that it stayed consistent each time the camera was set up on an ongoing basis. The goal of this setup was to provide a fixed point of reference, ensuring that the camera arrangement remained uniform and unchanged throughout each test series.

Photographs were taken once the structure was constructed and after completing each test. Once the test was completed, the overtopping volumes were measured and recorded. Once the test series was complete for the day, the instrumentation and equipment were removed or switched off, and the data generated from the test series was transferred. These checks were repeated for each test series.

4 RESULTS AND OBSERVATIONS

4.1 Test summary

The 2D physical model testing conducted of the Cubilok was performed in the flume at the CSIR. The entire test schedule includes sixteen single-layer and three double-layer test series. For each test series, the wave period and water level remain constant. The wave height was increased by 12% for each condition. The test was concluded once either all six conditions were completed or when the armour layer had taken significant damage. Once a test was finished, the armour units were removed, and the underlayer and armour layer were rebuilt. The test summary shown in Table 4-1 is based on the actual number of tests conducted with the wave steepness values indicated for each test run.

Table 4-1: Summary of tests conducted indicating wave steepness values.

Test series	Test Run 1	Test Run 2	Test Run 3	Test Run 4	Test Run 5	Test Run 6
A1_1	0.009	0.010	0.011	0.012	0.014	0.015
A2_1	0.034	0.038	0.042	0.047	0.053	0.059
A2_2	0.034	0.038	0.042	0.047	0.053	0.059
A2_3	0.034	0.038	0.042	0.047	0.053	0.059
A2_4	0.034	0.038	0.042	0.047	0.053	0.059
A3_1	0.021	0.024	0.027	0.030	0.034	0.038
B1_1	0.009	0.010	0.011	0.012	0.014	0.015
B2_1	0.034	0.038	0.042	0.047	0.053	0.059
B2_2	0.034	0.038	0.042	0.047	0.053	0.059
B2_3	0.034	0.038	0.042	0.047	0.053	0.059
B3_1	0.021	0.024	0.027	0.030	0.034	0.038
B3_2	0.021	0.024	0.027	0.030	0.034	0.038
C2_1	0.034	0.038	0.042	0.047	0.053	0.059
C2_2	0.034	0.038	0.042	0.047	0.053	0.059
C2_3	0.034	0.038	0.042	0.047	0.053	0.059
D3_1	0.019	0.022	0.025	0.030	0.020	0.024
D3_2	0.019	0.023	0.025	0.017	0.021	0.025

Test run completed	Test run stopped	Test run not performed

4.2 Wave conditions

In this section, an in-depth examination of the wave conditions is conducted, comprising key variables such as incidence wave height, wave period, and wave number.

4.2.1 Incident wave height

The calibration was completed before the structure was constructed within the flume. The procedure for calibration was completed by varying the input parameters, specifically the gain setting, for each wave height and period to ensure they fall within an error margin of ±3%. In this study, all the wave heights and periods were calibrated at the toe of the structure.

The wave height extracted from data sheets represents the total wave height, including the incident and reflected wave heights. The incident wave height was used in the stability and overtopping analysis. Equation 34 was used to determine the incident wave height (Mansard & Funke, 1980).

$$H_i = H_{m0} * \sqrt{\frac{1}{1 + {K_r}^2}} \tag{34}$$

where:

H_i	=	Incident wave height	m
H_{m0}	=	Significant wave height calculated from the spectrum $(H_i + H_r)$	m
K_r	=	Reflection coefficient	-

The graph in Figure 4-1 indicates the variability concerning the measured results compared to the target incident wave height. The calibrated results, which were measured without the structure in place, were within an error margin of ±3% of the target values. The variability in results could be due to several factors, including but not limited to structural variations, probe placement, and human errors.

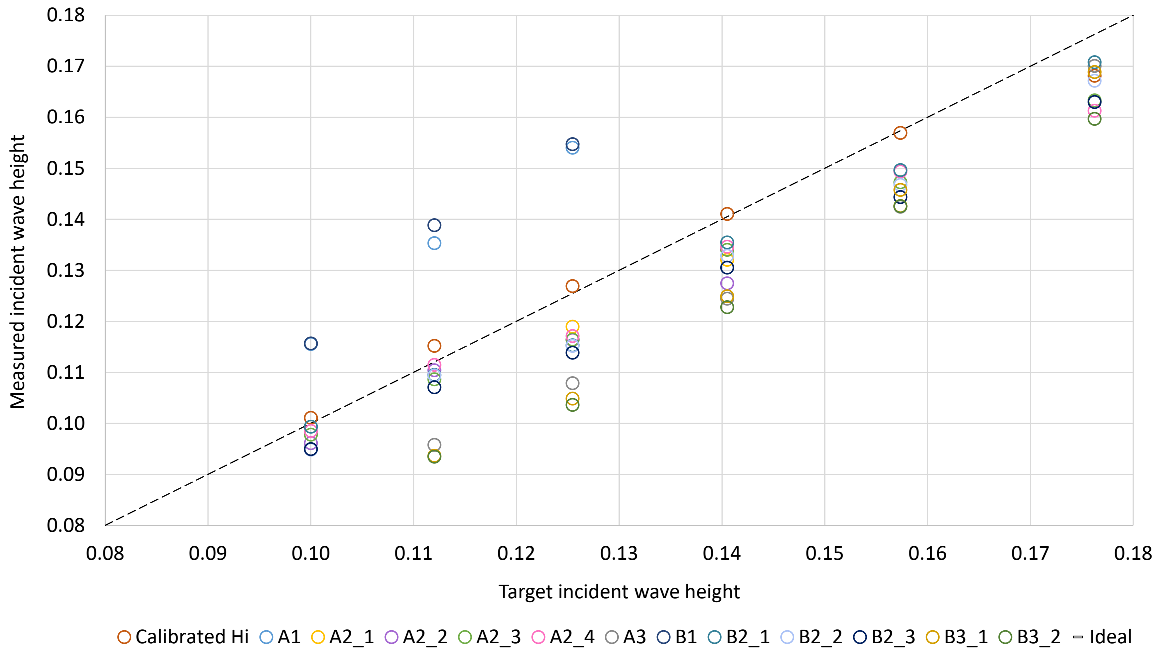

Figure 4-1: Target versus measured incident wave heights.

4.2.2 Wave period

The spectral wave period, $T_{m-1,0}$, is suitable for all types of wave spectra (such as bimodal and multi-peaked wave spectra) as it lends more weight to waves with longer durations in the wave spectrum. The peak wave period, T_P, was not suitable for all types of spectra and may result in significant inaccuracies if used. A clear relationship, shown in Equation 35, between the spectral and peak wave period may be defined when considering a singular peak wave spectrum (EurOtop, 2018).

$$T_P = 1.1T_{m-1,0} \tag{35}$$

The spectral period, $T_{m-1,0}$, is used for several wave run-up and overtopping calculations, as it lends greater weight to the longer wave periods in the spectrum and produces identical wave run-up or overtopping for the same values of Tm-1,0, and wave heights irrespective of the spectrum type. Therefore, wave run-up and overtopping for bimodal and 'flattened' spectra can be predicted without the use of more complex procedures (EurOtop, 2018).

For the experimental tests conducted, a set of four distinct wave periods was selected, as detailed in Table 4-2.

Table 4-2: Wave period and steepness ranges tested.

Peak wave period (s)	Test series	Wave steepness ranges (s_{op})
1.38	A2_1 – A2_4 B2_1 – B2_3 C1 – C3	0.034 – 0.059
1.55	N_0.63, N_0.65	0.038
1.73	A3, B3_1, B3_2	0.021 – 0.038
2.72	A1, B1	0.009 – 0.011

4.2.3 Number of waves

This section contains an analysis of the number of waves test series to determine a suitable number of waves. Figure 4-2 shows the results for the damage progression according to the number of units displaced. The tests run in 500 wave increments until structural failure or an equilibrium state was achieved. The selection of the wave condition for the Number of Waves test series included a wave height of 0.140 m and a wave period of 1.55 s, as these values served as effective representations of average wave conditions.

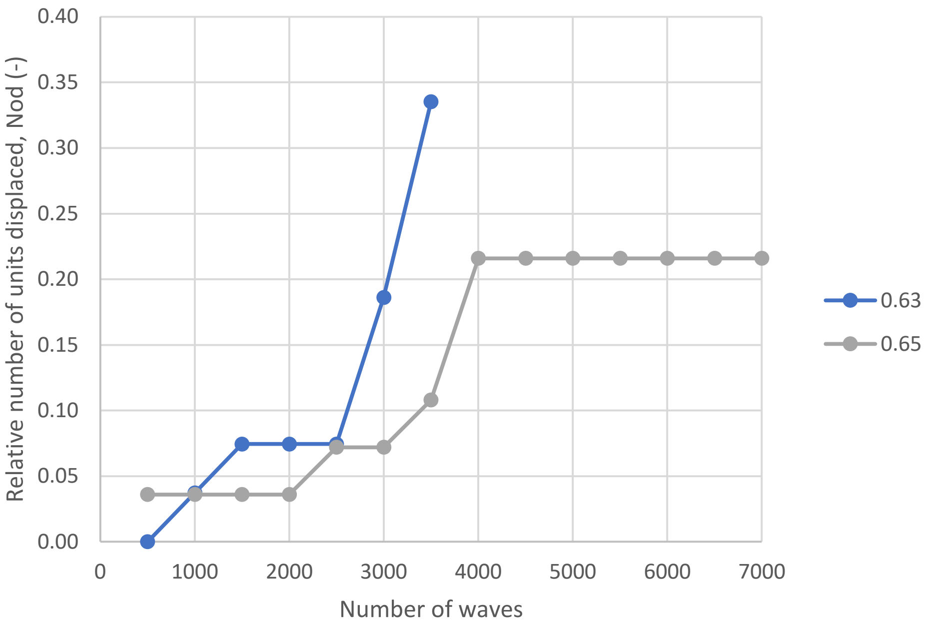

Figure 4-2: Damage progression.

The damage progression for the 0.63 packing density increases linearly until 1500 waves; the structure then stabilises briefly until 2500 waves, followed by a further linear increase until structural failure around 3500 waves. The damage progression for the 0.65 packing density maintains a constant damage number for the first 2000 waves, followed by a rapid increase in damage until the structure reaches an equilibrium state at 4000 waves. The figure above includes the relative number of displacements. In contrast, the graph in Section 5.2 includes the cumulative settlements and displacements for each test run, providing a more detailed description of the damage progression.

The damage progression for the number of waves test series at a packing density of 0.63 and 0.65 is provided in Figure 4-3 and Figure 4-4, respectively.

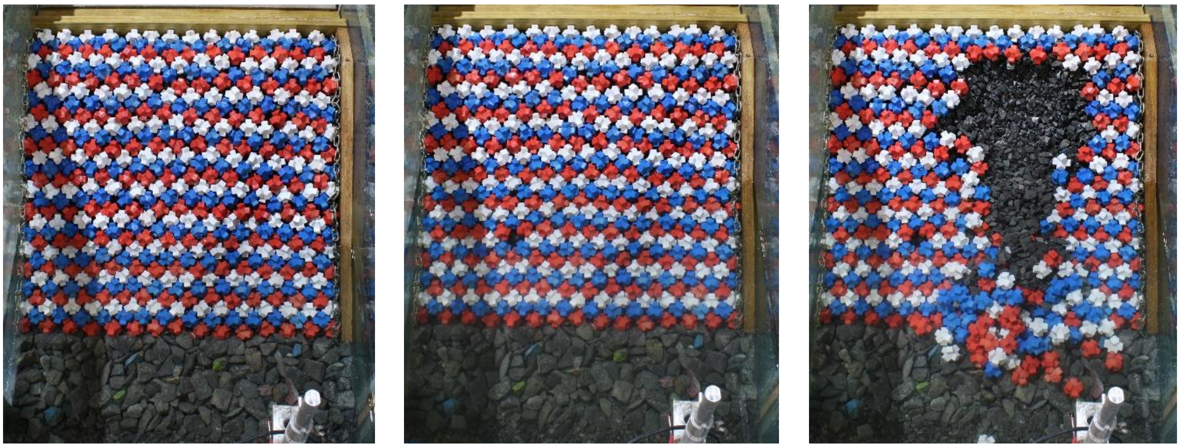

No Damage (N=500 waves) *Start of damage (N=1000 waves)* *Failure (N=3500 waves)*

Figure 4-3: Damage progression for Test Series N_0.63.

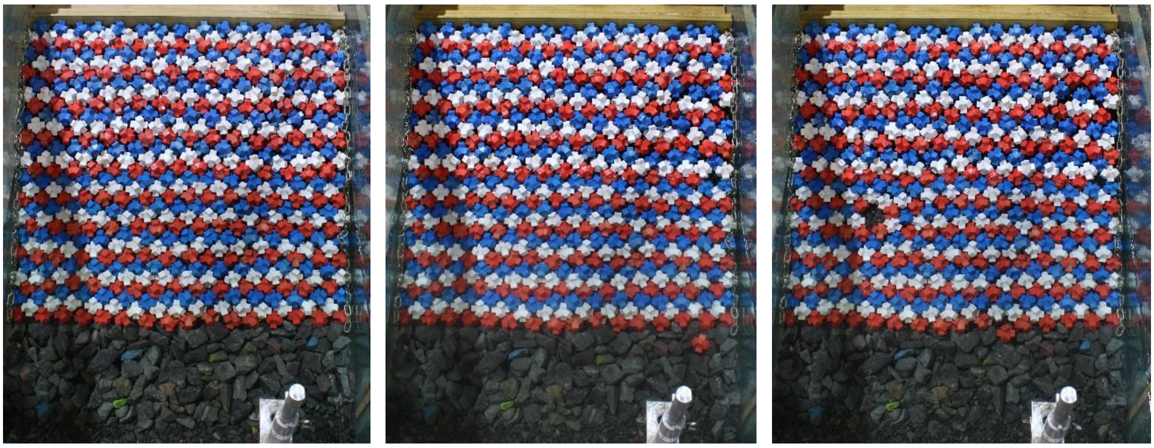

No Damage (N=0 waves) *Start of damage (N=500 waves)* *Equilibrium (N=4000 waves)*

Figure 4-4: Damage progression for Test Series N_0.65.

The start of damage occurs first in the 0.65 packing density, followed by a state of equilibrium; however, the start of damage occurs later in the 0.63 packing density, with the structure subsequently failing. It was evident that the performance of the 0.65 packing density significantly improved the stability of the slope compared to the 0.63 packing density. For this reason, the denser packing of 0.65 was selected for the tests conducted in a single layer.

It was decided to conduct the tests in this investigation using 1000 waves per test considering that 1000 waves were utilised in earlier studies for Accropode (DHL, 1987) and Xbloc (DMC, 2003b). The damage sustained remained consistent between 1000 – 2000 waves, this contributed to the decision to proceed with the selection of 1000 waves per test. It should be noted that the damage progression accelerates beyond 2000 waves, implying that greater structural deterioration should be expected.

It is crucial to acknowledge that these results may vary under different wave conditions, and the progression of damage could be further investigated for both higher and lower wave conditions in future testing. However, it was not included in this study due to time constraints.

4.3 Observations throughout testing

The settling of the slope is attributed to continuous wave exposure, leading to a denser packing near the waterline and decreased density above, particularly at the juncture between the slope and the crest. The types of failure observed during testing included progressive failure (start of damage and failure in one test run) due to gradual settlement or failure that occurs over several test runs. The latter occurred when one or more units were dislodged from the slope, and the surrounding units settled to fill the gaps, leading to instability in the regions where the units were extracted. An alternate result was observed, wherein the extraction of a unit led to the surrounding units filling the gap, all while preserving the structural integrity of the slope.

4.3.1 Single-layer test series

Table 4-3 and Table 4-4 summarizes the damage observations for Test A and B, respectively. The tables identify the start of damage as the first extraction from the slope, and failure occurs when a significant portion of the underlayer is exposed. These two series aim to determine the unit's stability at a slope of 1:1.5 and 1:1.33.

Table 4-3: Summary of Test Series A observations.

Test series	Observations
A1	During the third test, two units dislodged below the waterline, which led to the settlement, followed by complete structural failure 97% into the third test.

A2_1	The slope experienced significant settlement during the fourth test run, followed by structural failure along the structure edge 62% into the fifth test.
A2_2	Settlement occurred during the second test run, which led to the extraction of three units, followed by six units extracted from the same region during the third test, ultimately leading to structural failure 40% into the fourth test.
A2_3	During the fourth test, the first extraction occurred along the edge (which may indicate a model effect) and the second just below the waterline. These extractions led to further extractions in the same region and ultimately resulting in structural failure 44% into the sixth test.
A2_4	During the fifth test, the accumulated settlement led to the dislodgement of two units below the water line, followed by structural failure 52% into the sixth test.
A3	The gradual settlement throughout the first four test runs led to the first unit extraction in the fifth test, followed by eight extractions in the final test run.

Table 4-4: Summary of Test Series B observations.

Test series	Observations
B1	A significant amount of settlement was observed during the second run which led to rapid failure at the end of the third test.
B2_1	The continual settlement observed throughout testing ultimately led to the extraction of three units below the waterline at the end of the sixth test.
B2_2	The first unit extraction occurred during test three followed by separate extractions during test four, and five further extractions in the same region during test five. The extraction of the units in the same region led to the failure of the structure 60% into the sixth test.
B2_3	Settlement occurred along the glass wall which led to the extraction of ten units during test five and failure 20% into the sixth test.
B3_1	One unit was dislodged during test three, four, and five as a result of continuous settlement which led to the failure that occurred 80% into the sixth test.

B3_2	The gradual settlement of the slope led to the extraction of one unit in test three, two units during test four, three units during test five, which subsequently led to the failure of the structure 30% into the sixth test.

4.3.2 Double-layer test series

The aim was to determine an optimum packing density and whether the unit would be viable when placed in a double layer. To accomplish this, various packing densities were considered and then analysed. Three test series were all conducted at a slope of 1:1.5 and were constructed with varying packing densities. In the first series, Series C2_1, the slope was constructed with a packing density of $\emptyset = 1.17$, corresponding to a double layer of cubes (see Appendix A) and increased for the subsequent test series. The same wave conditions as test series A2 and B2 were used for the double-layer testing to ensure that the single- and double-layer results are comparable.

Figure 4-5 illustrates the damage accumulated after the fifth test run was concluded. In test series C2_1, structural failure occurred at the 95% mark during the fifth test run, whereas in Test series C2_2 and C2_3, only the outer armour layer experienced failure after the fifth test run. This suggests that the less dense armour packing of Ø = 1.17 was the least suitable for the Cubilok unit.

Test Series C2_1 (Ø = 1.17) Test Series C2_2 (Ø = 1.21) Test Series C2_3 (Ø = 1.30)

After test run 5 *After test run 5* *After test run 5*

Figure 4-5: Test Series C2 after test run 5.

Table 4-5 provides a summary of the packing densities employed and the corresponding damage observations documented during each test series conducted for the double layer.

Table 4-5: Summary of Test Series C observations.

Test series	Packing density	Observations
C2_1	1.17	Excessive settlement was observed in the settlement test, followed by a complete failure of the outer layer after the fourth test condition and failure of the structure after the fifth test condition.
C2_2	1.21	The packing density was increased in an attempt to limit the settlement. The second test series performed better than Series C2_1, and only the outer layer failed by the end of the sixth condition.
C2_3	1.3	This test series used a packing density of 1.3 (2 x single-layer packing density of $\emptyset = 0.65$). This allows for a direct comparison between the single and double layers. The first layer failed after the 5th test run, and structural failure after the sixth test run.

The results indicated no significant advantage when using the double layer over the single layer. Furthermore, increasing the packing density does not equate to a better result, thus concluding the double layer testing.

4.3.3 Unit extraction

During testing, the units often exhibited similar movements before their eventual extraction from the slope. Figure 4-6 illustrates the process of unit extraction from the slope.

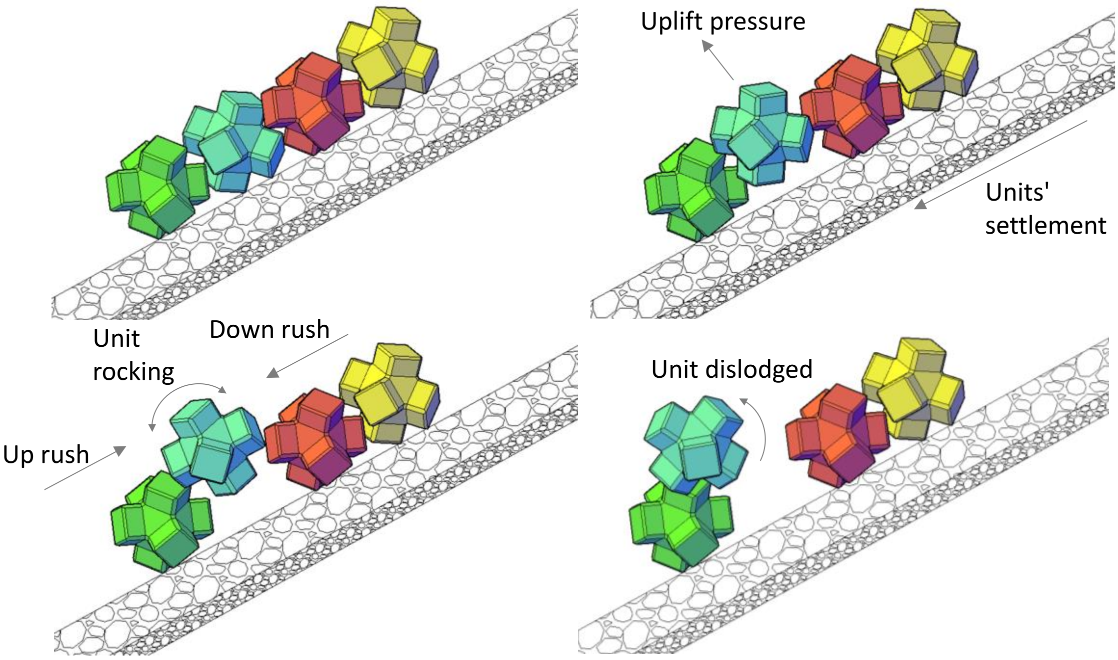

Figure 4-6: Failure mechanism identified for Cubilok.

Figure 4-7 provides examples of unit extraction that occurred during testing. It is worth noting that while rocking suggests potential unit extraction, it has occasionally resulted in the unit eventually settling into a stable position. The units are labelled in the photographs to clarify when referring to specific units (e.g., C refers to the same unit from the side and top views).

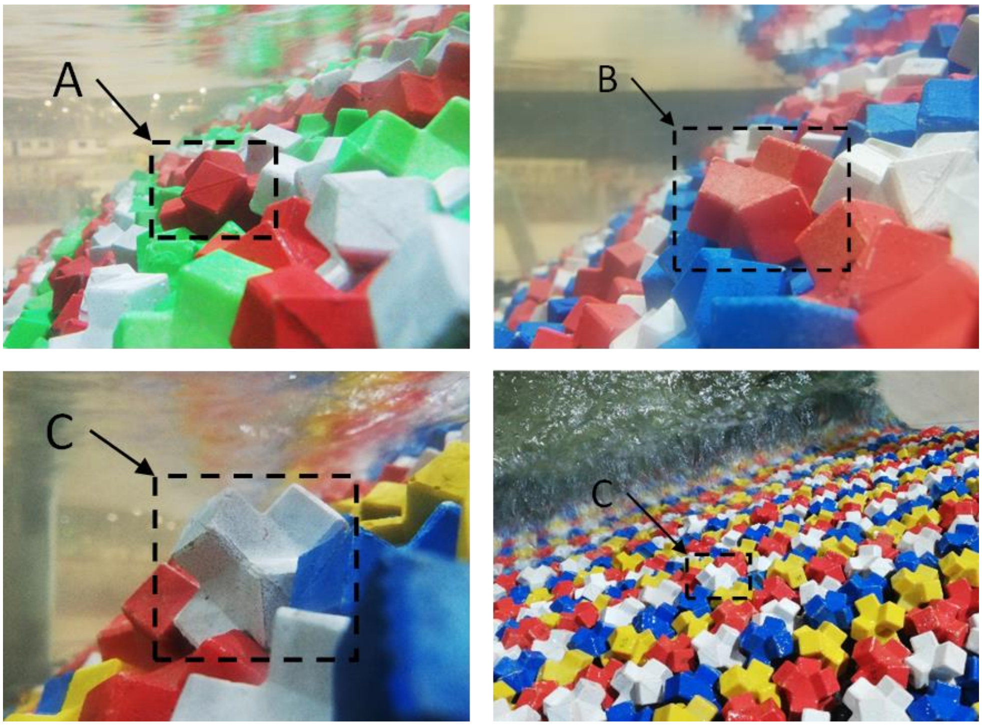

Figure 4-7: Examples of unit extraction in progress.

The total number of units extracted from the slope during test series A and B are indicated in Figure 4-8 and Figure 4-9, respectively.

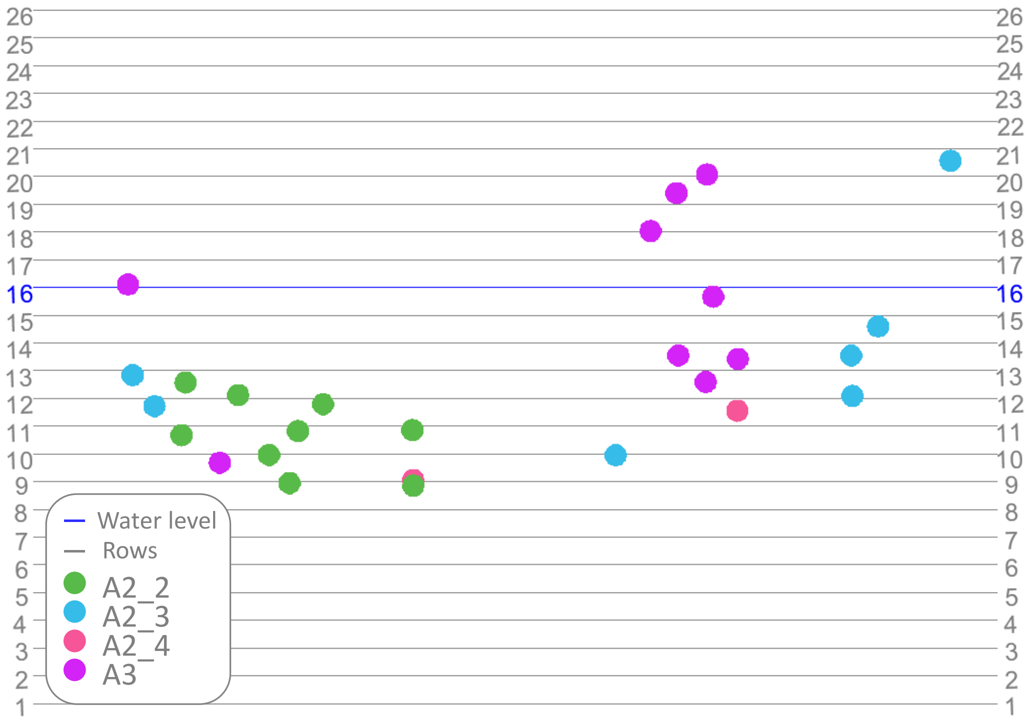

Figure 4-8: Units extracted during A-Series.

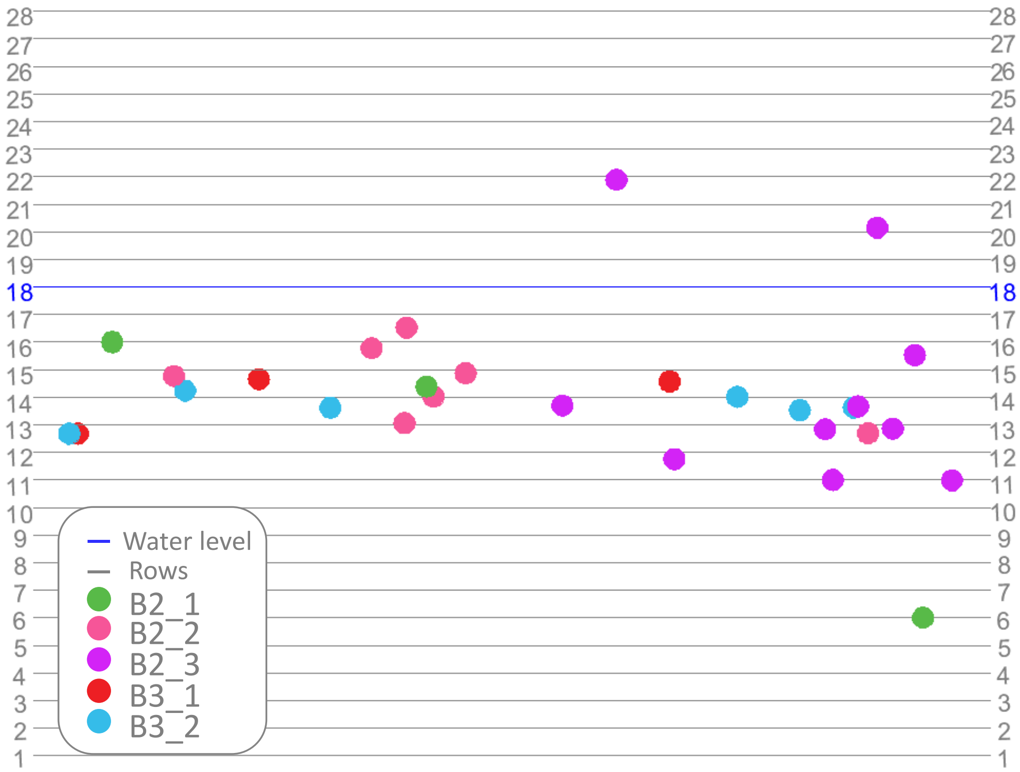

Figure 4-9: Units extracted during B-Series.

As illustrated in Figure 4-8 and Figure 4-9, the units extracted were mainly below the water line, with about 10% accounting for extractions occurring above the water line. The extractions were recorded during each test, with the number of units extracted per test varying significantly with respect to the wave condition and slope angle. It was qualitatively observed that the wave attack was most severe at the water line, coinciding with the start of damage (i.e., first unit extractions), which correlates with the depiction in the figure of the units extracted during testing.

A new configuration, which has not yet been tested, was suggested to increase the interlocking capability by extending the protuberance suggested in the previous tests conducted on the original unit shape (Wehlitz, 2020), as shown in Figure 4-10.

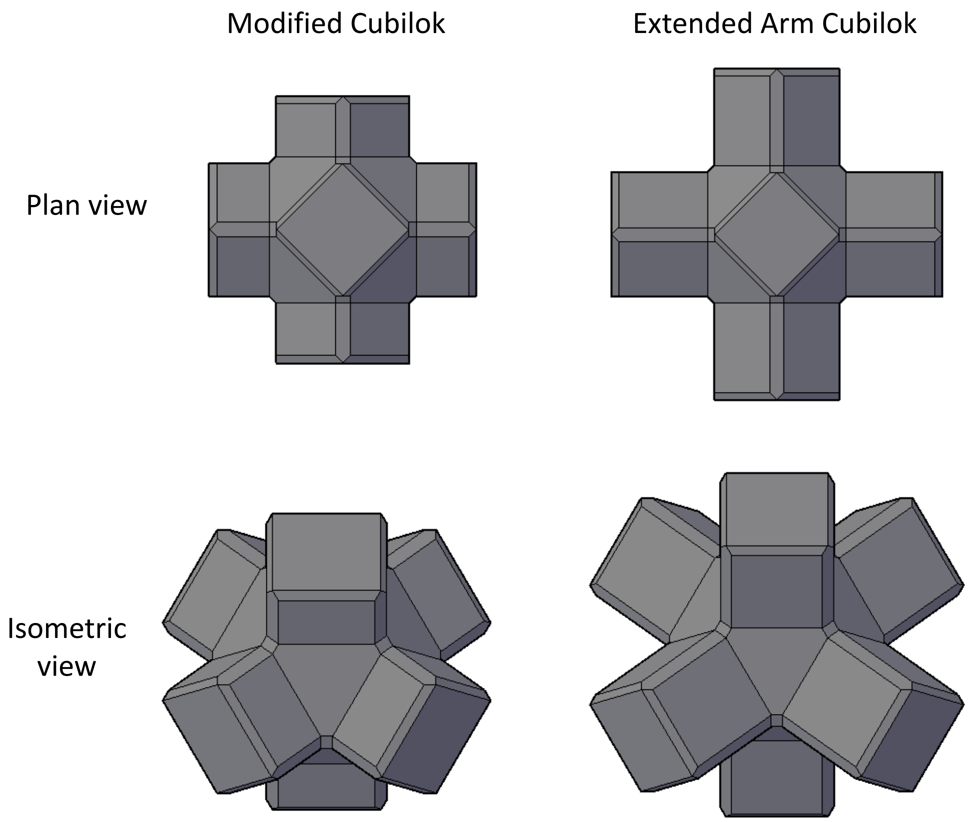

Figure 4-10: Plan and Isometric views of the proposed shape modifications.

5 HYDRAULIC STABILITY ANALYSIS

5.1 Repeatability of tests

The incremental increase of the total and incident wave height for the A2-Series, which was characterised by a slope of 1:1.33 and a wave period of 1.38 seconds, is illustrated in Figure 5-1. As seen in the graphs, the total wave height trendlines (dashed lines) run parallel to the calibrated values (the total wave height without the structure present), whereas the trendlines of the incident wave heights diverge with increasing wave heights. This indicates larger reflected waves with increasing wave heights.

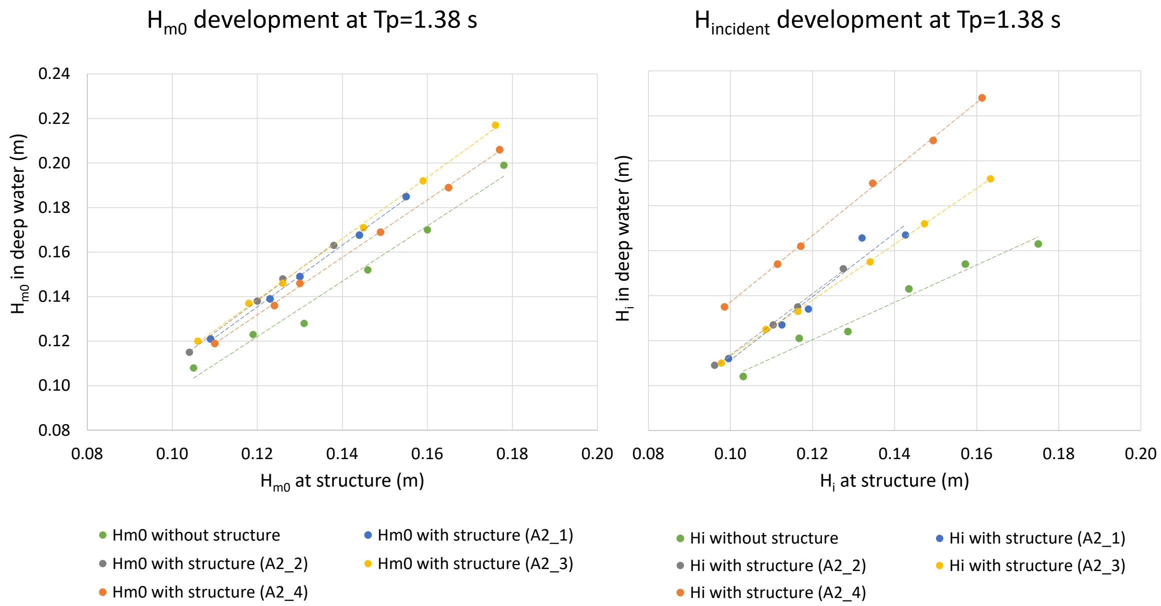

Figure 5-1: Comparison between the total and incident wave height.

The graph in Figure 5-2 illustrates the damage variability with respect to the stability for the A2-Series. An indication of the failure points was provided with respect to the relative number of displacements.

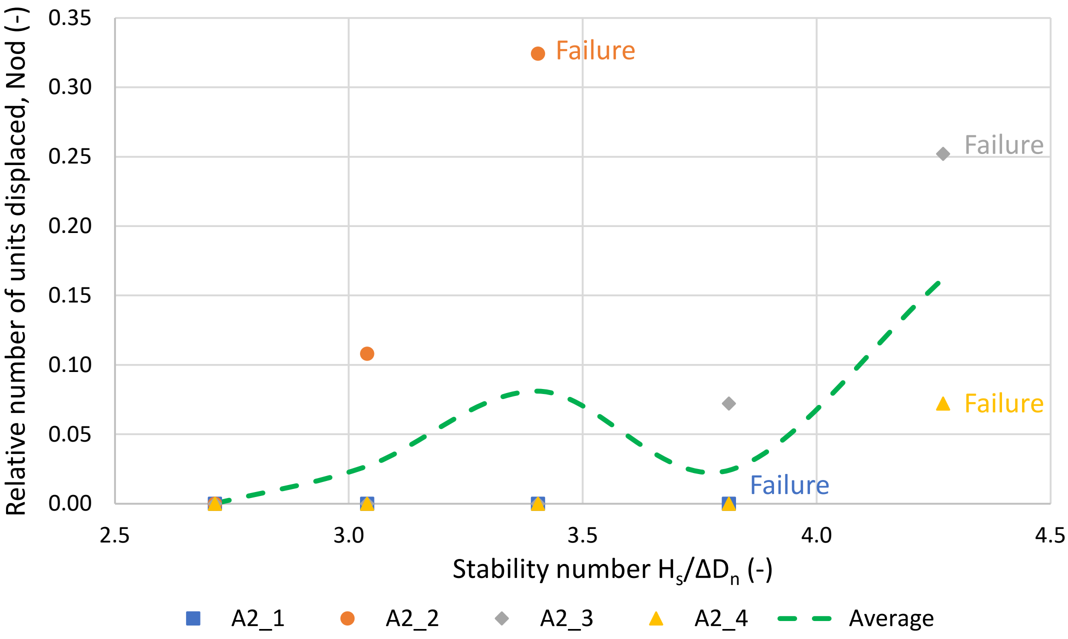

Figure 5-2: Damage progression for test series A2.

Figure 5-3 illustrates the damage accumulated after the fourth test run was concluded. Test A2_02 was terminated after 9 minutes, equating to roughly 40% of the test duration. After the fourth test run, the state of the slope was very similar for three of the four test series performed for this wave condition, as seen in the photographs. Initially, three tests were performed for test series A2; however, the wide range of results prompted the execution of an additional test series (A2_4) to validate the results employing the same wave conditions.

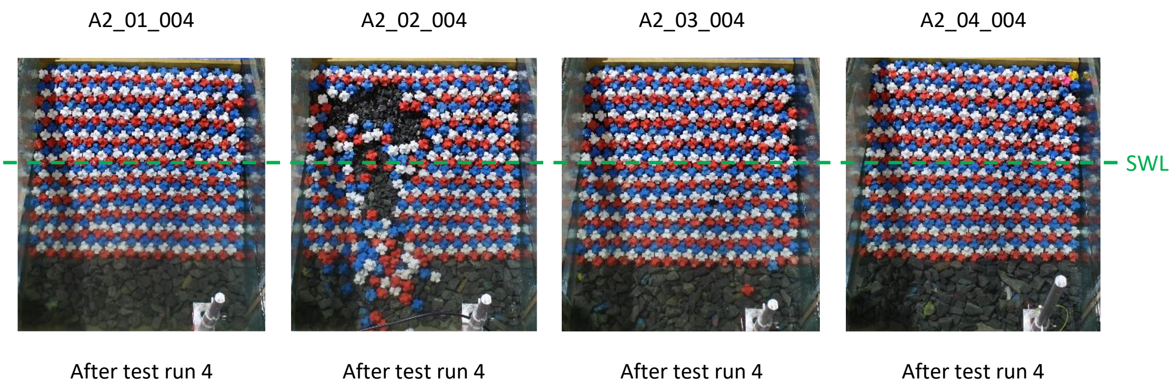

Figure 5-3: Slope damage after test 4 for Test series A2.

Figure 5-4 illustrates the damage progression observed in each test series within the B2 series.

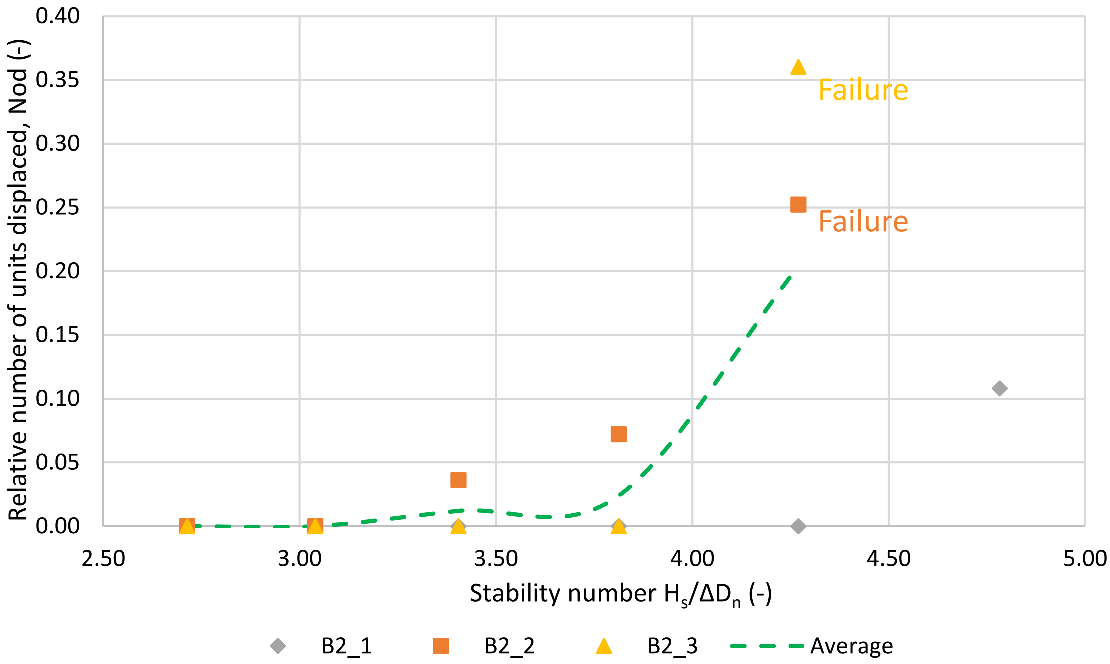

Figure 5-4: Damage progression for test series B2.

The damage progression for test series B2, illustrated in Figure 5-5, follows a similar trend throughout the repeated tests. The damage occurs suddenly in the final test run with the exception of test B2_2, where the level of damage continuously increases (as indicated in Figure 5-4).

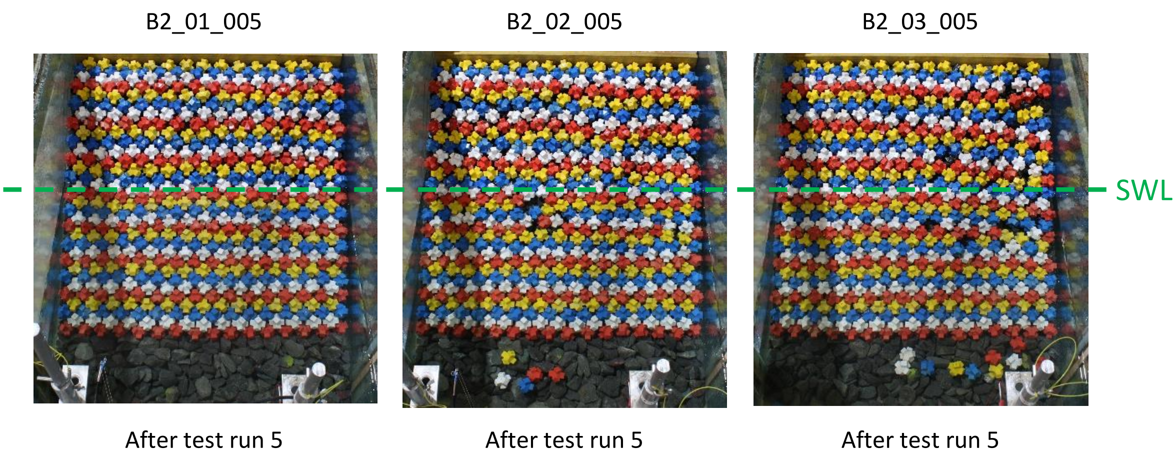

Figure 5-5: Slope damage after test 5 for Test series B2.

The results of the repeatability tests highlight the significance of variability in conducting physical model studies.

5.2 Damage by movement

The graph in Figure 5-6 illustrates the incremental settlement for the duration of the test series. The settlement percentage (described by Equation 36) was calculated by dividing the sum of the number of movements, which were categorised as ratios of D_n indicated on the graph, by the total number of units on a given slope.

$$S_{\%} = \frac{Sum\ of\ movements\ as\ a\ ratio\ of\ Dn}{Total\ number\ of\ units\ on\ slope} \tag{36}$$

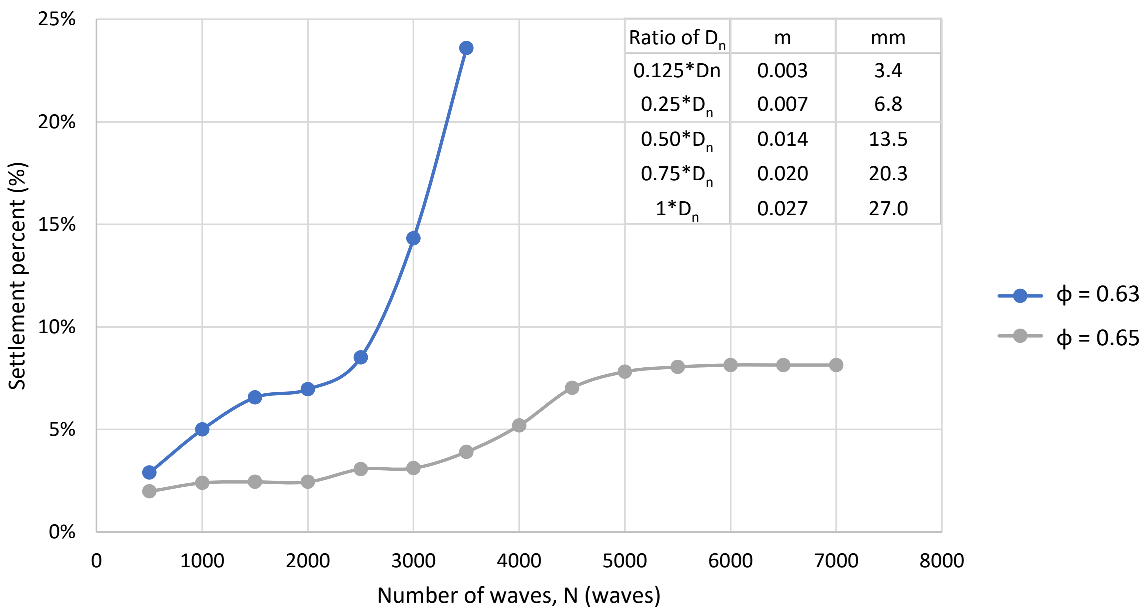

Figure 5-6: Settlement over time.

The graph depicts settlement at packing densities of 0.63 and 0.65. The 0.63 packing density's settling increased continually until failure. The settlement for the 0.65 packing density follows an alternate trend, with minimal settlement until approximately 3000 waves, followed by an increase until roughly 5000 waves, where the slope reaches equilibrium. The graph demonstrates a notable reduction in settlement with a marginal increase in packing density. Specifically, for an approximate 7% increase in the total number of units used on the slope, there is the potential to achieve an approximately eight times lower settlement. This implies that the increased packing density substantially improved the settlement experienced by the unit.

5.3 Damage progression

The level of damage was divided into three categories, as indicated in Table 5-1. The first units dislodging from the slope describe the start of damage. Additionally, failure is described by the deterioration of the armour layer to the extent that the underlayer becomes exposed. Assume progressive failure (the first displacement and total structural failure within one test run) has occurred where no start has been indicated for the damage value.

Table 5-1: Stability numbers for the single-layer tests

Test Series	No Damage	Start of Damage	Failure	% damage between the start of damage and failure (ΔH_S)
	Stability number, $N_S = H_S/\Delta D_n$			
A1	3.67	-	4.18	-
A2_1	3.58	-	3.87	-
A2_2	2.61	3.00	3.46	15%
A2_3	3.16	3.64*	4.43	22%
A2_4	3.65	4.05	4.38	8%
A3	3.38	3.87	No Failure (Max value = 4.62)	No failure
B1	3.77	-	4.20	-
B2_1	4.06	4.64	No Failure (Max value = 4.64)	No failure
B2_2	2.97	3.13	4.54	45%
B2_3	3.54	3.92	4.42	13%
B3_1	2.54	2.85	4.58	61%
B3_2	2.04	2.54	4.33	71%

* Start of damage on flume wall (boundary effect)

The parameter, ΔH_S, describes the increase in wave height from the first unit extraction to the ultimate failure of the structure. The wave height increases by 12% for each consecutive test until the sixth condition or failure of the structure. In test series B3, the margin between the start of damage and failure was significantly greater than in the other tests, indicating that the structure retained its damaged state for an extended duration before failure.

As illustrated in Figure 5-7 and Figure 5-8, all the test series eventually failed except for Series A3 and B2_1. The relative damage number, which was described by the number of units displaced, provides a good indication of the unit's potential performance under a certain wave condition at a specific slope. The relative damage number progressed rapidly from the start of the damage until failure for the slope of 1:1.33. The slope of 1:1.5, on the other hand, retains its damaged state from the initial displacement before eventually failing. At each data point, wave steepness is indicated, while the test series name is displayed at the final data point before failure occurs.

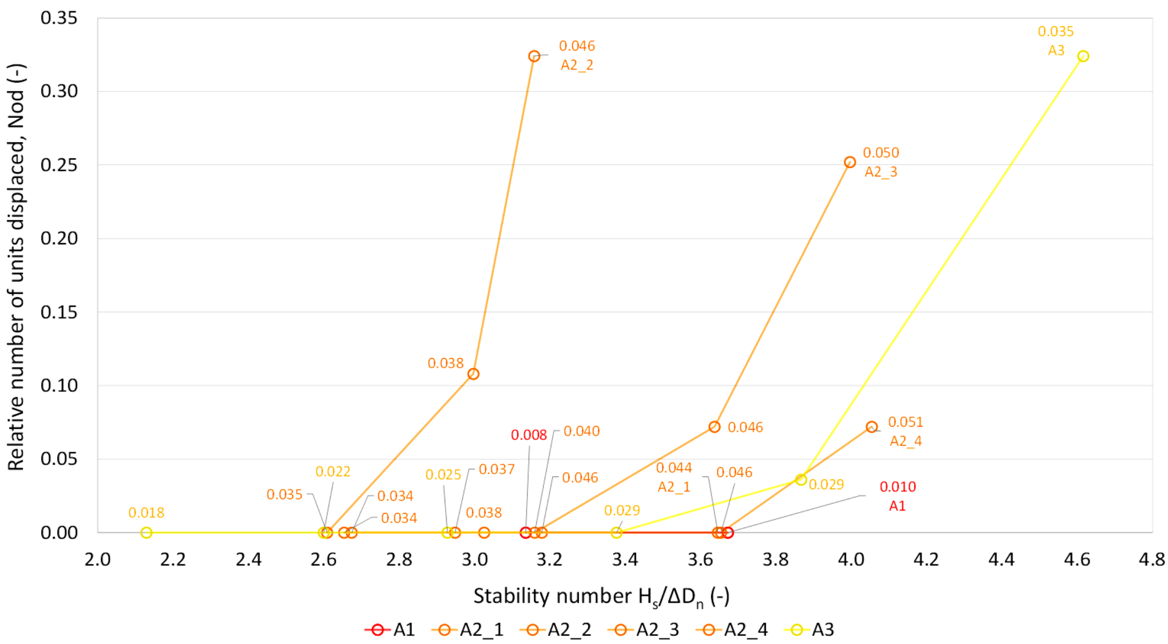

Figure 5-7: Relative damage number as a function of the stability for A-Series (Slope of 1:1.33).

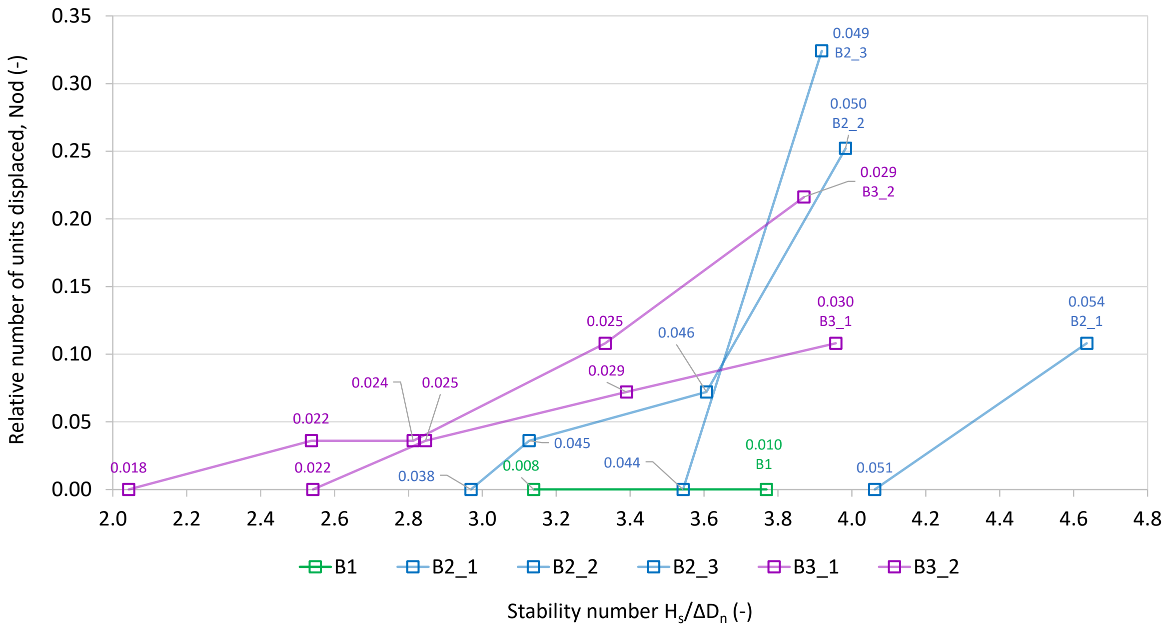

Figure 5-8: Relative damage number as a function of the stability for B-Series (Slope of 1:1.5).

The variability in results was far more apparent for the milder slope than for the steeper slope. The stability number (N_S) for no damage for the A-Series was roughly 3.4, whereas N_S ranges from 2 to 2.5 for the B-Series. In test series A3 and B3, the onset of damage for the identical wave condition was roughly 3.8 for Series A and ranges from 2.5 to 2.8 for Series B. When designing a breakwater with a single-layer unit, the no-damage value becomes critical as any displacement would expose the underlayer to wave attack. The graph illustrates that the steeper slope can withstand greater wave heights without undergoing damage, highlighting the influence of the slope on the unit's performance.

Figure 5-9 illustrates several degrees of damage, including no damage, the start of damage, and failure. The value surrounding each data point represents the wave steepness for the specific test.

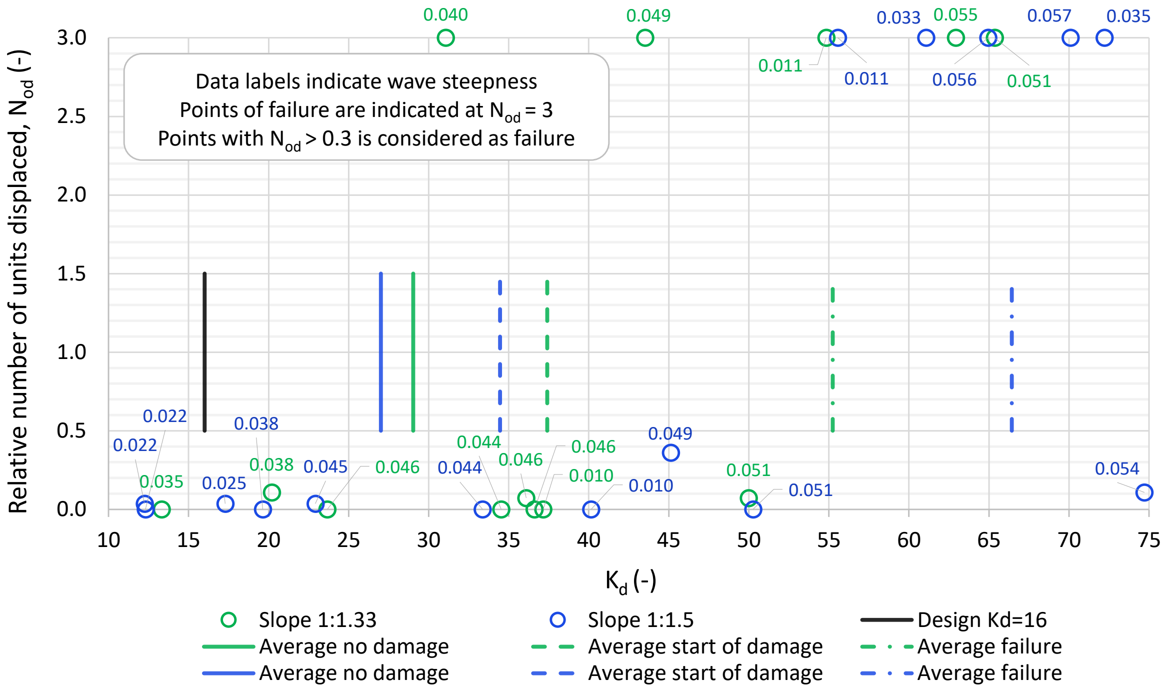

Figure 5-9: Damage as a function of K_d for Test Series A (1:1.33) and B (1:1.5).

Table 5-2 provides descriptive statistics for the stability parameter, K_d, including the minimum, average, maximum, and standard deviation. The table also summarises the percentage of values that fall within one standard deviation away from the average. This parameter is useful for describing the variability in the dataset.

Table 5-2: Data analysis of stability parameter, K_d.

Description	Test Series A (1:1.33)			Test Series B (1:1.5)		
Stability parameter, K_d	No damage	Start of damage	Failure	No damage	Start of damage	Failure
Minimum	13	20	31	6	12	56
Average	29	37	55	27	34	66
Maximum	37	50	74	50	75	75
STDEV	8	11	14	16	23	7
Percentage within 1 * STDEV	83%	50%	67%	67%	80%	67%

Considering the steeper slope, a sufficiently high confidence interval was achieved when the structure had taken no damage, indicating that the majority of the stability numbers fall within plus/minus one standard deviation from the mean. In contrast, a confidence interval of 50% was obtained at the onset of damage, signifying the substantial variability within this parameter. Consequently, the value of one standard deviation below the mean was deemed an unreliable representation of this parameter. Furthermore, the percentage achieved at failure also indicates that one standard deviation below the average is not a reliable value.

For the milder slope, a high confidence interval was attained at the onset of damage, indicating that data within one standard deviation of the average were considered reliable. The result that has been attained at no damage and failure displays a certain level of confidence; however, it was deemed unreliable. It is crucial to emphasize that the reliability of statistical parameters depends on the quality of the dataset from which they are derived.

5.4 Effect of wave period

The stability of the armour layer was tested with a peak wave period ranging from T_P = 1.38 – 2.72 seconds. The relationship between the relative number of units displaced and the wave period is described in Figure 5-10. At each data point, stability numbers are denoted by data labels, while solid fill represents points that have not yet experienced failure.

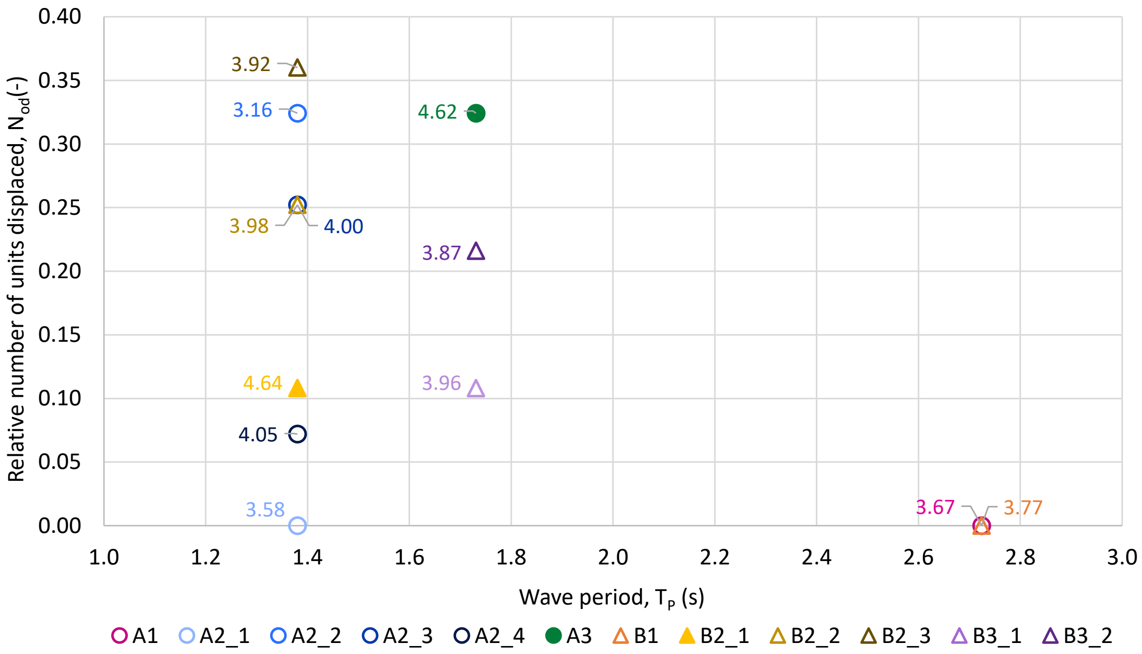

Figure 5-10: Effect of wave period.

The results show that test Series B2 sustains a larger damage number than Series A2 before reaching failure. In contrast, Series A3 outperformed Series B3, resulting in inconclusive data on the effect of the slope change. The third test run of test series A1 and B1 failed without preceding damage. The relative number of displaced units increased with decreasing wave periods (increasing wave steepness values), except for test series A3 and B2_1, which did not experience failure by the final test run. Additionally, the stability number exhibited an increase with rising wave steepness values, with the exception of test series A2_2. This indicates that the unit has a greater capacity to withstand damage before reaching failure when exposed to higher wave steepness values. In practical application, longer wave periods would necessitate the use of larger concrete armour units due to the lower stability achieved for these conditions. Further testing would be required to make any conclusive statements regarding the effect of the wave period.

5.5 Effect of surf similarity parameter

The surf similarity parameter, or Iribarren parameter, in relation to the stability number, is indicated in Figure 5-11. The stability number as a function of the Iribarren parameter is represented at the start of damage (SoD). The figure does not include test series that undergo progressive failure where the start of damage and failure occur within the same test. The variation of the Iribarren parameter was greater for series A2. The results from the figure indicate that, on average, the SoD stability for Series A2 was less than for Series B2. In contrast, Series A3 outperformed Series B3. Based on the inconsistency of the SoD results, the effect of the slope change has no conclusive impact on stability.

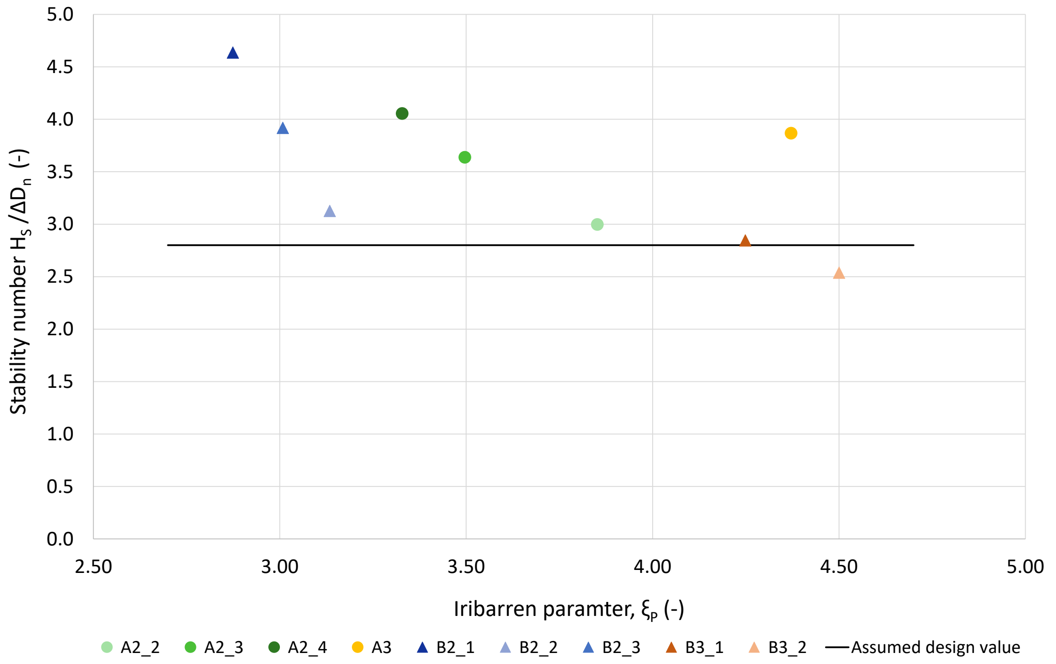

Figure 5-11: Start of damage - Iribarren parameter.

This stability number in relation to the Iribarren parameter was described at failure in Figure 5-12. The hollow shapes indicate the structures that have not yet reached failure at the end of the sixth condition.

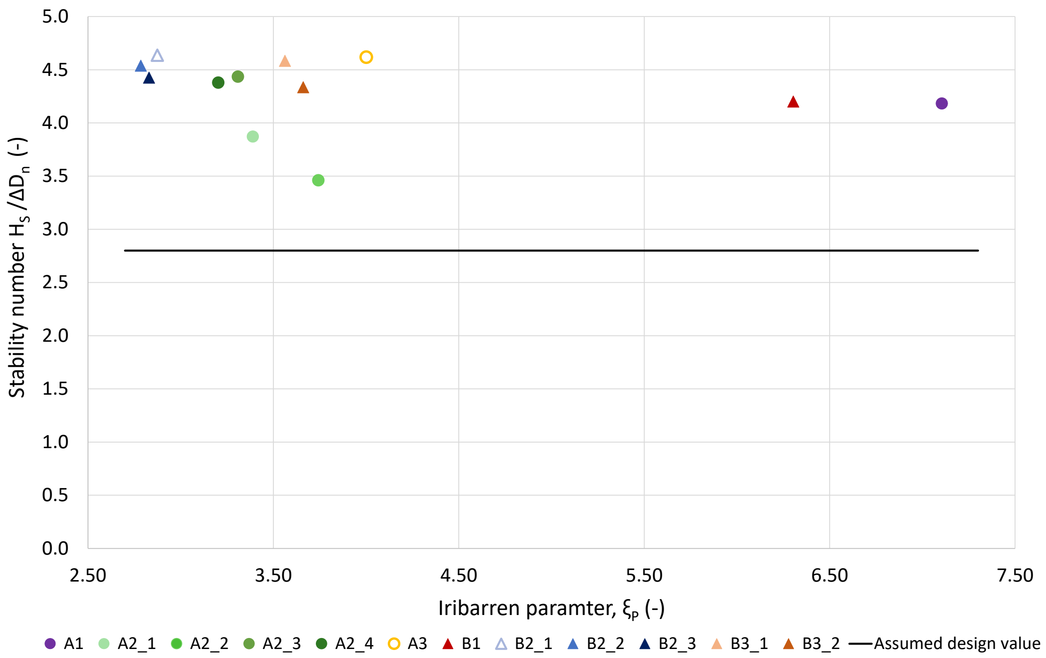

Figure 5-12: Failure - Iribarren parameter.

The graphic includes the progressive failures that occur in test series A1, B1 and A2_1. Considering the stability at failure, the results obtained for Series B2 were considered fairly reliable, whereas there was an increase in the variance of the results generated for Series A2. Series A3 and B3 results fall within a similar range of stability numbers. However, it is important to note that while test series B3 reached failure, series A3 still maintains its structural integrity. Finally, Series A1 and B1 underwent rapid failure in the third test run, resulting in a similar stability result.

5.6 Design stability

Table 5-3 provides descriptive statistics for the stability parameter, N_S, including the minimum, average, maximum, and standard deviation. The range of the minimum and maximum value relative to the average was broad in certain instances, as seen in Table 5-3 (which represents the same data as that of Table 5-2). Therefore, using an average to determine a design stability number was considered unreliable. The average stability number determined during testing for a slope of 1:1.33 ranges from 3.34 to 4.16, whereas for the 1:1.5 slope the stability numbers range from 3.15 to 4.45 (In a test series where no failure occurred, the highest stability number determined was used).

Table 5-3: Data analysis of stability parameter, N_S.

Description	Stability parameter, N_S							
	Test Series A (1:1.33)				Test Series B (1:1.5)			
	Min	Average	Max	STDEV	Min	Average	Max	STDEV
No damage	2.61	3.34	3.67	0.37	2.04	3.15	4.06	0.71
Start of damage	3.00	3.64	4.05	0.40	2.54	3.41	4.64	0.76
Failure	3.46	4.16	4.62	0.39	4.20	4.45	4.64	0.15

Although average values are useful for offering a general perspective on recorded data, they can occasionally distort the actual data trends. This becomes particularly relevant in the context of breakwater design using a single-layer armour system, where the no damage parameter becomes crucial as any extraction from the slope leads to potential underlayer exposure to waves. Consequently, the minimum no-damage value is adopted as the basis for determining the design stability number of the Cubilok. As a result, the design values are highly conservative, and less conservative values may be considered cautiously. Table 5-4 shows the design stability number for each slope.

Table 5-4: Design stability numbers for each slope.

Description		Stability number	
		A-Series (1:1.33)	B-Series (1:1.5)
Minimum start of damage		3.00	2.54
Safety factor		1.15	1.25
Design stability number	N_S	2.61	2.04
	K_d	13	6

From the table, it can be seen that the mildest slope achieves a lower stability number compared to the steeper slope. In the context of physical model testing, this implies that the same size armour unit can withstand a greater wave height on a steeper slope. In practical application, this would allow for the use of smaller concrete armour units on steeper slopes compared to milder slopes. This would reduce the amount of concrete required and result in a more cost-effective structure.

6 OVERTOPPING ANALYSIS

The interaction between the waves and the structure induces several hydraulic responses. These include wave transmission, reflection, and overtopping. The recorded data reflects the total wave height, and the reflected wave height is extracted to obtain the incident wave height used in the analysis. The wave overtopping is recorded for every test, while this study does not consider wave transmission. Table 6-1 provides a summary of the overtopping discharge and the percentage of overtopping waves relative to the incident wave heights recorded at the structure's toe. In the test series indicated in the table the wave height (based on the spectrum, H_{m0}) determined at the toe of the structure was considered.

Table 6-1: Summary of the overtopping results.

Test series	Wave period (s)	Incident wave height (m)	Overtopping discharge (l/s/m)	Percentage of overtopping waves (%)
A1	2.724	0.116 – 0.154	0.33 – 1.35	11 – 37
A2_1	1.380	0.100 – 0.143	0.03 – 0.30	3 – 29
A2_2	1.380	0.096 – 0.127	0.03 – 0.16	2 – 18
A2_3	1.380	0.098 – 0.163	0.03 – 0.88	3 – 43
A2_4	1.380	0.099 – 0.161	0.05 – 0.75	3 – 41
A3	1.731	0.078 – 0.170	0.05 – 3.22	0 – 47
B1	2.724	0.116 – 0.155	0.63 – 2.29	11 – 37
B2_1	1.380	0.099 – 0.171	0.03 – 0.95	3 – 47
B2_2	1.380	0.095 – 0.167	0.03 – 0.68	2 – 45
B2_3	1.380	0.095 – 0.163	0.02 – 0.38	2 – 43
B3_1	1.731	0.076 – 0.169	0.05 – 1.17	0 – 46
B3_2	1.731	0.075 – 0.143	0.04 – 0.80	0 – 40
C2_1	1.380	0.089 – 0.160	0.04 – 0.53	1 – 41
C2_2	1.380	0.091 – 0.174	0.02 – 0.48	1 – 49
C2_3	1.380	0.090 – 0.186	0.02 – 0.46	1 – 55

6.1 Wave overtopping discharge

6.1.1 Wave steepness

Figure 6-1 presents the rate of overtopping per meter as a function of the mean energy wave steepness. The three-test series A, B and C, indicate the slope of 1: 1.33 for A and 1: 1.5 for B and C. The numbers referenced in the legend refer to the wave period used, with 1,2 and 3 representing a mean wave period of 2.48, 1.26 and 1.57 seconds, respectively.

There appears to be a significant increase in the overtopping per meter for a mean wave steepness between 0.01 and 0.02, which implies that longer wave periods result in larger overtopping volumes. The graph shows that for lower wave steepness, the overtopping rate increases rapidly with each consecutive test.

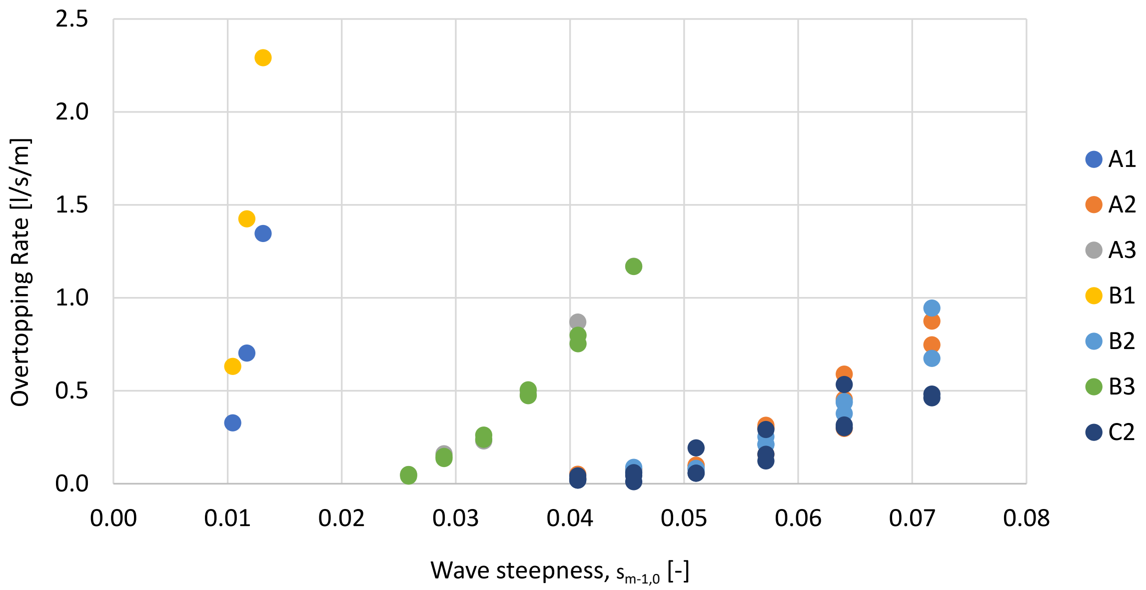

Figure 6-1: Influence of wave steepness on the rate of overtopping.

Equation 18 from Section 2.7.1 was used to determine the roughness factor (γ_f) for Test series A, B and C.

$$\frac{q}{\sqrt{g \times H_{m0}^3}} = 0.09 \times \exp[-(1.5\frac{R_c}{H_{m0} \times \gamma_f \times \gamma_\beta})^{1.3}$$

The roughness influence factors were determined using the measured data range from approximately 0.5 – 1, where one represents a smooth, impermeable surface (EurOtop, 2018). Test series A1, B1, A3, and B3 account for the highest roughness factors and include the longest wave periods ($T_{m-1,0}$) tested, with a maximum $T_{m-1,0}$ of 2.48 seconds for test series A1 and B1, indicated in Figure 6-2. Overall, the roughness factors were high relative to other single-layer units. The majority of the tests exceed the roughness factor of a singular rock layer with an impermeable core ($\gamma_f = 0.6$). This could indicate that the measured overtopping was relatively large, preventing the waves from experiencing surface roughness.

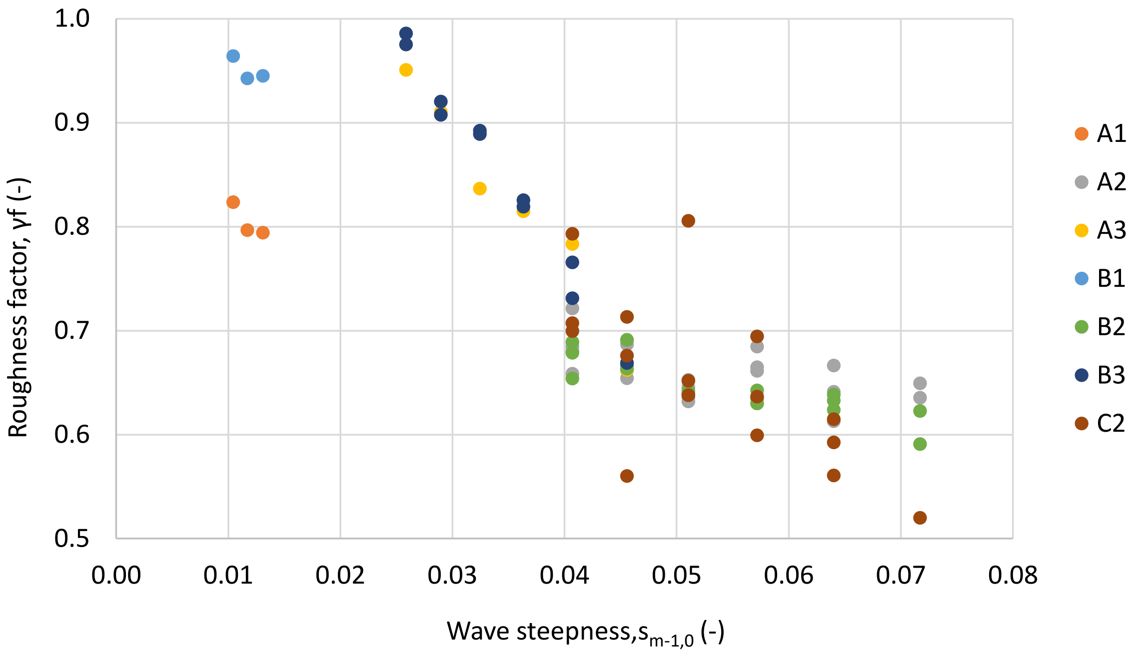

Figure 6-2: Roughness factor as a function of the wave steepness.

6.2 Dimensionless crest level

Figure 6-3 illustrates the relative overtopping rate as a function of the relative crest height for each test series. The boundaries of the roughness factor are depicted in the graph by black solid and dashed lines, with the solid line indicating the smooth impermeable profile and the dashed line indicating a single rock layer with a permeable core. Typically, an armour unit has a roughness factor ranging from 0.38 for Tetrapods to a maximum of 0.49 for a single layer of Cubes or Cubipods (EurOtop, 2018). The assumption is that the shape complexity should yield a roughness factor lower than that of a single layer of Cubes or Cubipods. However, the results obtained in the graph appear inconsistent with this assumption.

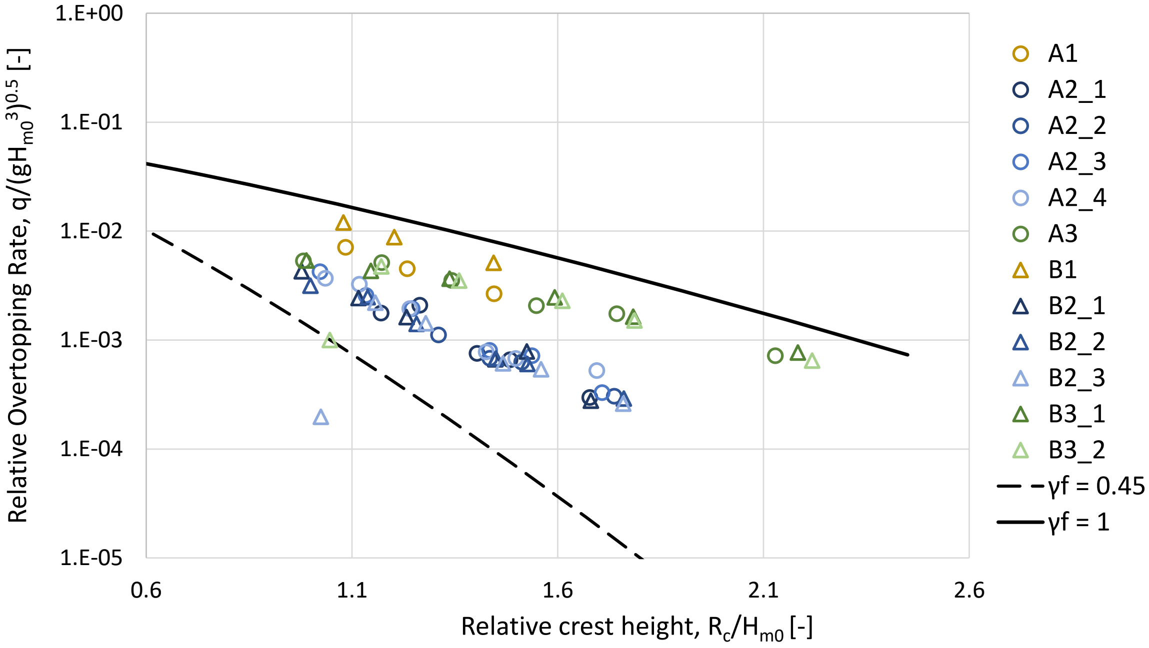

Figure 6-3: Relative overtopping rate as a function of the relative crest height.

The relative wave overtopping rate increases as the dimensionless crest height decreases. Furthermore, the relative overtopping rate increases with increasing wave periods. In practical terms, this implies that longer wave periods would require increased crest heights to mitigate overtopping.

6.3 Percentage of wave overtopping

The probability of overtopping, P_{OV}, was illustrated as a function of the incident wave height in Figure 6-4. The probability of overtopping increases for a low wave steepness, as indicated with test series A1 and B1 (s_{op} = 0.01).

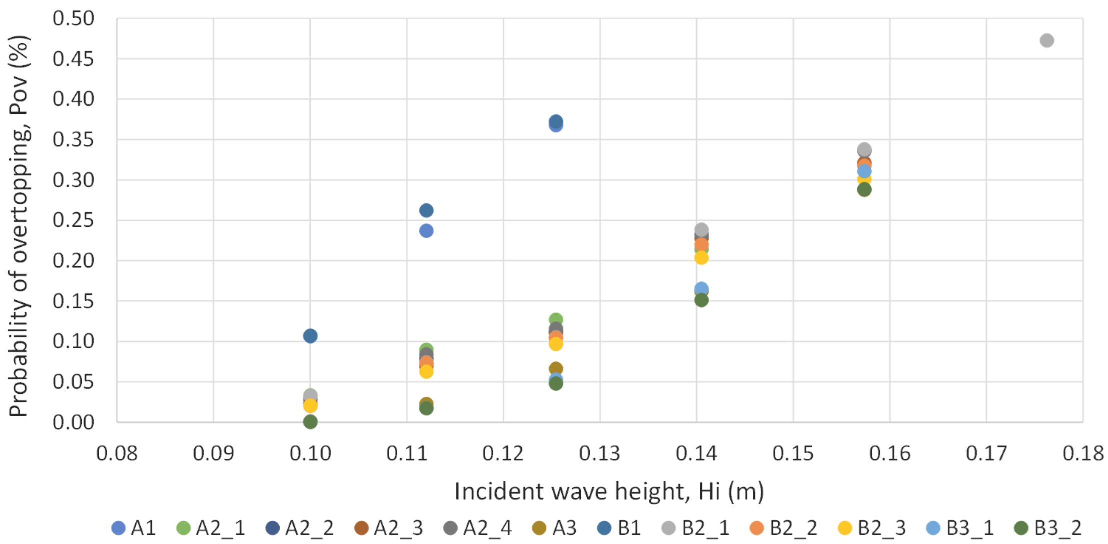

Figure 6-4: Probability of wave overtopping.

7 COMPARISON WITH OTHER SINGLE-LAYER UNITS

7.1 Shape comparison

A comparison of several single-layer units was provided in Figure 7-1. A view of each unit in the XY, XZ, and YZ planes was provided in the figure. This assists in the visualisation of the unit in various planes. For the Xbloc, the unit is symmetrical in two planes, whereas for the Cubilok, Crablock and Hexapod, the units are symmetrical in all planes. The symmetrical nature of the unit should provide ease of placement as the orientation of the unit was not limited to a specified number of placements. This comparative analysis seeks to illustrate that Cubilok holds the potential to adopt established guidelines from similar units, thereby paving the way for the development of specific Cubilok guidelines.

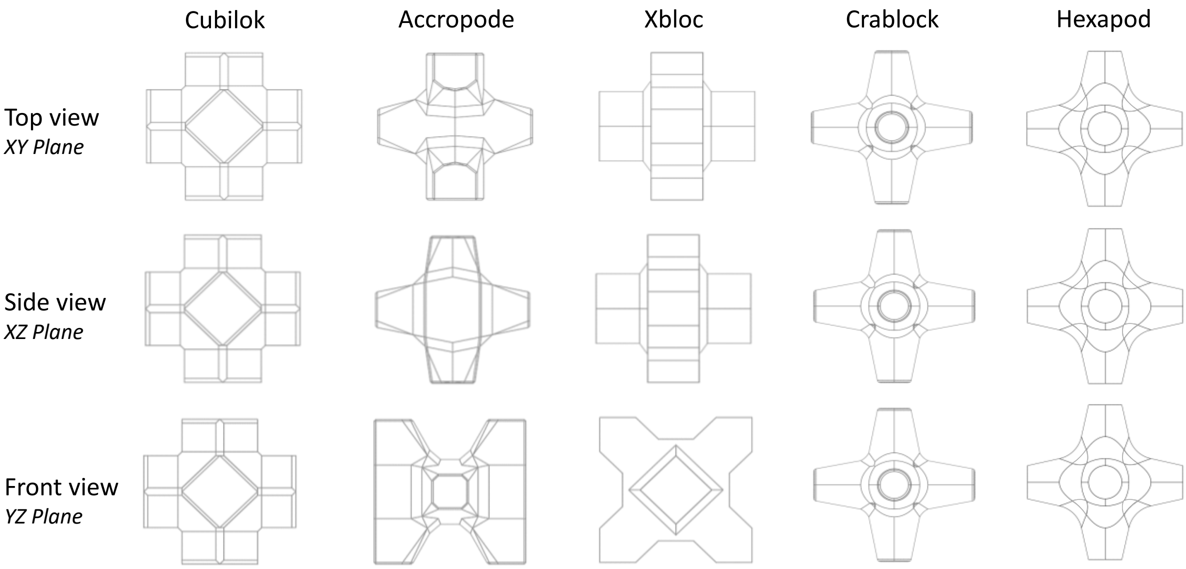

Figure 7-1: Plane comparison of the unit.

A summary of several other armour units' slenderness ratios is provided in Figure 7-2.

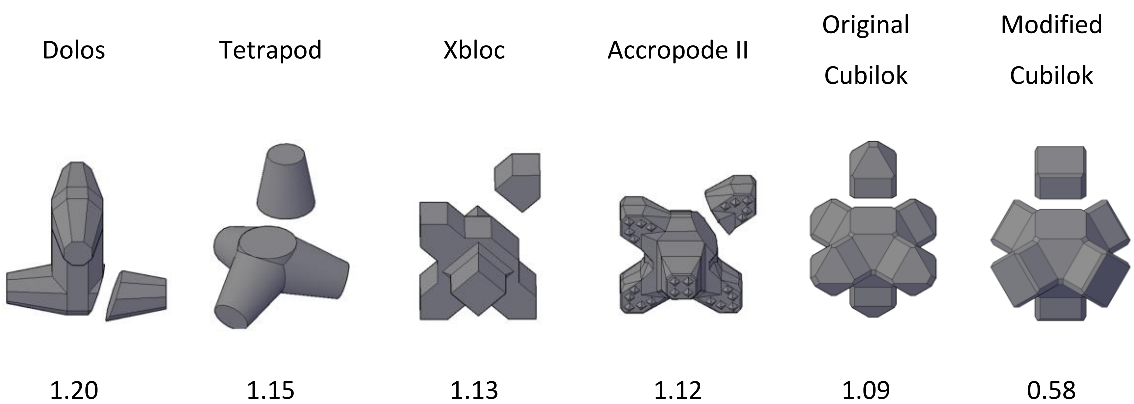

Figure 7-2: Slenderness ratios of various concrete armour units.

Figure 7-3 depicts the footprint of several popular armour units. The footprints of several popular armour units show that the original Cubilok has a significantly larger footprint than the modified Cubilok. According to Wehlitz and Schoonees (2023), the increased surface area may have contributed to the settlement achieved in prior testing. The modified unit features a smaller surface area, corresponding to the footprints established for other units, in an attempt to reduce settlement.

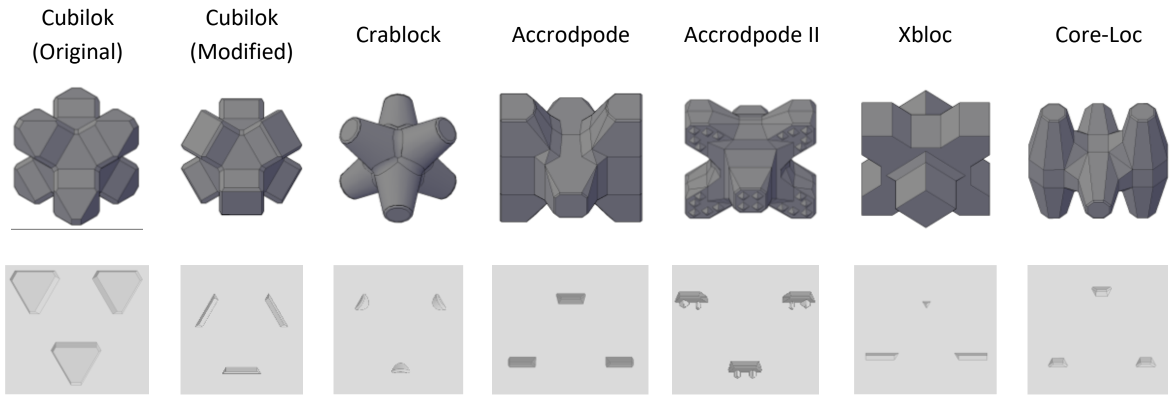

Figure 7-3: Footprint of several armour units.

The Cubilok follows a configuration similar to the Xbloc, Crablock and Hexapod (Jackson, 1968), termed centre-based construction. These slender concrete armour units comprise several bars placed in various directions. The bars are constructed in three perpendicular directions for the units illustrated in Figure 7-4, resulting in the centralised construction (Bonfantini, 2014). It is clear that each of the units has four protuberances visible from the front side and an additional protuberance in the centre. The protuberances are similar for Cubilok, Crablock, and Hexapod, whereas they differ for the Xbloc.

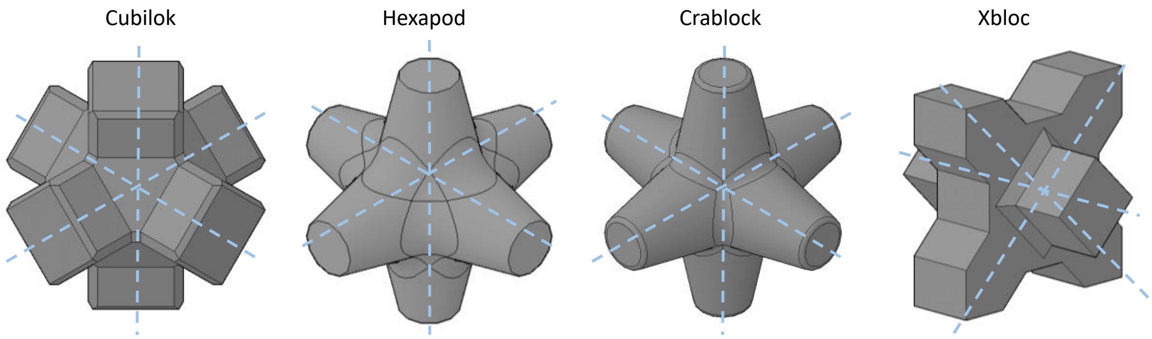

Figure 7-4: Centre-based construction, adapted from Bonfantini (2014).

An alternate construction configuration consists of stacked adjacent bars in alternating directions, as seen in Figure 7-5.

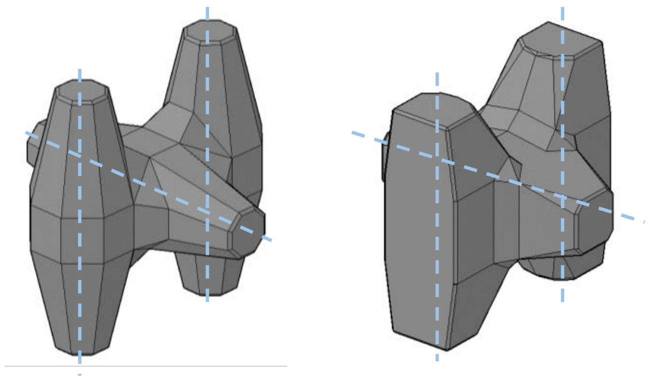

Figure 7-5: Stacked bars, adapted from Bonfantini (2014).

7.2 Stability analysis

The level of damage was divided into three categories, as indicated in Table 7-1. The damage numbers in the table represent the relative number of displaced units, N_{0d}, and the percentage of displaced units, N_d, on the slope. The table addresses two of the three damage categories, as instances of intermediate damage were infrequent in the recorded outcomes.

Table 7-1: Comparison of damage numbers (CIRIA, 2007).

Armour type	Damage number	Damage level		
		Start of damage	Intermediate damage	Failure
Cube	N_{od}	0.2 – 0.5	1	2
Tetrapod		0.2 – 0.5	1	1 – 5
Accropode		0	–	> 0.5
Cubilok		0	–	> 0.5
Cube	N_d	–	4%	–
Tetrapod		0 – 2%	–	≥ 15%
Accropode		0%	1 – 5%	≥ 10%
Cubilok		0%	–	≥ 5%

A comparison between the stability of the Cubilok and several other single-layer systems is analysed in this section. The single-layer systems include the Xbloc (which the model section in this study was based on), Crablock, and Accropode. The physical model configuration was comparable for all of these structures, each featuring a section of deep water where the waves were produced and a foreshore that sloped at a ratio of 1:30 (V:H). The spectrums employed in the tests vary, with the JONSWAP wave spectra used for the Cubilok, Xbloc (DMC, 2003b), and Crablock (Broere, 2015) and the Pierson-Moskovitz spectrum used for the Accropode (DHL, 1987). Furthermore, the Accropode was tested with a consistent wave height, whereas the other units were tested using increasing wave heights. Table 7-2 provides the packing densities tested in the physical models of each unit.

Table 7-2: Packing densities tested for each unit.

Concrete armour unit	Packing density
Accropode	0.64
Xbloc	0.55-0.59
Crablock	0.66-0.69
Core-Loc	0.62-0.64
Cubilok	0.63
	0.65

Figure 7-6 illustrates the comparison of the stability numbers as a function of the Iribarren parameter for the Xbloc, Accropode, and Cubilok. The range of stability numbers at the start of damage was greater for the Cubilok than the Xbloc and Accropode.

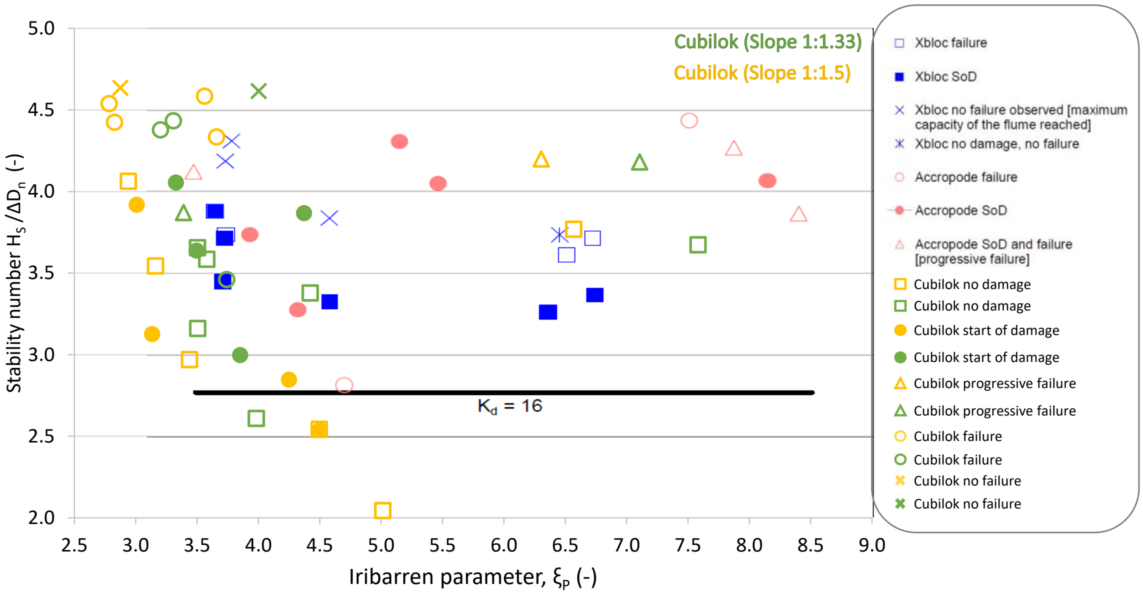

Figure 7-6: Comparison with Accropode and Xbloc, adapted from DMC (2003b).

Figure 7-7 compares the relative damage number as a function of the stability numbers for the Cubilok, Accropode, and Xbloc. For the Cubilok, the points where the slope reached failure were plotted at a relative number of displaced units (N_{od}) equaling three. This was done since determining the N_{od} at failure was impractical due to the severity of the failure. The data points in the graph above are representative of the three levels of damage indicated in the legend.

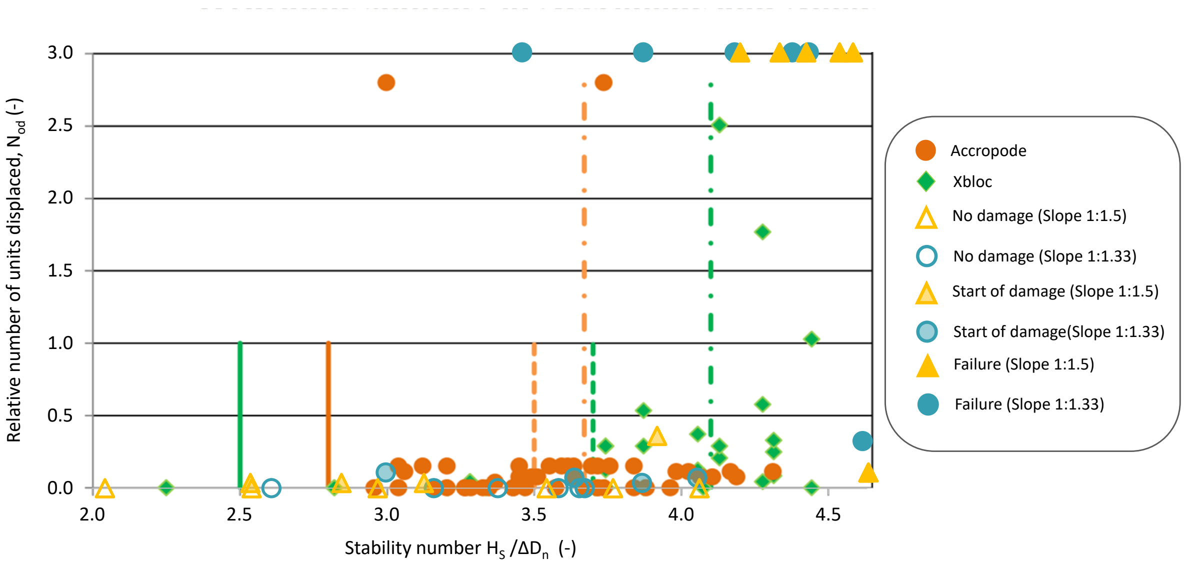

Figure 7-7: Comparison with Accropode and Xbloc, adapted from Bonfantini (2014).

The minimum stability number illustrated on the graph was for the Cubilok at a slope of 1:1.5.

The lowest recorded stability numbers at the onset of damage for the Accropode and Xbloc were $N_S = 3.28$ and $N_S = 3.04$, respectively. The minimum stability number recorded at the onset of damage for the Cubilok was $N_S = 2.54$ and 3.00 for the milder and steeper slope, respectively.

Figure 7-8 summarises the data points indicated in the previous graph. The dot, dashed, and dash-dot lines represent the design value, the start of damage, and failure, respectively.

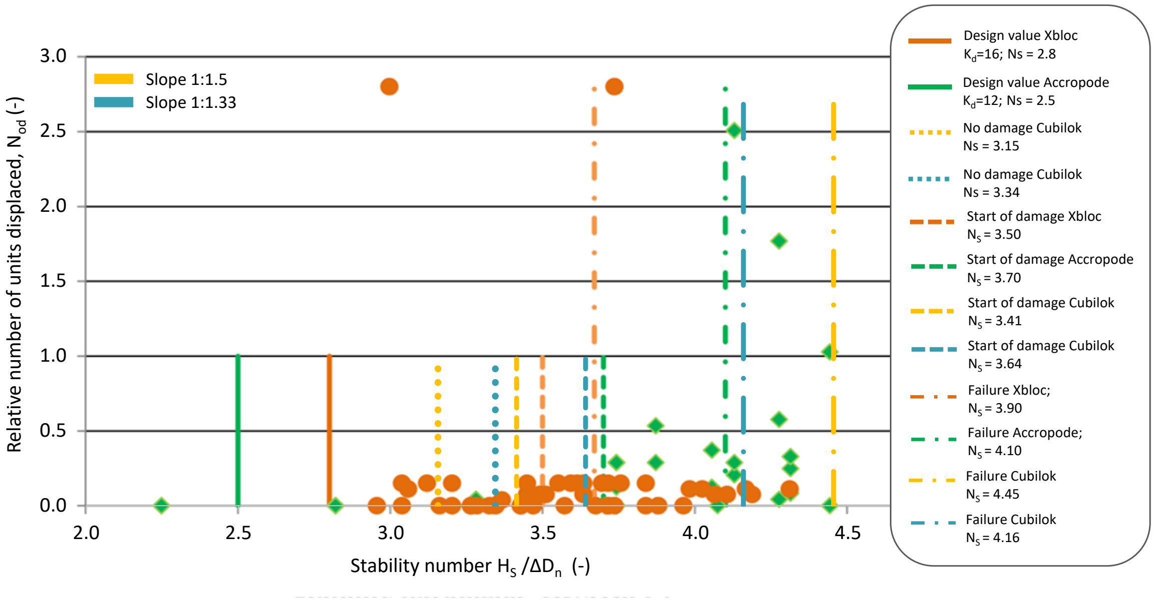

Figure 7-8: Average damage unit comparison, adapted from Bonfantini (2014).

A summary of the average stability numbers for each unit is provided in the Table 7-3.

Table 7-3: Summary of the stability values achieved for the Cubilok, Accropode, and Xbloc.

Stability number N_S (-)	Concrete Armour Unit			
	Cubilok (1:1.33)	Cubilok (1:1.5)	Xbloc	Accropode
Design	2.61	2.04	2.80	2.50
Minimum no damage	2.61	2.04	2.96*	2.25*
Average no damage	3.34	3.15	-	-
Average start of damage	3.64	3.41	3.50	3.70
Average failure	4.16	4.45	3.90	4.10

*Approximated from Figure 7-8

The average stability number at failure for the Cubilok outperformed both the Xbloc and the Accropode independent of the slope. However, the start of damage for the milder Cubilok slope achieved the lowest stability number out of the tests compared. The stability numbers for the onset of damage were greater for the steeper slope; however, at failure, the stability of the milder slope exceeds the steeper slope. This indicates that the milder slope (B-Series) retains its damaged state for longer than the steeper slope (A-Series). According to the findings, it was clear that Cubilok's performance was improved on the steeper slope.

Considering the minimum no-damage values attained for the armour units outlined in Table 7-3, it is observed that the Xbloc's design value falls below its minimum no-damage threshold, thus leading to a structure's design stability number of 2.8. An extra 5% safety margin is incorporated before the minimum no-damage number is reached. Meanwhile, the Accropode is assigned a design stability number of 2.5, and during testing, the minimum damage number achieved is 9% lower than the design value.

Figure 7-9 and Figure 7-10 compare the relative number of units displaced as a function of the stability number for the Cubilok and Xbloc. The legend on the right of the graph indicates the name of each test series for both the Cubilok and Xbloc (DMC, 2003b) results. The wave steepness was indicated in the brackets for the Xbloc Test Series (“TS" indicated by the grey lines), whereas the wave steepness for the Cubilok is indicated for each data point on the graph. The solid-filled data points represent test series in which failure was not achieved.

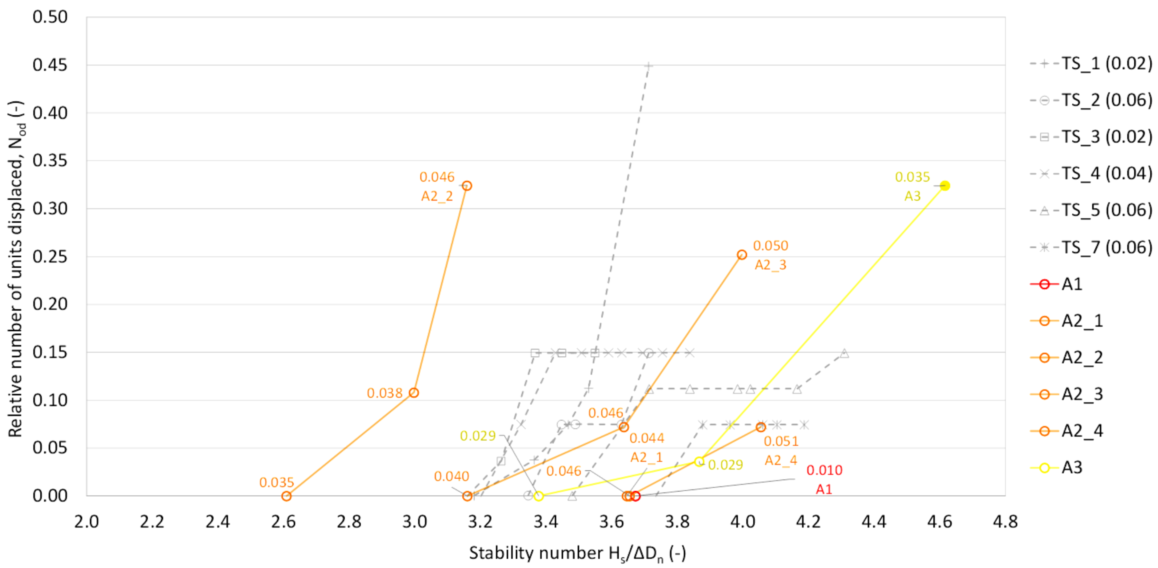

Figure 7-9: Comparison of Cubilok with Xbloc for a slope of 1:1.33, adapted from (DMC, 2003b).

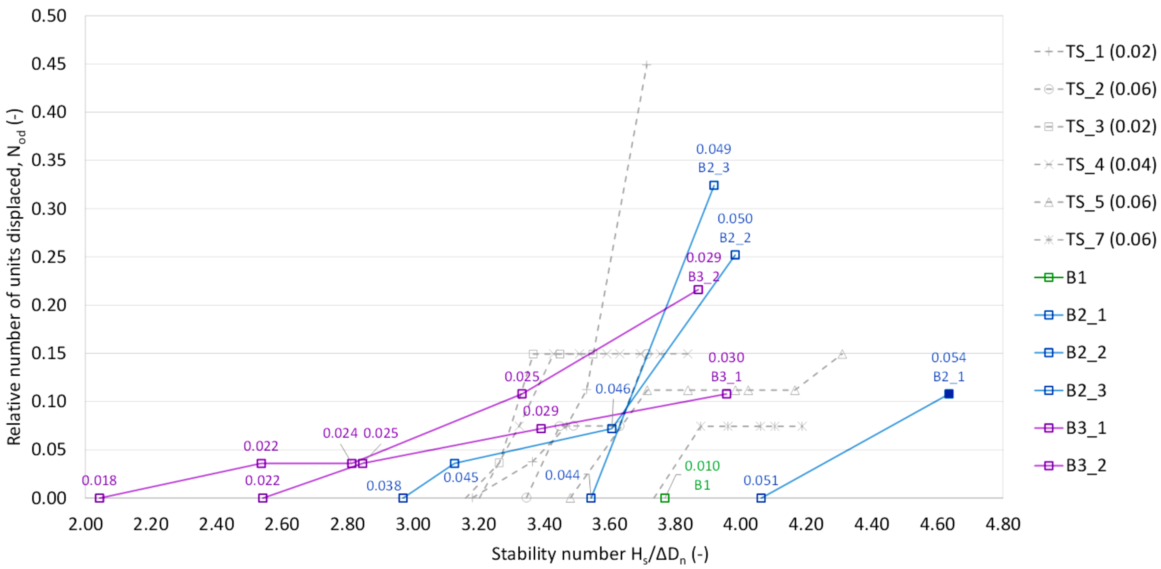

Figure 7-10: Comparison of Cubilok (1:1.5) with Xbloc (1:1.33), adapted from DMC, 2003b.

The test series for the steeper slope (1:1.33) and the milder slope (1:1.5) follow a similar trend for a wave steepness of s_{op} = 0.01, where sudden failure occurs during the third test. For intermediate wave steepness values, the Cubilok unit demonstrated greater stability than the Xbloc when considering the steeper slope. In tests involving high wave steepness values, the stability range for Xbloc was estimated to be between 3.7 to 4.3, whereas for the steeper slope Cubilok variation, the stability range was wider, with stability numbers from roughly 3.1 to 4.1. When comparing the milder Cubilok slope with the steeper Xbloc configuration, it becomes evident that the Cubilok's overall performance is comparatively less favourable when compared to the Xbloc.

Although the Cubilok has promising initial stability findings, there is some unit unreliability to consider given the wide range of results, particularly for the milder slope and the steeper slope in one instance (test A2_2). The steeper Cubilok slope proves to be competitive with the other units studied in this analysis when taking into account the design stability data.

7.3 Overtopping

Figure 7-11 compares the dimensionless overtopping rate measured with the Cubilok unit in the 2D hydraulic flume testing and the results from previous model tests conducted on several single-layer armour units extracted from the CLASH (2004) database and DMC (Salauddin, et al., 2015). The overtopping rate for the Cubilok was larger than the overtopping rates extracted from the CLASH (2004) database; however, the results were similar to the Crablock and Xbloc® (DMC) test results.

The test results determined in the CLASH (2004) database using 2D-model testing included wave steepness's, s_{op} = 0.02, 0.035 and 0.05. This study contains wave steepness values from $s_{m-1,0}$ = 0.01 – 0.07 (s_{op} = 0.009 – 0.059). The tests conducted at a lower wave steepness (s_{op} = 0.01) fall outside the range of data covered in the CLASH database, resulting in an overestimation of wave overtopping compared to the database. The experimental model tests from the CLASH (2004) database were performed without the inclusion of a foreshore slope. This study uses a foreshore slope of 1:30, similar to the tests conducted on the Xbloc® (DMC) and Crablock, influencing the waves at the toe of the structure (Salauddin, et al., 2015).

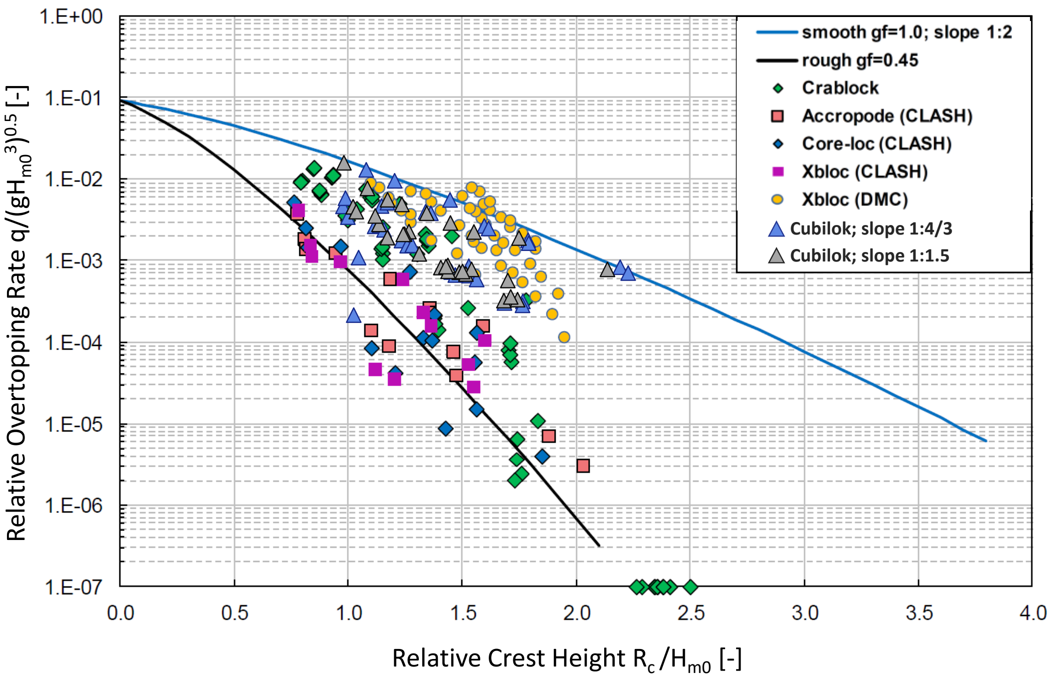

Figure 7-11: Mean overtopping discharge verse relative crest height, adapted from Salauddin et al. (2015)

A significant number of the Cubilok results fall within a rough armour layer category; specific data points for both slopes fall on or near the "smooth" line. These data points were likely due to a lower wave steepness, resulting in an over-estimated overtopping rate.

Figure 7-12 compares the dimensionless overtopping rate against the relative crest height, as measured with the Cubilok unit in the 2D hydraulic flume testing, against the outcomes from previous model tests conducted on several single-layer armour units extracted from the CLASH (2004) database (Schüttrumpf, et al., 2009). The overtopping rate for the Cubilok was greater compared to the overtopping rates extracted from the CLASH (2004) database.

This graph includes the test series conducted at a slope of 1:1.5 which relates to the B- and C-Series in this study. Single-layer units such as Accropode™, CORE-LOC®, Xbloc® and the Cube are indicated with a solid shape, whereas double-layer units are indicated with a hollow shape. Single-layer structures tend to have higher overtopping rates than double layers structures (EurOtop, 2018).

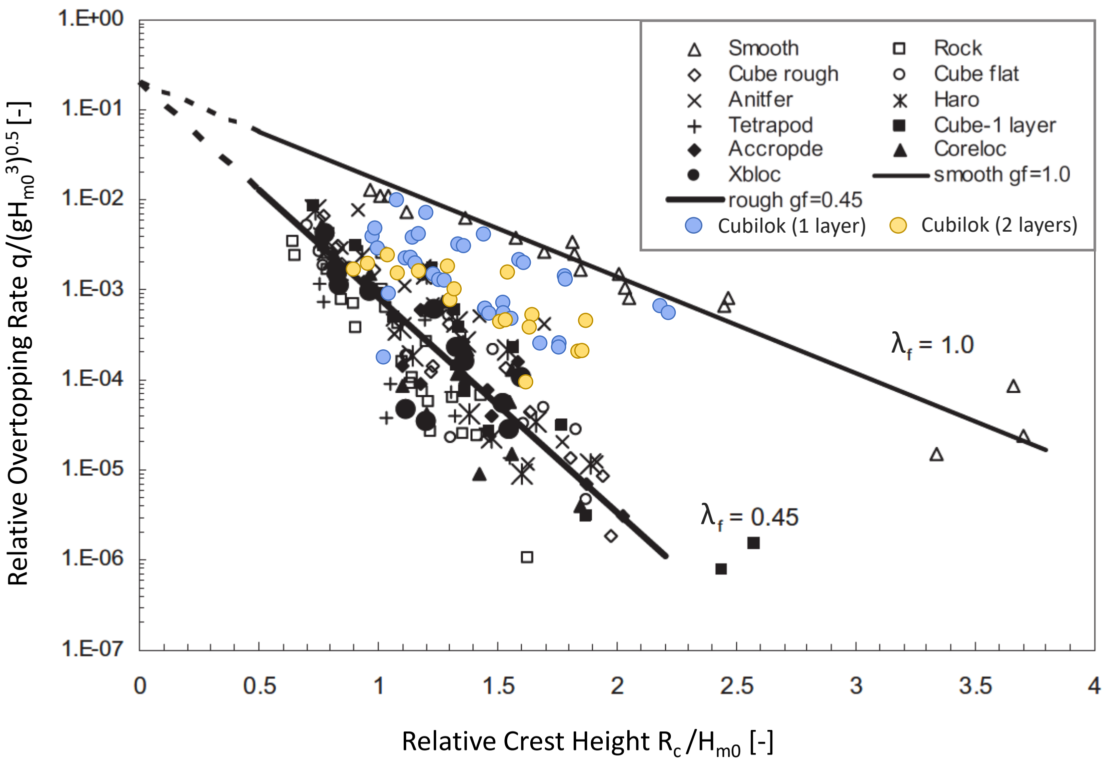

Figure 7-12: Mean overtopping discharge verse relative crest height, adapted from Schüttrumpf et al. (2009).

7.4 Settlement

To ensure a direct comparison could be made between the original and modified Cubilok, two additional test series (Series D3_1 and D3_2) were conducted on the original Cubilok at a packing density of 0.65. As stated beforehand, the modified Cubilok has a mass of around 46.6 g, whereas the original Cubilok has a mass of 61.8 g. The cross-sectional dimensions were increased proportionately to accommodate the larger unit. The D-Series were subjected to the same wave conditions as the A3- and B3-Series.

Figure 7-13 illustrates the variation in settlement between the modified unit (graph on the left) and the original unit (graph on the right). The graph indicates that the settlement difference is relatively small for the modified unit. In contrast, the settlement for the original unit follows a similar path up to roughly 3000 waves and concludes with an approximate fivefold difference by the end of the sixth condition. This demonstrates the original unit's sensitivity to slope level variations.

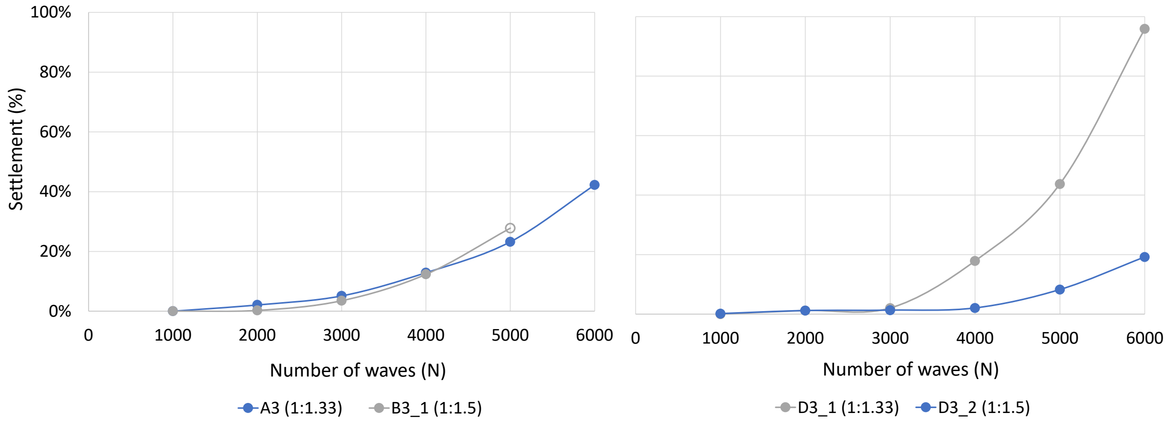

Figure 7-13: Settlement comparison with modified (left) and original Cubilok (right), respectively.

Figure 7-14 compares the settlement of the modified unit directly with the original unit, differentiating by the slope level. Considering the graphs, the steep slope has a significantly greater variation in settlement than the milder slope. This indicates that the milder slope reduces settlement which is in line with what was mentioned in Chapter 2. The modified unit outperformed the original on the steeper slope, indicating that the settlement problem has been addressed for a slope of 1:1.33. In contrast, the original unit outperforms the modified unit when considering the milder slope.

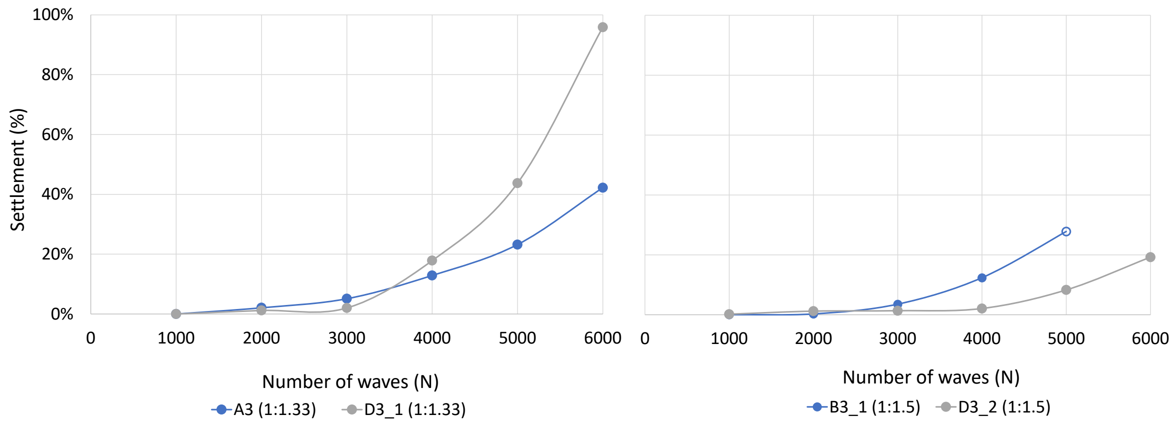

Figure 7-14: Settlement with respect to the slope level.

Figure 7-15 presents a summary of all the settlement tests that were analysed for comparative purposes. Considering the graph, the lowest settlement result was achieved for the original Cubilok at a slope of 1:1.5, whereas the settlement for the same unit and the slope of 1:1.33 resulted in the highest recorded settlement.

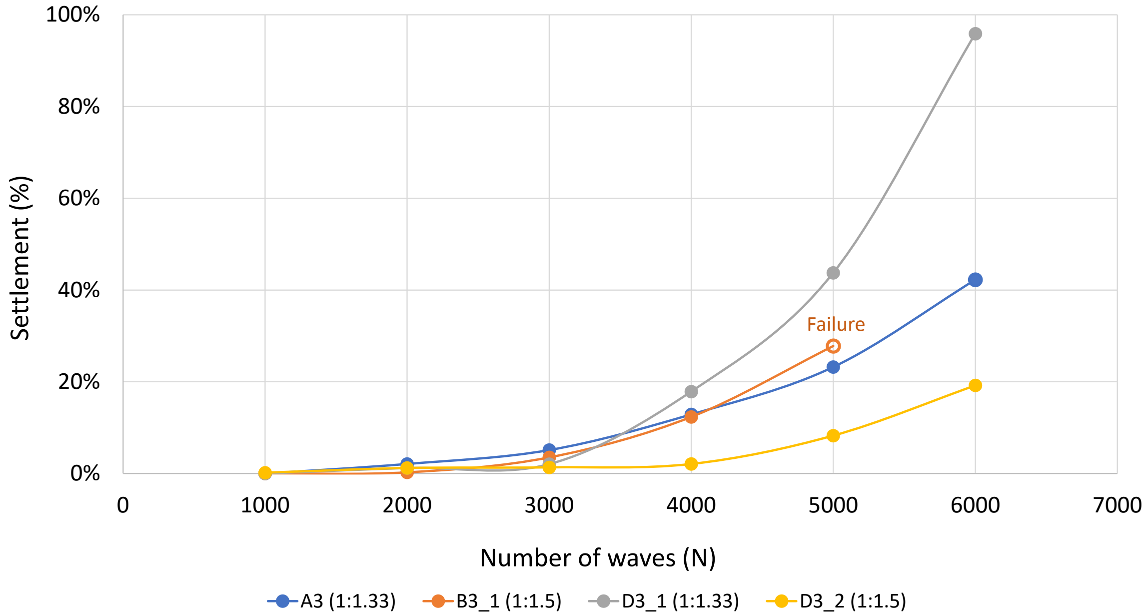

Figure 7-15: Overall settlement analysis.

The graph emphasizes the influence of slope and packing density on the settlement of both the original and modified units. The disparity in settlement is considerably greater for the original unit compared to the modified one, suggesting that the settlement concern has been partially addressed. Nevertheless, additional testing is necessary to draw a definitive conclusion regarding the impact of settlement.

8 ECOLOGICAL ENHANCEMENT OF CONCRETE ARMOUR UNITS

An expanding field of study known as ecological enhancement, often referred to as ecological engineering, focuses on incorporating environmentally conscious designs into hard engineering structures in order to extend or otherwise improve habitat biodiversity (ITRC, 2004). These methods may be applied to existing structures or introduced when designing new structures and aim to promote habitat biodiversity without impairing the integrity of the structure.

The majority of marine life inhabits coastal regions, and modifications resulting from human activities along coastlines are a significant factor leading to the deterioration of coastal habitats and the associated loss of services provided by ecosystems (Spalding, et al., 2007). Maritime infrastructure (i.e., breakwaters and revetments) often displaces these ecologically diverse habitats, endangering these vulnerable ecosystems (Dugan, et al., 2012).

8.1 Comparison of ECOncrete® and Standard Antifer

The ECOncrete®Antifer (EA) project will employ three concrete matrices with enhanced ecological attributes (M1-M3) that have demonstrated promising outcomes in the laboratory and prior field tests. The EA units were created in moulds with a flexible lining in order to create an intricate concrete texture, including cavities and grooves. This technique was developed to provide refuge spots for various biological organisms within the units, promoting marine biodiversity (Sella & Perkol-Finkel, 2015). A comparison is undertaken between the EA and the Standard Antifer (SA), with the units indicated in Figure 8-1.

Standard Armouring (SA)   ECOncrete® Antifers (EA)

Figure 8-1: Standard and ECOncrete Antifers (Sella & Perkol-Finkel, 2015).

According to Sharma (2009), more than 50% of concrete marine infrastructure was built with Portland cement, known for being an unsuitable material for biological enhancement, which may result from its high pH levels (basic pH ≈ 13 compared to a less basic pH ≈ 8 for saltwater) and substances harmful to marine life (Artificial Reef Subcommittees, 2019). Traditional coastal infrastructure fails to offer favourable conditions for the emergence of varying marine organisms with its limited surface complexity and artificial material composition indicated in Figure 8-2, resulting in an influx of invasive species able to endure the harsh marine environment (Firth, et al., 2015; Mineur, et al., 2012).

Concrete marine infrastructure sites have been identified as susceptible locations for the rapid increase of invasive species. The prevalent composition of concrete marine infrastructure, often comprising uniform smooth-surfaced units constructed from artificial materials, including concrete or quarry run, tends to attract non-indigenous species that exhibit high adaptability to diverse environments (Glasby, et al., 2007; Vaselli, et al., 2008).

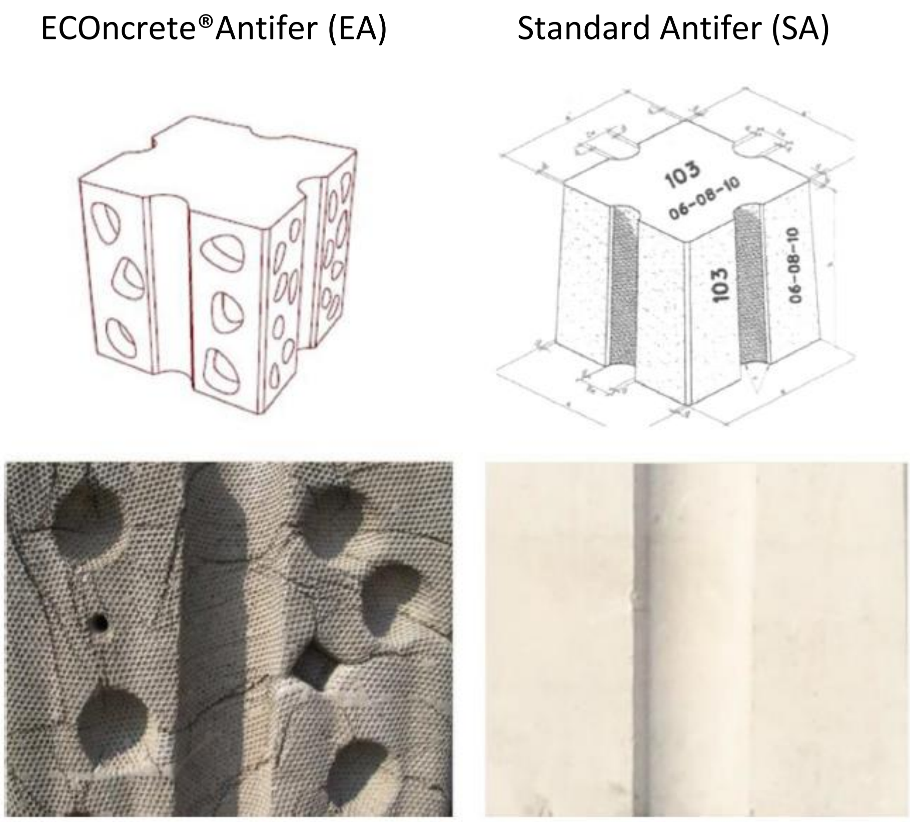

Figure 8-2: EA has a complicated concrete surface with grooves and crevices, whereas SA has a smooth surface with no complexity (Sella & Perkol-Finkel, 2015).

Each EA matrix outperformed the Portland cement used in the SA. Over a span of 2 years, the EA units displayed a notable abundance of marine life cover, which was characteristic of their intricate surface design. The accumulation of biogenic materials (shown in Figure 8-3) has been associated with greater structural robustness, lower susceptibility to chloride infiltration, and increased resistance to erosion and abrasion, all of which decrease required maintenance and, as a result, extend the structure's operational lifespan. This process is usually referred to as bioprotection (Sella & Perkol-Finkel, 2015; Perkol-Finkel, et al., 2018).

Aside from contributing to the mass of the unit, the presence of biogenic formations results in a stronger link between neighbouring armouring units. This is made possible by the growth of marine organisms serving as a natural glue, absorbing wave forces and decreasing the structural impact of surges (Perkol-Finkel & Sella, 2014).

Usual marine cover found on SA

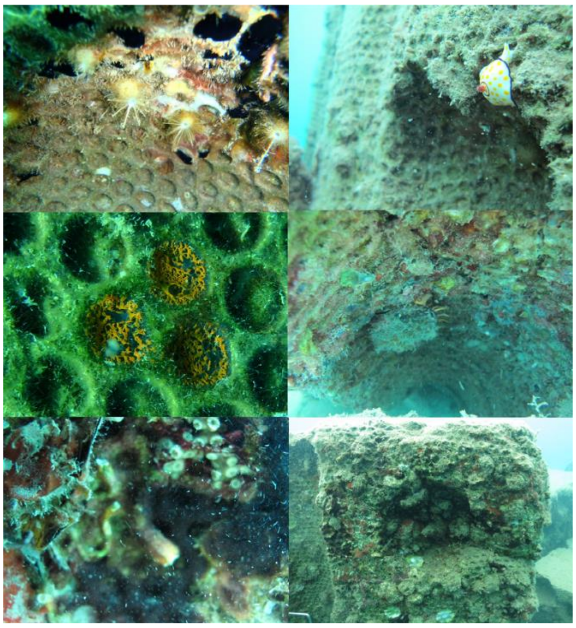

Usual marine cover found on EA

Figure 8-3: SA versus EA after two years (Sella & Perkol-Finkel, 2015).

In the context of SA structures, benthic species have a notably low presence. EA installations provide significant habitat value for these species. These species usually inhabit holes and grooves provided by the design of EAs, which promotes biodiversity and protective environments not found in conventional grey engineering designs. The findings from the study indicate that it is possible to boost the abundance of marine life by incorporating minor adaptations without compromising the performance of coastal protection (Sella & Perkol-Finkel, 2015).

The outcomes of these studies affirm the premise and establish that alterations in material composition, surface roughness, and design may enhance the ecological significance of concrete-based maritime infrastructure. Consequently, this progress aligns with the principles of sustainable and flexible marine development in accordance with the research conducted by Perkol-Finkel et al. (2014; 2015; 2018).

8.2 Potential Cubilok modifications

Figure 8-4 illustrates potential Cubilok modifications aimed at enhancing the ecological value of the unit. Various designs, inspired by real-world and conceptual ideas, are depicted on the Cubilok to demonstrate the diverse modifications possible for the unit. However, the consequences of these alterations on the unit's structural integrity remain uncertain and warrant thorough investigation. Integrating these modifications with ecologically enhanced concrete, similar to the composition of the ECOncrete®Antifer, could foster sustainable and environmentally beneficial marine structure development.

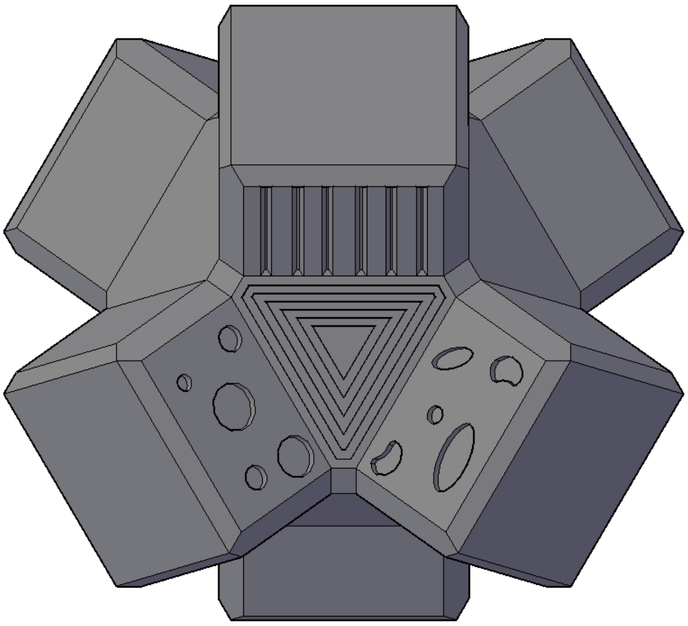

Figure 8-4: Potential model unit modifications.

9 CONCLUSIONS AND RECOMMENDATIONS

The final remarks and research study findings are described in this chapter, along with suggestions for further research.

9.1 Conclusions

This study investigated the potential of the newly trademarked concrete armour unit, Cubilok, to function as a suitable breakwater armour unit. The hydraulic stability and overtopping were explored for the Cubilok with respect to the slope, excluding the toe and the transition between the crest and slope, in the 2D physical model. This research aims to gain an understanding of the functionality of the Cubilok armour unit and, as a result, its potential practical applications. Furthermore, a limited investigation was conducted to explore the ecological enhancements associated with concrete armour units and strategies for ecologically engineering the Cubilok. The exploration of ecological enhancement highlighted two main categories: the investigation of ecologically engineered concrete armour units and the utilization of eco-concrete within concrete armour units.

Seventeen test series were conducted on the modified Cubilok unit with varying slopes and layers. An additional two test series were conducted on the original Cubilok unit with the aim of comparing the settlement between the units. The investigation was divided into four distinct categories, labelled as test series A, B, C, and D. In test series A and B, single-layer experiments were conducted using identical wave conditions but on two different slopes. Specifically, test series A was conducted at a slope of 1:1.33, while test series B was carried out at a slope of 1:1.5. Series C involved the evaluation of a double-layer system at a slope of 1:1.5. Lastly, test series D considers the original Cubilok in a single-layer system, with testing conducted at slopes of 1:1.33 and 1:1.5. Test series D was undertaken to quantify the impact of settlement between the original and modified Cubilok units, enabling a direct and meaningful comparison between these two variations.

9.1.1 Effect of wave period

Three wave periods were tested and considered a wide variety of wave steepness values. The wave periods tested include a T_P = 1.38, 1.73 and 2.74 seconds. The stability numbers determined for longer wave periods (lower wave steepness) indicate progressive failure of the structure, where the start of damage and failure occur within the same test (no increase in wave height).

For the tests conducted, progressive failure was not commonly observed in shorter wave periods (higher wave steepness). Instead, the damage typically accumulated gradually over multiple test runs. The study demonstrated increased stability as wave steepness values increased, implying a positive correlation between wave steepness and stability.

9.1.2 Effect of packing density

A potential cause for the extraction of units may be the lack of interlocking once a unit shifts out of its original position. The absence of interlocking may be attributed to the reduced length of protuberances resulting from the flattened configuration in the modified unit.

The effect of packing density was evaluated for the single and double-layer systems. The number of waves test series presented the damage progression for the unit at a slope of 1:1.33 (V:H) with two different packing densities. The damage progression for the 0.63 packing density progressed rapidly until failure, whereas the 0.65 packing density progressed slowly until an equilibrium state was achieved. These preliminary results indicate that denser packing enhances the unit's overall stability, aligning with findings achieved for the original Cubilok shape. The subsequent single-layer tests were carried out at a packing density of 0.65 for the modified Cubilok shape.

Three packing densities were examined for the double-layer system: 1.17 (based on a double layer of cubes), 1.21, and 1.3. The packing density of 1.21 aimed to mitigate the settlement experienced at 1.17 packing density. While the 1.21 density notably reduced settlement, the double layer still exhibited inferior performance compared to a single layer under identical slope and wave conditions. Testing a final density of 1.3 (twice that of the single layer packing of $\emptyset = 0.65$) aimed to assess the viability of the double layer. This, however, resulted in insufficient interlocking between layers, leading to earlier failure compared to the 1.21 density. It was determined that, for staggered grid placement, the double-layer armour system does not notably enhance stability or slope protection.

9.1.3 Effect of slope

The relative damage number was discussed as a function of the unit stability. Two slopes were tested in this study: a slope of 1:1.33 (steeper slope) and a slope of 1:1.5 (milder slope). The extent of the variability in testing was clearly illustrated when considering the repeat tests conducted at the slopes mentioned above. From the findings, it becomes clear that the steeper slope has less variability than the milder slope. The less variability attained, the more reliable the outcome was seen to be, making this a critical aspect to consider when determining design values for new concrete armour units. Three levels—no damage, the start of damage, and failure—were considered when determining the severity of the damage to the slopes. The onset of damage occurs first for the steeper slope despite meeting increased no-damage criteria than the milder slope. The no-damage criterion was crucial as any extraction from the slope would expose the underlayer to direct wave attack.

The unit relies heavily on its interlocking capability both with the adjacent units and the underlayer rock. The steeper slope provides a tighter interlocking as a result of the increased gravitational force acting on the units. The influence of the unit interaction was seen when comparing the steeper slope to the milder, where the relative damage number increased for the milder slope.

9.1.4 Overtopping

Smaller wave steepness values were found to be correlated with higher overtopping discharges. This observation suggests that longer-period waves resulted in larger overtopping volumes. The overtopping rate increased rapidly for each consecutive test run with decreasing wave steepness values. The overtopping results showed an increase in the overtopping volume for the milder slope in comparison to the steeper slope. The calculated roughness influence factor, determined from the collected data, ranged from 0.5 to 1. The most significant factors contributing to increased roughness coefficients, with values nearing 1, were associated with longer wave periods. This outcome was unexpected, and though the exact rationale remains unclear, it could be attributed to the excessive overtopping volumes observed. Regarding the influence of roughness, definitive conclusions could not be drawn.

9.1.5 Comparison with other units

The no-damage parameter is crucial when considering single-layer armouring, as any extraction in this configuration exposes the underlayer directly to wave action. The Cubilok had a 16% increase over the Accropode for a minimum no-damage stability number and a 13% decrease compared to the Xbloc. Considering the results obtained, it is evident that the stability performance of the Cubilok showed a notable improvement on steeper slopes. This implies its potential competitiveness among the other single-layer units discussed, subject to further investigation. After evaluating the no-damage and design parameters, a finding emerged, with the Cubilok outperforming the Accropode when employed on a 1:1.33 slope. It is worth mentioning that the design parameter for the Xbloc surpasses that of the Cubilok by 7%. The wide range of stability numbers observed for the Cubilok units led to the conclusion that the average value for this study was not a reliable indicator of the unit's performance. Instead, a conservative approach should prioritize the consideration of the minimum no-damage parameter.

9.2 Recommendations

The model tests were primarily conducted using a packing density of 0.65, with the exception of the number of wave test series conducted at 0.63. Additionally, all the tests were conducted with the staggered grid placement pattern. Further research investigating the impact of packing densities and arrangement patterns could provide valuable insights into the unit's behaviour. This research may encompass the examination of packing densities at levels such as 0.63, 0.64, 0.65, and 0.66. However, it is important to exercise caution when considering higher packing densities, as they may lead to uneconomical consumption of concrete. While exploring packing densities lower than 0.63 is possible, caution is advised, as tests conducted at this density yielded unfavourable results for the original Cubilok shape. The study did not explore the effects of varying row numbers. Future research endeavours should explore the influence of row numbers on stability. Preliminary testing on the original Cubilok shape suggested a connection between the row number and stability, consistent with findings in other single-layer units. However, the initial investigation did not extensively examine the impact on stability.

In this study, tests were carried out on slopes with ratios of 1:1.33 and 1:1.5, and it was found that the steeper slope yielded better results compared to the milder one. Conducting additional testing with a range of slopes, such as 1:1.2, 1:1.4, and 1:1.6, would yield a comprehensive evaluation of the slope's influence on stability, thus contributing to an enhanced understanding of various slopes' influence on hydraulic stability. Beyond assessing the impact of the slope gradient, it is advisable to extend research by examining the influence of underlayer size on stability, an aspect not explored in this study. While this study considered an underlayer size of $M_a/10$, future investigations could focus on $M_a/5$ and $M_a/15$ underlayer sizes.

The overtopping analysis consistently revealed unit roughness coefficient values indicative of a smooth, impermeable surface, mainly for longer wave periods. Conducting tests that specifically examine the factors influencing overtopping discharge could substantially contribute to developing strategies for mitigating overtopping for specific design scenarios. Further research could focus on identifying the impact of various crest levels on overtopping and the unit's roughness coefficient. This could be achieved by conducting tests with varying freeboard levels.

Given the settlement results obtained in the preliminary comparison between the original and modified shape, it is advisable to conduct additional testing on the original shape, specifically at a slope of 1:1.5. This particular shape exhibited the least settlement when compared to the modified unit based on the limited testing conducted, thus warranting a more thorough investigation. In contrast, the modified unit displayed a significant decrease in settlement compared to the original shape for the steeper slope of 1:1.33.

The slenderness of the unit may be easily varied by adjusting the length of the protuberance, where a greater length translates into a slender unit. The degree of unit optimization opens up various possibilities, enhancing the unit's versatility. Further research into the influence of protuberance length on unit stability would be valuable in defining the unit's design attributes. This could be accomplished through experimentation involving various protuberance lengths, thus investigating the impact of protuberance length on the stability of the unit.

A prospective avenue for ecological enhancement could involve exploring strategies to adapt the unit in order to promote biodiversity. For future investigations, it is advisable to integrate scaled-down model units to assess the potential effects of the modifications on structural stability.

10 REFERENCES

Artificial Reef Subcommittees, 2019. *Guidelines for marine artificial reef materials.* Third ed. s.l.:s.n.

Battjes, J., 1974. *Computation of set-up, longshore currents, run-up and overtopping due to wind-generated waves.* s.l.:s.n.

Bonfantini, F., 2014. *Set-up to design guidance for the Crablock armour unit: Comparison of single layer armour units investigation,* s.l.: UNESCO-IHE (Institute for Water Education).

Broere, A., 2015. *Physical model tests on stability and interlocking of new breakwater armour block Crablock,* s.l.: Delft University of Technology, UNESCO-IHE.

Burcharth, H. F., 1993. *Structural Integrity and Hydraulic Stability of Dolos Armour Layers,* Aalborg: Department of Civil Engineering, Aalborg University.

Burcharth, H., Liu, Z. & Troch, P., 1999. *Scaling of core material in rubble mound breakwater model.* Cape Town, South Africa, Proceedings of the 5th International Conference on Coastal and Port Engineering in Developing Countries, pp. 1518-1528.

CEM, C. E. M., 2006. *Volume VI Chapter 2: Types and Functions of Coastal Structures.* Washington, D.C.: U.S. Army Corps of Engineers.

Chadwick, A., Morfett, J. & Borthwick, M., 2013. *Hydraulic in civil and environmental engineering.* 5th ed. s.l.:CRC Press.

CIRIA, C., 2007. *The Rock Manual. The use of rock in hydraulic engineering.* 2nd ed. s.l.:C683, CIRIA, London.

CLI, C. L. I., n.d. *CLI concrete armour units to protect port and coastal structures.* [Online] Available at: https://www.concretelayer.com/en/solutions/technologies/cli-concrete-armour-units-protect-port-and-coastal-structures
[Accessed 2023].

Dalrymple, R. A., 1985. "Introduction to Physical Models in Coastal Engineering" . In: *Physical Modelling in Coastal Engineering.* The Netherlands: A.A. Balkema Rotterdam, pp. 3-9.

DHL, D. h. l., 1987. *Stability of rubble mound breakwaters: Stability formula for breakwaters armoured with ACCROPODE (R),* s.l.: s.n.

DMC, D. M. C., 2003a. Development of concrete breakwater armour units. *Canadian Society for Civil Engineering.*

DMC, D. M. C., 2003b. *Xbloc armour unit development - hydraulic performance of Xbloc armour units, 2D model tests at WL Delft,* s.l.: BAM Infraconsult - DMC.

DMC, D. M. C., 2008. *Design of Concrete Armour Layers,* s.l.: s.n.

Dugan, J. E. et al., 2012. Estuarine and coastal structures: environmental effects, a focus on shore and nearshore structures. In: *Treatise on estuarine and coastal science.* s.l.:Academic Press.

EurOtop, 2018. *Manual on wave overtopping of sea defences and related structures.* 2nd ed. s.l.:s.n.

Firth, L. B. et al., 2015. Facing the future: the importance of substratum features for ecological engineering of artificial habitats in the rocky intertidal. *Marine and Freshwater Research,* 67(1), pp. 131-143.

Glasby, T. M., Connell, S. D., Holloway, M. G. & Hewit, C. L., 2007. Nonindigenous biota on artificial structures: could habitat creation facilitate biological invasions?. *Marine Biology,* p. 887–895.

Goda, Y., 2000. *Random seas and design of maritime strutures.* 2nd ed. s.l.:World Scientific Publishing Co. Pte. Ltd.

Hughes, S. A., 1993. *Physical models and laboratory techniques in coastal engineering, Advanced series on Ocean Engineering - Volume 7.* s.l.:World Scientific Publishing .

ITRC, T. I. T. &. R. C., 2004. *Making the Case for Ecological Enhancements,* s.l.: s.n.

Jackson, R. A., 1968. *Design of cover layers for rubble-mound breakwaters subjected to nonbreaking waves,* s.l.: s.n.

Jan Steendam, G. et al., 2004. The international database on wave overtopping. *ResearchGate.*

Mansard, E. & Funke, E., 1980. *The Measurement of Incident and Reflected Spectra Using a Least squares Method,* s.l.: Charleston, American Society of Civil Engineers..

Mineur, F. et al., 2012. Changing coasts: marine aliens and artificial structures. *Oceanography and Marine Biology,* Volume 50, pp. 189-233.

Muttray, M. & Reedijk, J., 2008. *Design of Concrete Armour Layers,* s.l.: s.n.

Oever, E. t., 2006. *Theoretical and experimental study on the placement of Xbloc ,* s.l.: TUDelft.

Perkol-Finkel, S. et al., 2018. Seascape architecture – incorporating ecological considerations indesign of coastal and marine infrastructure. *The Journal of Ecosystem Restoration.*

Perkol-Finkel, S. & Sella, I., 2014. *Ecologically Active Concrete for Coastal and Marine Infrastructure: Innovative Matrices and Designs.* s.l., Proceeding of the 10th ICE Conference: from Sea to Shore - Meeting the Challenges of the Sea.

PRDW, 2019. *New Breakwater Armour Unit: Cubilok,* s.l.: PRDW.

Salauddin, M., 2018. A Review on the Development and Applications of Single-layer Concrete Armour Units in the Design of Rubble Mound Breakwaters. *Jordan Journal of Civil Engineering,* 12(1).

Salauddin, M. et al., 2015. A New Symmetrical Unit for Breakwater Armour: First Tests. *Proceedings 7th Coastal Structures conference.*

Schiereck, G. J. & Verhagen, H. J., 2012. *Introduction to Bed, bank and shore protection.* 2nd ed. Delft, The Netherlands: VSSD.

Schüttrumpf, H. et al., 2009. Wave Run-Up and Wave Overtopping at Armored Rubble Slopes and Mounds. In: *Handbook of Coastal and Ocean Engineering.* s.l.:s.n., pp. 383-409.

Sella, I. & Perkol-Finkel, S., 2015. Blue is the new green – Ecological enhancement of concrete basedcoastal and marine infrastructure. *The Journal of Ecosystem Restoration.*

Sharma, P., 2009. *Coastal Zone Management.* s.l.:Global India Publications.

Spalding, M. et al., 2007. Marine ecoregions of the world: A bioregionalization of coastal and shelf areas. *BioScience,* 57(7), pp. 573-583.

van der Meer, J., 2017. Application and stability criteria for rock and artificial units.. In: K. Pilarczyk, ed. *Chapter 11: Dikes and Revetments. Design, Maintenance and safety Assessment.* s.l.:IAHR.

van der Meer, J. W., 1988a. *Rock Slopes and Gravel Beaches under Wave Attack ,* Delft: Delft University of Technology.

van der Meer, J. W., 1988b. Stability of cubes, tetrapods and accropode. In: *Design of Breakwaters.* London: Proc conf Breakwaters ’88, Eastbourne, 4–6 May, pp. 71-80.

Vaselli, S., Bulleri, F. & Benedetti-Cecch, L., 2008. Hard coastal-defence structures as habitats for native and exotic rocky-bottom species. *Marine Environmental Research,* pp. 395-403.

Wehlitz, C.-P., 2020. *Hydraulic stability of the new Cubilok armour unit on a 3:4 slope (Master's thesis),* Stellenbosch: University of Stellenbosch.

Wehlitz, C. & Schoonees, J., 2023. Hydraulic stability of the new Cubilok™ armour unit on a 3:4 slope. *Elsevier: Coastal Engineering,* Volume 183, p. 12.

APPENDIX A: CHARACTERISTICS OF CONCRETE ARMOUR UNITS

Type of armour	Design N_S $(\mathbf{H}_s/\Delta\mathbf{D}_n)$	No. of layers	$\mathbf{k_t}$	Packing density
Cube	2,2	2	1,10	1,17
Tetrapod	2,2	2	1,04	1,02
Dolosse	2,8	2	0,94	0,83
Cubipod	3,48	2	1.10	1.16
Accropode	2,7	1	1,51	0,66
Core-Loc^{TM}	2,8	1	1,51	0,60
Xbloc^{TM}	2,8	1	1,49	0,58
Cubilok (1:1.33)	2,61	1	1,50*	0,65

*Determined using the average of the other single/ double layer units.

APPENDIX B: GRADING

A sample size of approximately two hundred stones is measured and plotted to compare against the Rosin Ramler curve. The size of the underlayer stone is selected from the 12-19 mm range, which resulted in a light average stone mass. A 13.2 mm sieve is then used to extract some of the finer material, resulting in a mean mass of 4.1 g. It has been decided to use the mass irrespective of it being lower than the target mass of 4.6 g.

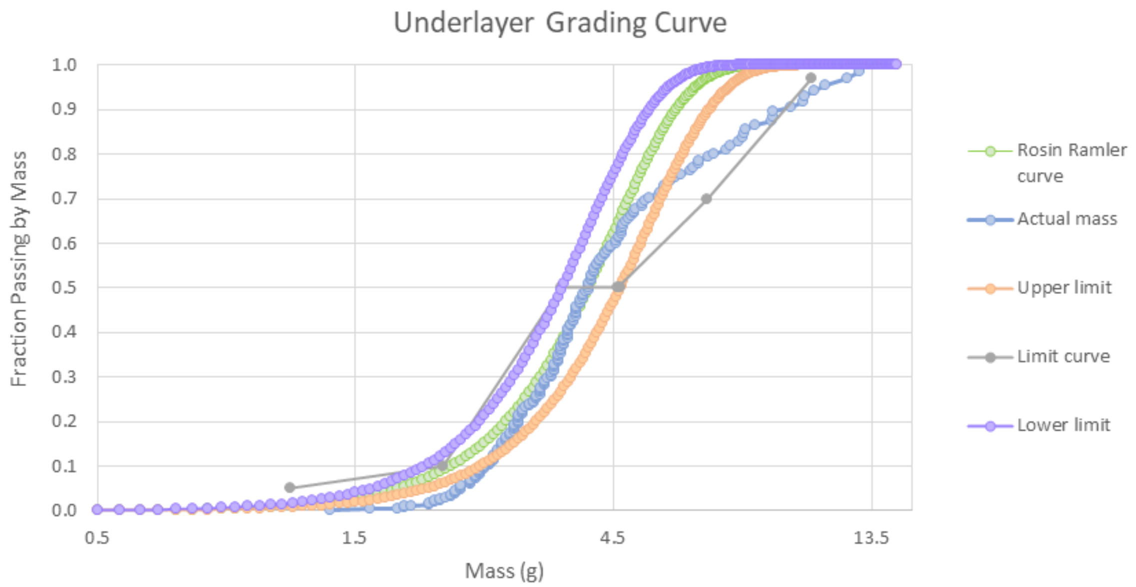

APPENDIX C: DATA OUTPUT FROM CALIBRATION AND TESTING

Sensor calibration is done before every test series to ensure no errors in the data acquisition process. There are two primary checks done before the equipment may be cleared. The first is ensuring the graph points are linear, and the second is confirming that the error values are within a specific range.

Calibrated by: 230308_MCC Calibration Status: NORMAL
Project: Cubilok_2 Facility: CSIR
Sensor: P_01 Model: WG50 Serial No. N/A
Programmable Gain: 1 Plug-In Gain: 1 Filter Frequency: 20.0 Hz

Data Point No.	Input Signal (volts)	Physical Value (m)	Fitted Curve (m)	Error (m)
1	−2.627	−0.050000	−0.050003	+0.25593E−05
2	−1.626	0.000000	0.000005	0.51231E−05
3	−0.625	0.050000	0.049997	+0.25630E−05
Maximum Error = 0.00512% of Calibration Range				

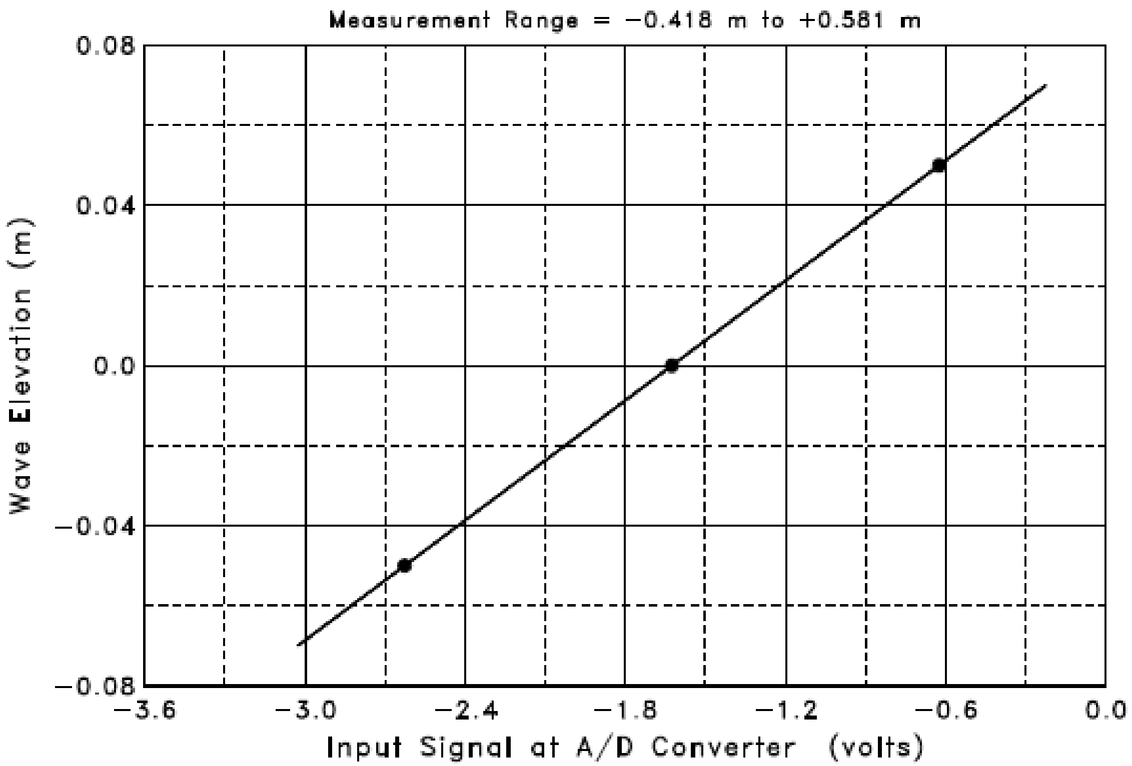

The image below is a snip of the data sheet used to determine the wave heights and periods.

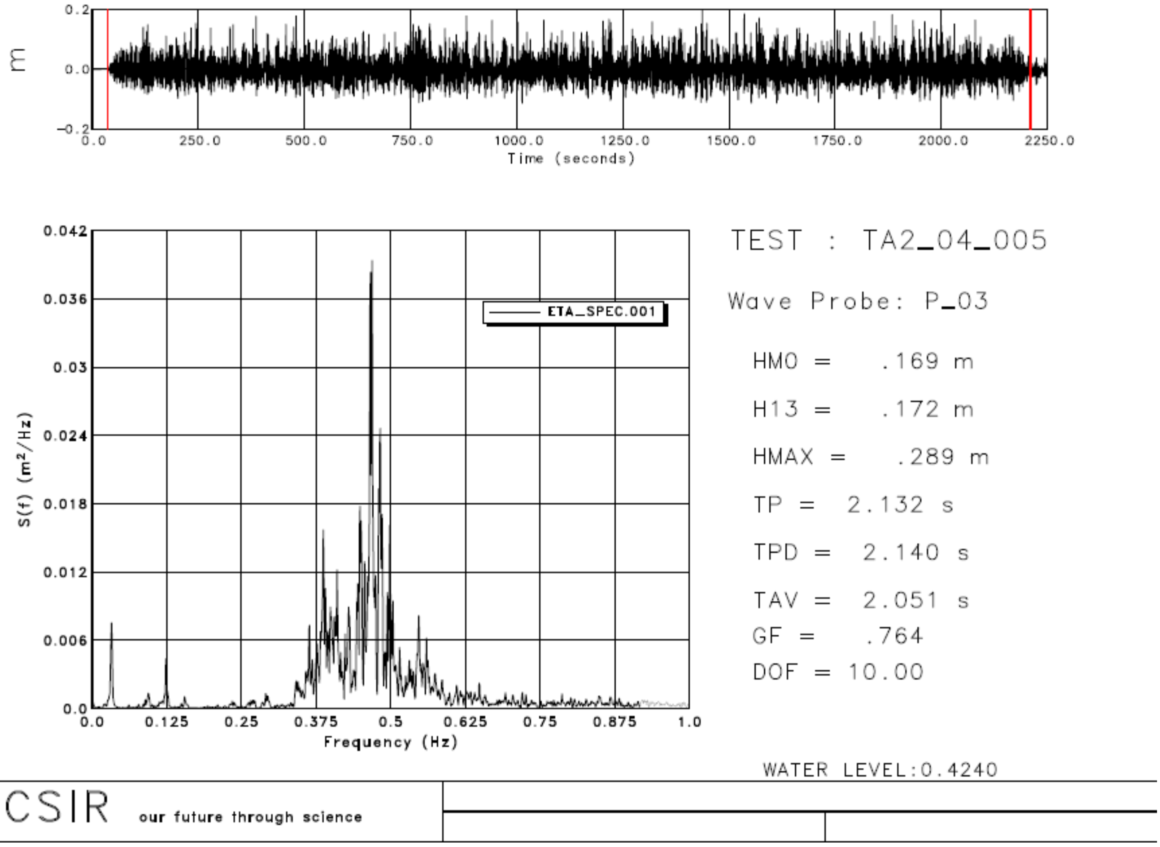

APPENDIX D: MANUFACTURING THE MODEL UNITS

v This study is the first model scale test for the new Cubilok configuration. PRDW developed the unit mould using AutoCAD, illustrated in the images below.

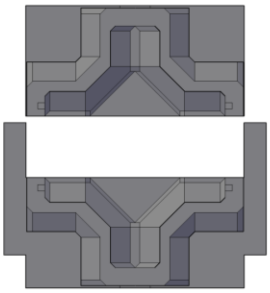

Top view.

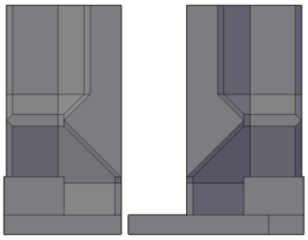

Side view.

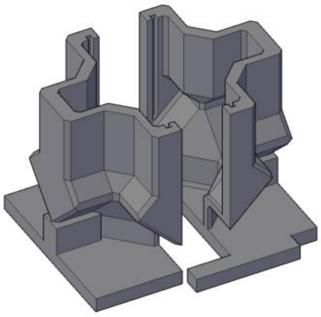

Isometric view.

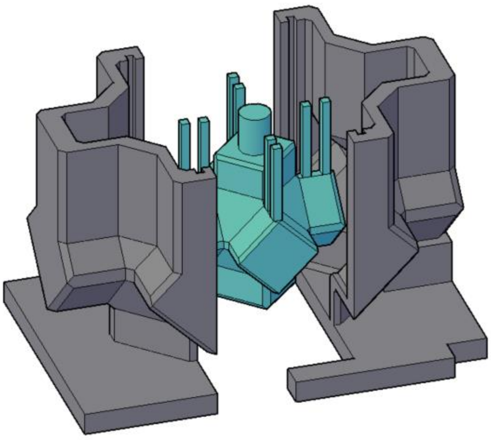

Isometric view of the mould and unit.

The model units are manufactured by PRDW, and the process will be described in this section. The master unit is developed by an external company and used in the making of all the moulds. The 3D-printed shell, developed by PRDW, is designed to follow the contours of the unit shape to minimise the required materials.

3D-printed shell

Master unit in the shell

Silicone setting.

Once the silicone is set, the mould is cut into two parts and is ready for the unit mixture. The unit mixture consists of a Resin solution, Accelerant, Barium sulphate, and a Catalyst.

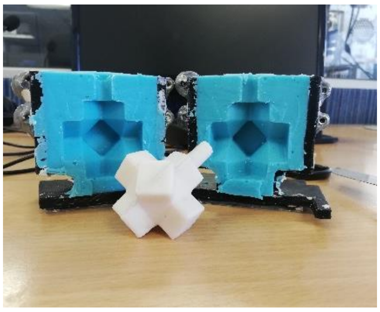

The mould is cut into two parts, and the master unit is removed.

The syringe is used to input the mixture into the mould.

The units are then set aside to cure for about an hour.

Once the units are almost cured, the units are carefully removed from the mould, and the vents used to prevent bubbles from forming are removed. The units are then left to harden further and the density is usually recorded the next day. The unit number and density are written on each unit to ensure they are documented accurately.

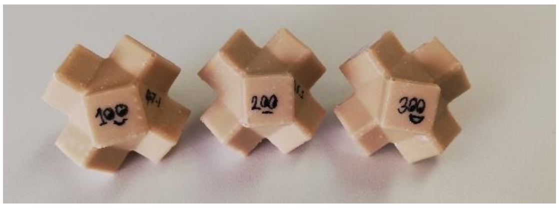

The units were made in a batch of around 10 units, with over 850 units being manufactured at the end of the process. Two failure modes that impact the structure of the unit are identified. The first is the thinning of a mould to the extent that a hole forms and the second is the deformation of the mould. Both these failures are because of the heat the units reach while curing.

Thinning resulting in a mould breakage

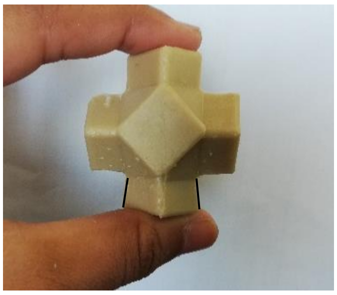

Unit from a deformed mould

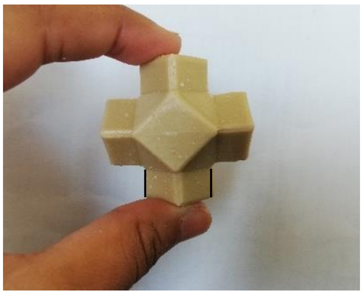

Unit from a useable mould

APPENDIX E: MODEL UNIT PROPERTIES

The graph below illustrates the mass of each unit which are colour coordinated according to the batch produced (i.e., Test #). An upper and lower limit is determined based on 5% variance from the mean. The units are also excluded based on the densities and physical deformities .

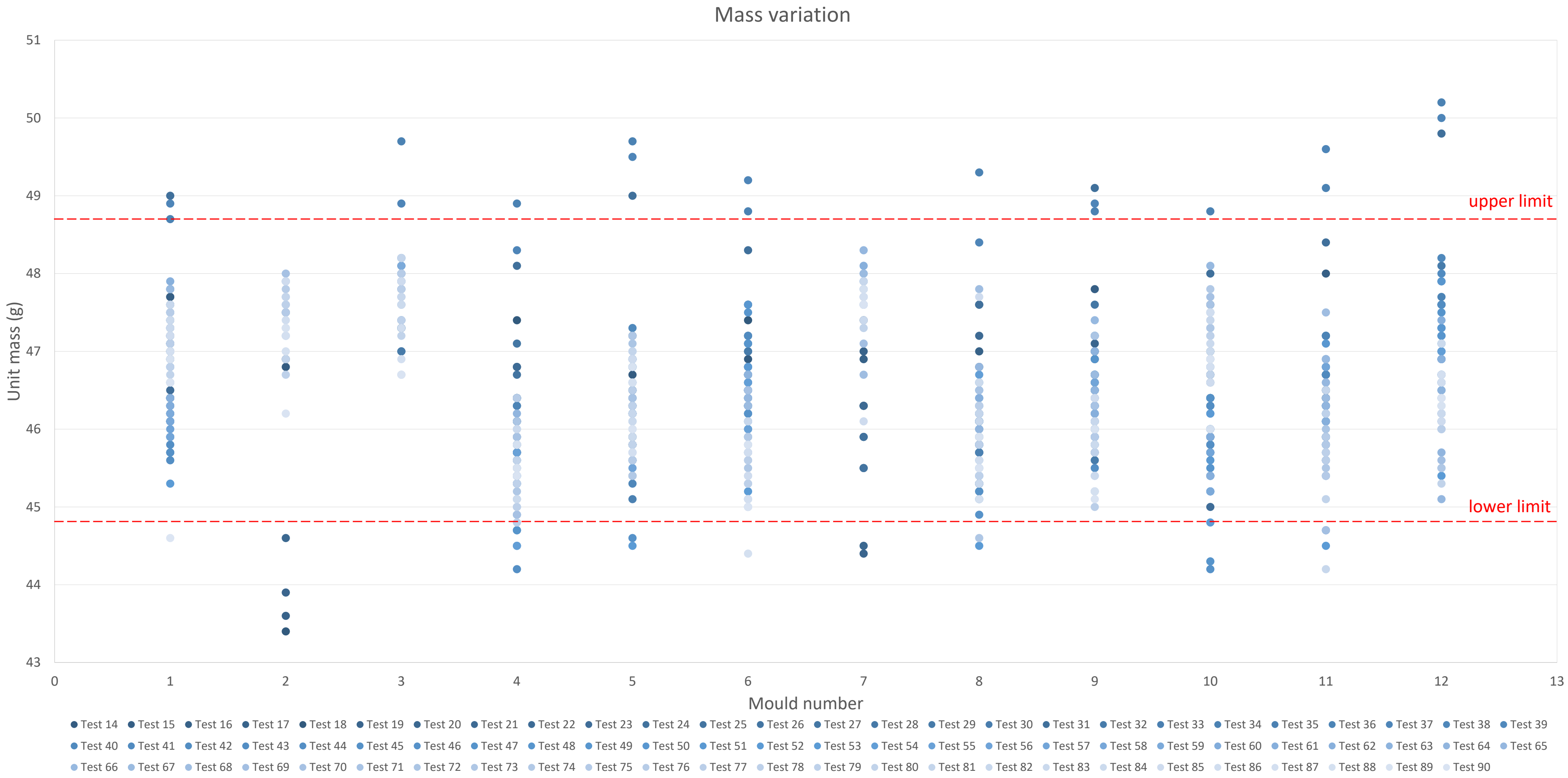

The graph below indicates the normal distribution of the units which were manufactured.

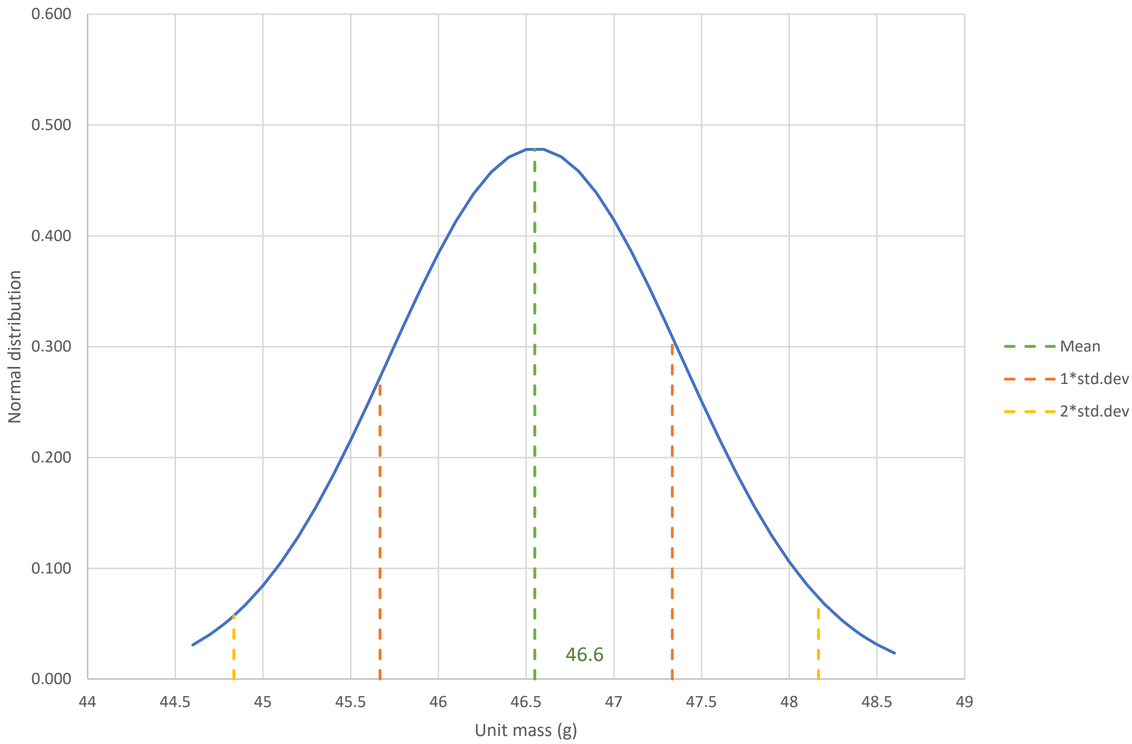

APPENDIX F: DRY PACKING AND MODEL BUILD

Dry packing is an efficient way to develop packing techniques and test out various packing densities. Three single-layer slopes were packed, as well as one double-layer slope.

Packing density = 0.61

Packing density = 0.63

Packing density = 0.65

Packing density = 0.585

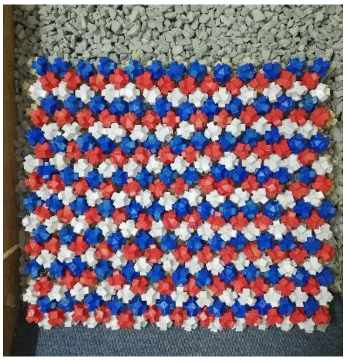

Packing density = 1.17

Once the 1:30 slope is constructed, the concrete blocks are placed, the core is packed, and the crown wall is placed. The toe, underlayer, and armour are then constructed in that sequence.

Core and Toe placed

Underlayer placed

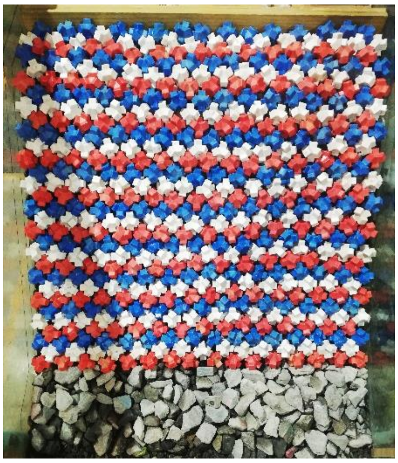

Armour layer placed

APPENDIX G: TARGET AND MEASURED CONDITIONS

The following table presents each series and test's target and measured conditions. As mentioned before, each test was performed until structural failure was achieved.

Test series	cotα	Target conditions				Measured conditions			
		H_i (m)	T_P (s)	s_{op} (-)	N_S (-)	H_i (m)	T_P (s)	s_{op} (-)	N_S (-)
N_63	1.33	0.140	1.545	0.038	3.800	0.124	1.667	0.029	3.38
						0.125	1.667	0.029	3.38
						0.125	1.667	0.029	3.38
						0.125	1.667	0.029	3.38
						0.125	1.667	0.029	3.38
						0.127	1.667	0.029	3.44
						0.126	1.667	0.029	3.41
						0.128	1.667	0.029	3.47
N_65		0.140	1.545	0.038	3.800	0.125	1.667	0.029	3.39
						0.125	1.667	0.029	3.40
						0.124	1.667	0.029	3.37
						0.125	1.667	0.029	3.40
						0.125	1.667	0.029	3.39
						0.125	1.667	0.029	3.40
						0.124	1.667	0.029	3.37
						0.125	1.667	0.029	3.40
						0.124	1.667	0.029	3.37
						0.124	1.667	0.029	3.37
						0.127	1.667	0.029	3.44
						0.123	1.667	0.028	3.35
						0.124	1.667	0.029	3.37
						0.124	1.667	0.029	3.37
A1	1.33	0.100	2.72	0.009	2.71	0.116	2.977	0.008	3.14
		0.112		0.010	3.04	0.135	2.977	0.010	3.67
		0.125		0.011	3.40	0.154	2.976	0.011	4.18
A2_1		0.100	1.38	0.034	2.71	0.100	1.366	0.034	2.70
		0.112		0.038	3.04	0.113	1.366	0.039	3.05
		0.125		0.042	3.40	0.119	1.277	0.047	3.23
		0.140		0.047	3.81	0.132	1.388	0.044	3.58
		0.157		0.053	4.27	0.143	1.366	0.049	3.87
A2_2		0.100	1.38	0.034	2.71	0.096	1.318	0.035	2.61
		0.112		0.038	3.04	0.110	1.366	0.038	3.00
		0.125		0.042	3.40	0.116	1.277	0.046	3.16
		0.140		0.047	3.81	0.127	1.426	0.040	3.46
A2_3		0.100	1.38	0.034	2.71	0.098	1.366	0.034	2.65
		0.112		0.038	3.04	0.109	1.366	0.037	2.95
		0.125		0.042	3.40	0.116	1.277	0.046	3.16
		0.140		0.047	3.81	0.134	1.366	0.046	3.64
		0.157		0.053	4.27	0.147	1.371	0.050	4.00
		0.176		0.059	4.78	0.163	1.427	0.051	4.43
A2_4		0.100	1.38	0.034	2.71	0.099	1.364	0.034	2.67
		0.112		0.038	3.04	0.111	1.364	0.038	3.03

		0.125		0.042	3.40	0.117	1.277	0.046	3.18
		0.140		0.047	3.81	0.135	1.372	0.046	3.65
		0.157		0.053	4.27	0.149	1.373	0.051	4.05
		0.176		0.059	4.78	0.161	1.373	0.055	4.38
A3		0.100	1.73	0.021	2.71	0.078	1.653	0.018	2.13
		0.112		0.024	3.04	0.096	1.653	0.022	2.60
		0.125		0.027	3.40	0.108	1.652	0.025	2.93
		0.140		0.030	3.81	0.124	1.665	0.029	3.38
		0.157		0.034	4.27	0.142	1.761	0.029	3.87
		0.176		0.038	4.78	0.170	1.761	0.035	4.62
B1	1.5	0.100	2.72	0.009	2.71	0.116	2.977	0.008	3.14
		0.112		0.010	3.04	0.139	2.939	0.010	3.77
		0.125		0.011	3.40	0.155	2.977	0.011	4.20
B2_1		0.100	1.38	0.034	2.71	0.099	1.366	0.034	2.70
		0.112		0.038	3.04	0.110	1.421	0.035	2.97
		0.125		0.042	3.40	0.115	1.378	0.039	3.13
		0.140		0.047	3.81	0.135	1.366	0.047	3.68
		0.157		0.053	4.27	0.150	1.366	0.051	4.06
		0.176		0.059	4.78	0.171	1.426	0.054	4.64
B2_2		0.100	1.38	0.034	2.71	0.095	1.366	0.033	2.57
		0.112		0.038	3.04	0.109	1.366	0.038	2.97
		0.125		0.042	3.40	0.115	1.277	0.045	3.13
		0.140		0.047	3.81	0.133	1.366	0.046	3.61
		0.157		0.053	4.27	0.147	1.371	0.050	3.98
		0.176		0.059	4.78	0.167	1.367	0.057	4.54
B2_3		0.100	1.38	0.034	2.71	0.095	1.364	0.033	2.58
		0.112		0.038	3.04	0.107	1.423	0.034	2.91
		0.125		0.042	3.40	0.114	1.276	0.045	3.09
		0.140		0.047	3.81	0.131	1.372	0.044	3.54
		0.157		0.053	4.27	0.144	1.372	0.049	3.92
		0.176		0.059	4.78	0.163	1.372	0.056	4.42
B3_1		0.100	1.73	0.021	2.71	0.076	1.652	0.018	2.08
		0.112		0.024	3.04	0.094	1.652	0.022	2.54
		0.125		0.027	3.40	0.105	1.652	0.025	2.85
		0.140		0.030	3.81	0.125	1.655	0.029	3.39
		0.157		0.034	4.27	0.146	1.759	0.030	3.96
		0.176		0.038	4.78	0.169	1.757	0.035	4.58
B3_2		0.100	1.73	0.021	2.71	0.075	1.652	0.018	2.04
		0.112		0.024	3.04	0.093	1.652	0.022	2.54
		0.125		0.027	3.40	0.104	1.652	0.024	2.81
		0.140		0.030	3.81	0.123	1.759	0.025	3.33
		0.157		0.034	4.27	0.143	1.763	0.029	3.87
		0.176		0.038	4.78	0.160	1.756	0.033	4.33
C1		0.100	1.38	0.034	2.71	0.089	1.365	0.031	2.42
		0.112		0.038	3.04	0.101	1.365	0.035	2.75
		0.125		0.042	3.40	0.108	1.277	0.042	2.94
		0.140		0.047	3.81	0.129	1.365	0.044	3.51
		0.157		0.053	4.27	0.160	1.439	0.050	4.35
C2		0.100	1.38	0.034	2.71	0.091	1.363	0.031	2.46
		0.112		0.038	3.04	0.103	1.363	0.036	2.80
		0.125		0.042	3.40	0.110	1.276	0.043	3.00

		0.140		0.047	3.81	0.128	1.366	0.044	3.48
		0.157		0.053	4.27	0.143	1.366	0.049	3.87
		0.176		0.059	4.78	0.174	1.425	0.055	4.73
C3		0.100	1.38	0.034	2.71	0.090	1.363	0.031	2.44
		0.112		0.038	3.04	0.102	1.363	0.035	2.77
		0.125		0.042	3.40	0.109	1.276	0.043	2.95
		0.140		0.047	3.81	0.126	1.366	0.043	3.43
		0.157		0.053	4.27	0.154	1.366	0.053	4.19
		0.176		0.059	4.78	0.186	1.388	0.062	5.04

APPENDIX H: TEST SERIES A PHOTOGRAPHS

TEST SERIES A1

Settlement test

Test 1

Test 2

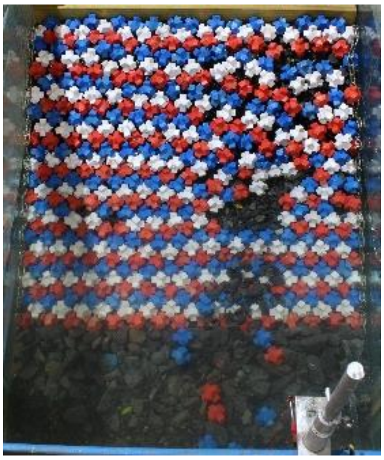

Test 3

TEST SERIES A2_1

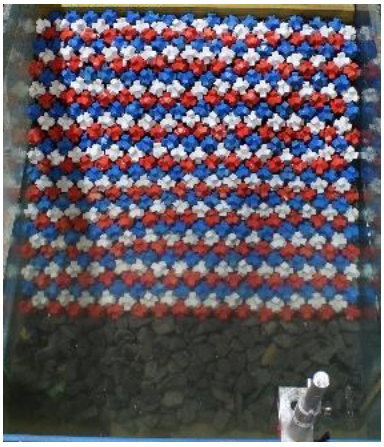

Settlement test

Test 1

Test 2

Test 3

Test 4

Test 5

TEST SERIES A2_2

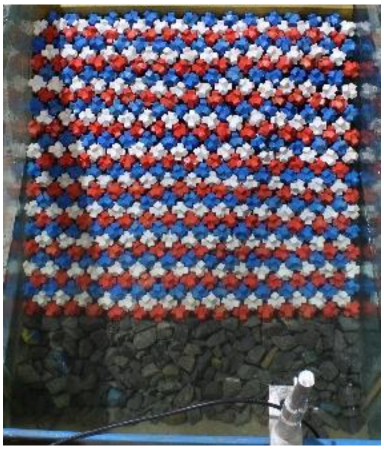

Settlement test

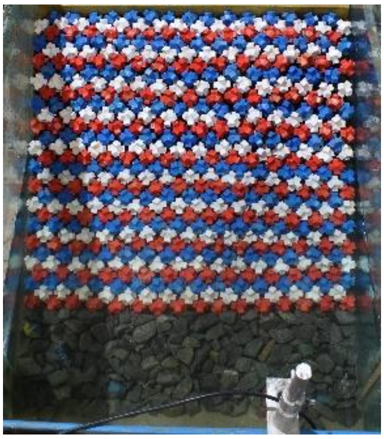

Test 1

Test 2

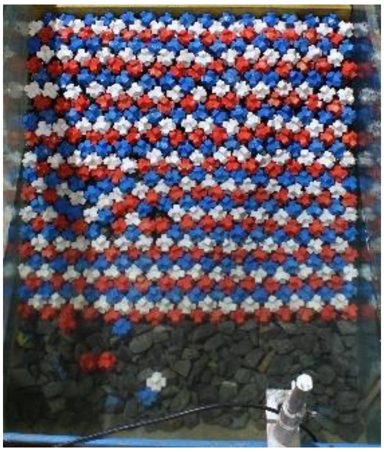

Test 3

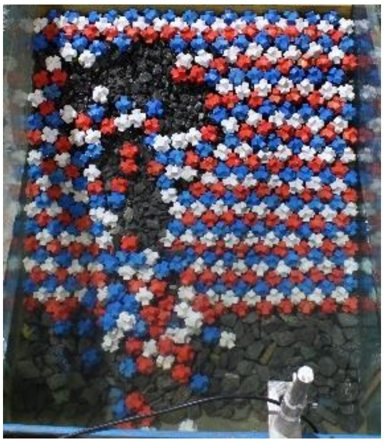

Test 4

TEST SERIES A2_3

Settlement test

Test 1

Test 2

Test 3

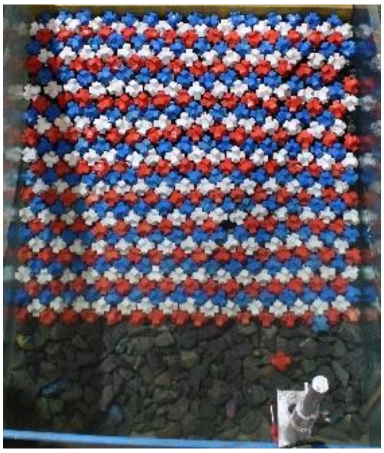

Test 4

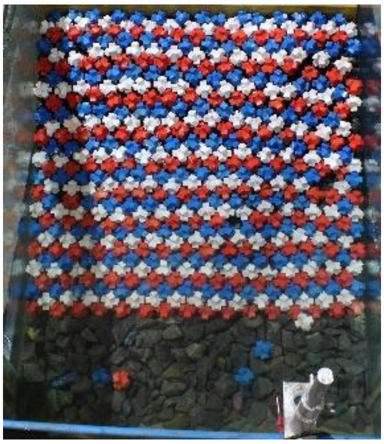

Test 5

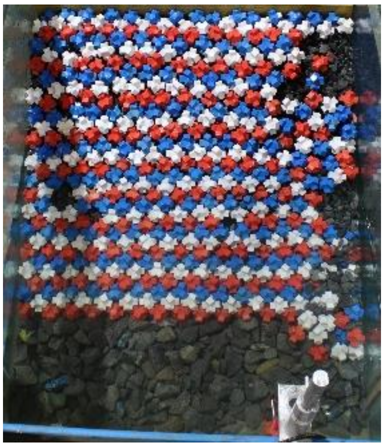

Test 6

TEST SERIES A2_4

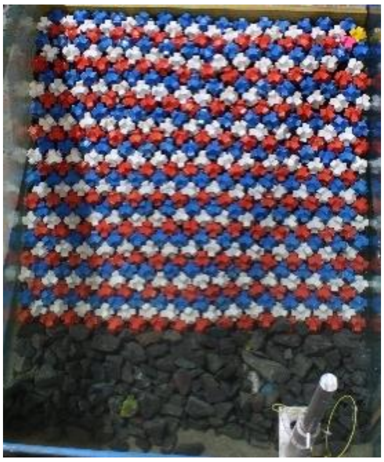

Settlement test

Test 1

Test 2

Test 3

Test 4

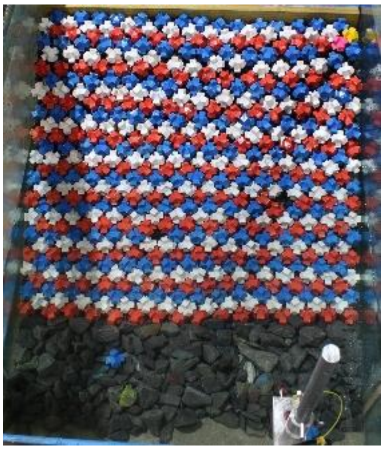

Test 5

Test 6

TEST SERIES A3

Settlement test

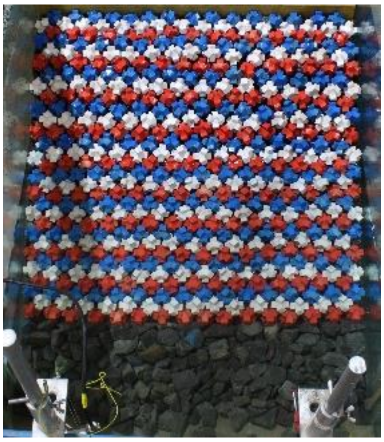

Test 1

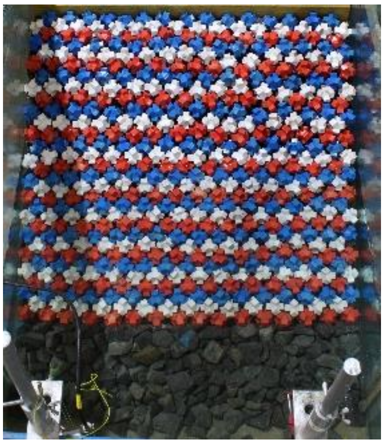

Test 2

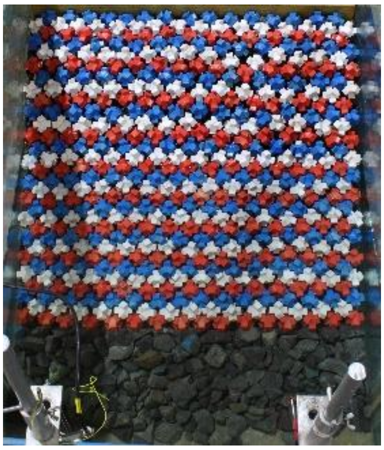

Test 3

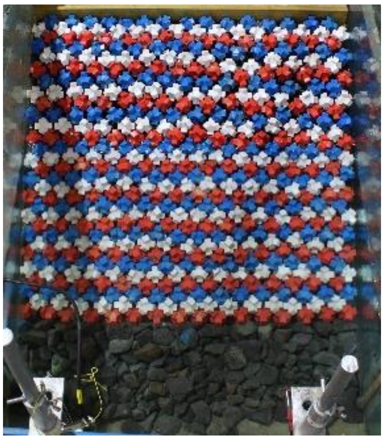

Test 4

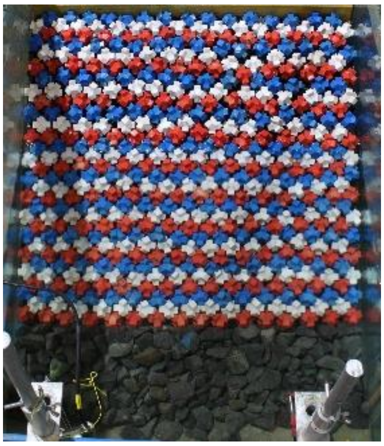

Test 5

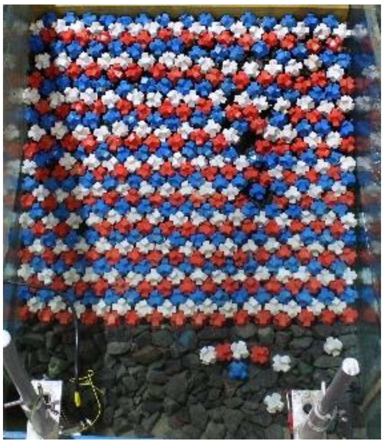

Test 6

APPENDIX I: TEST SERIES B PHOTOGRAPHS

TEST SERIES B1

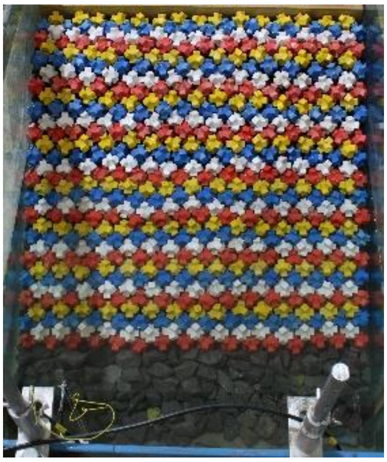

Settlement test

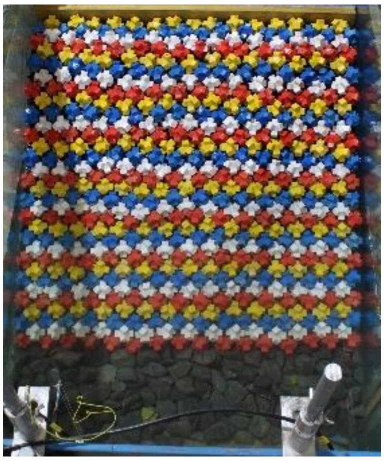

Test 1

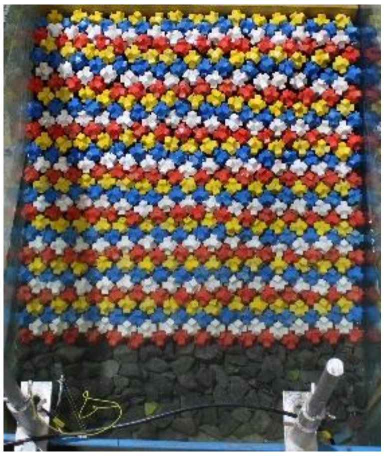

Test 2

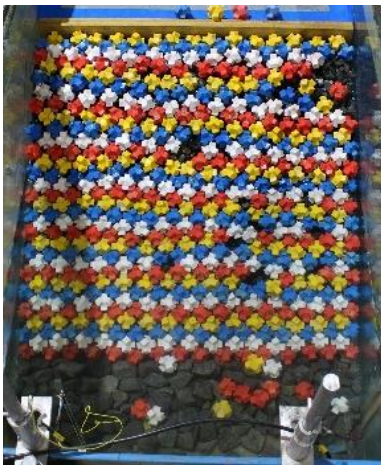

Test 3

TEST SERIES B2_1

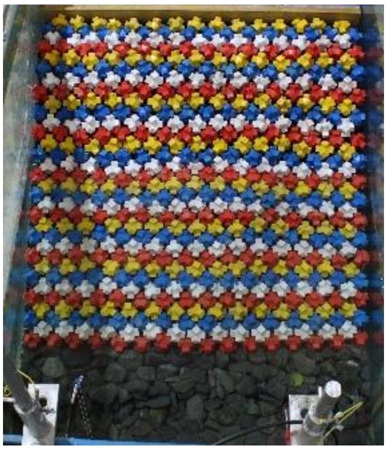

Settlement test

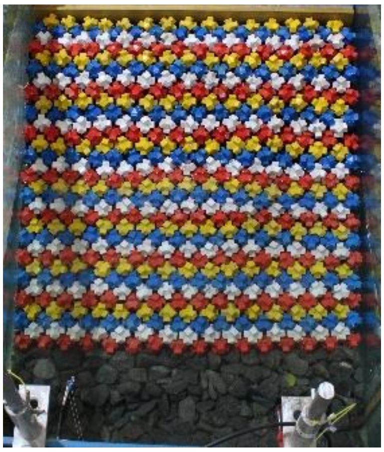

Test 1

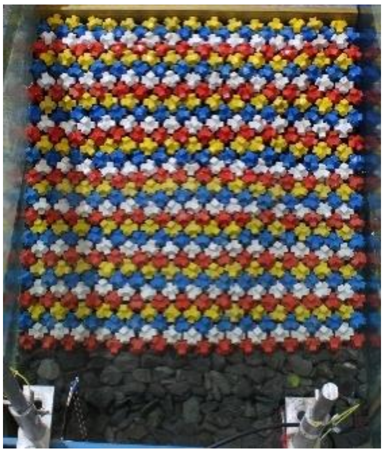

Test 2

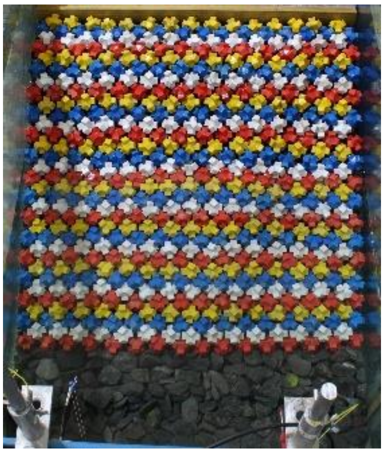

Test 3

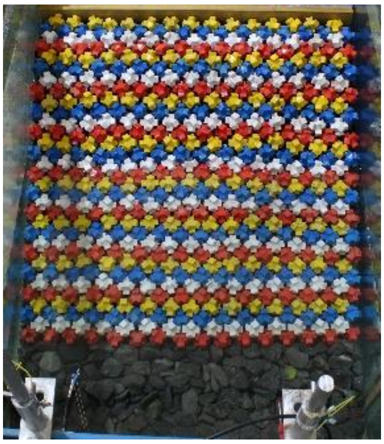

Test 4

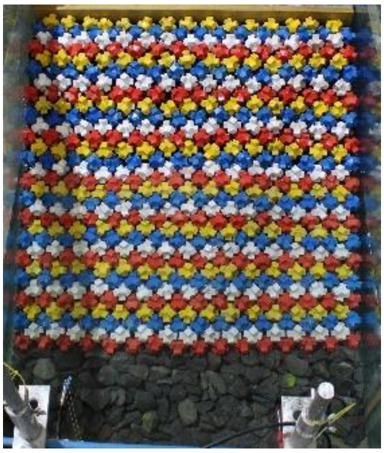

Test 5

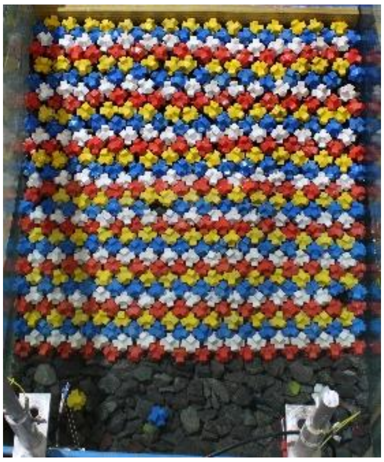

Test 6

TEST SERIES B2_2

Settlement test

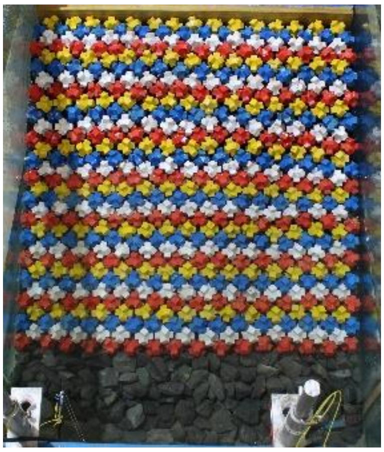

Test 1

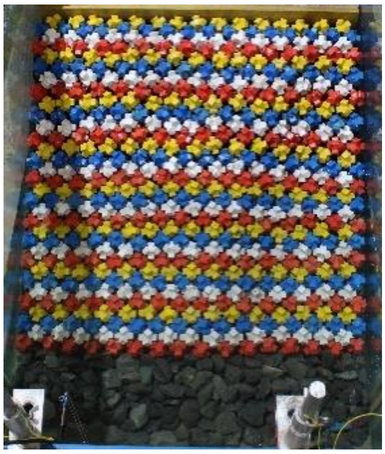

Test 2

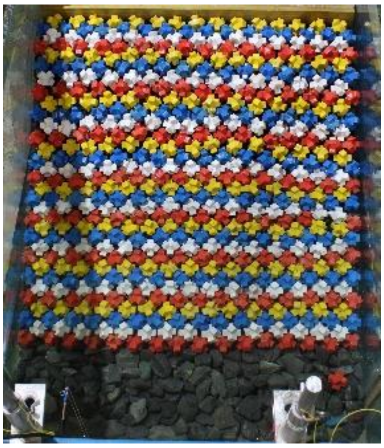

Test 3

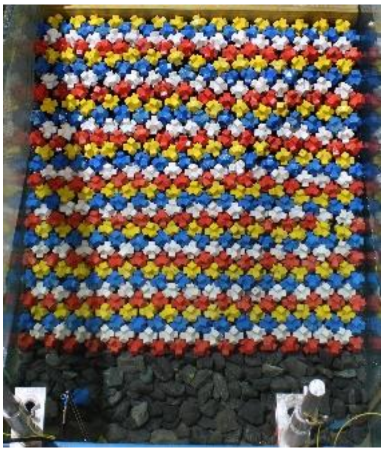

Test 4

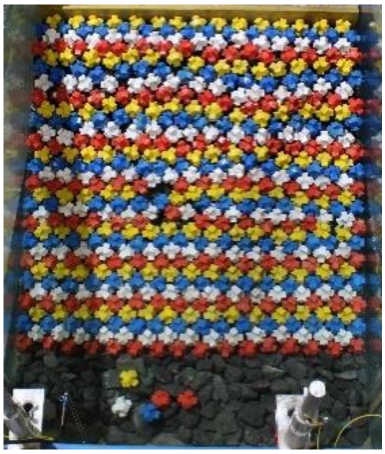

Test 5

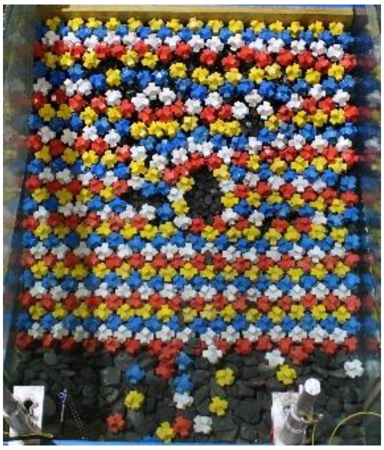

Test 6

TEST SERIES B2_3

Settlement test

Test 1

Test 2

Test 3

Test 4

Test 5

Test 6

TEST SERIES B3_1

Settlement test

Test 1

Test 2

Test 3

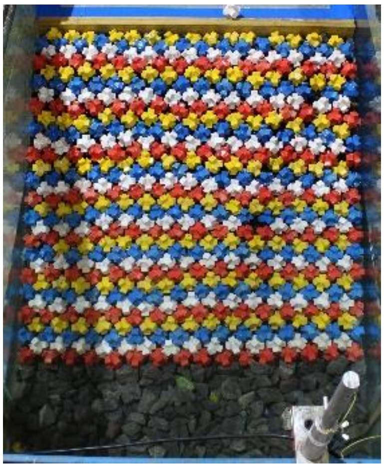

Test 4

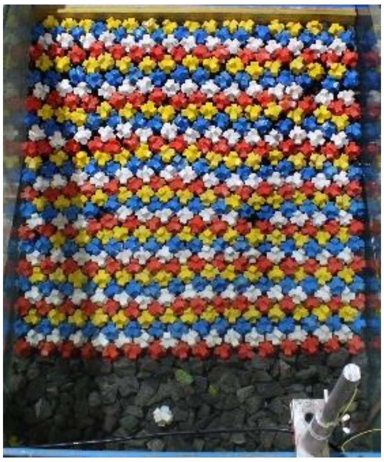

Test 5

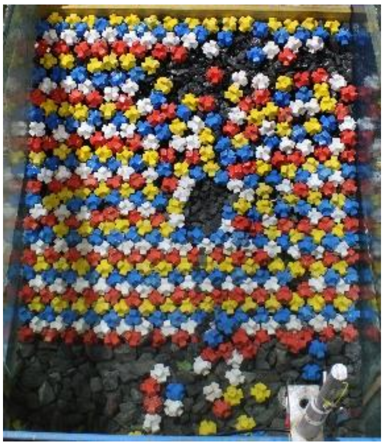

Test 6

TEST SERIES B3_2

Settlement test

Test 1

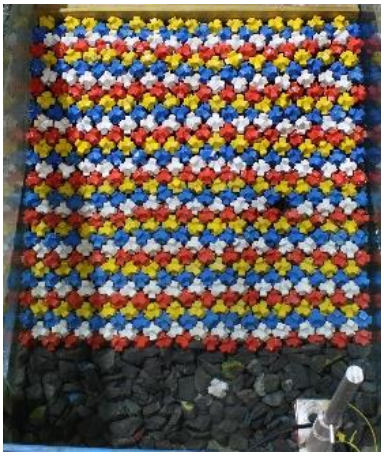

Test 2

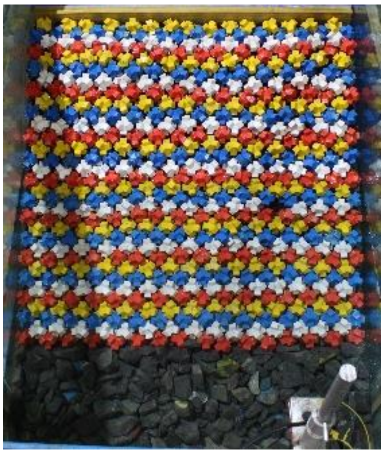

Test 3

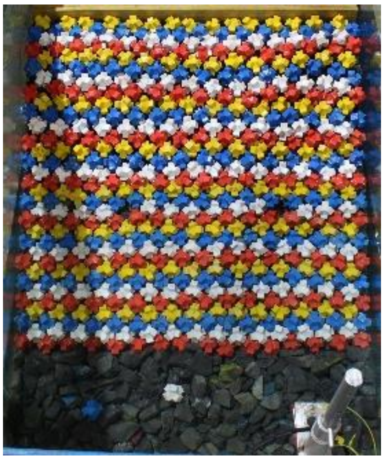

Test 4

Test 5

Test 6

APPENDIX J: TEST SERIES C PHOTOGRAPHS

TEST SERIES C2_1

Settlement test

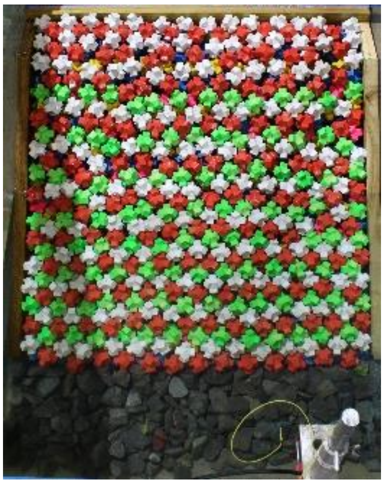

Test 1

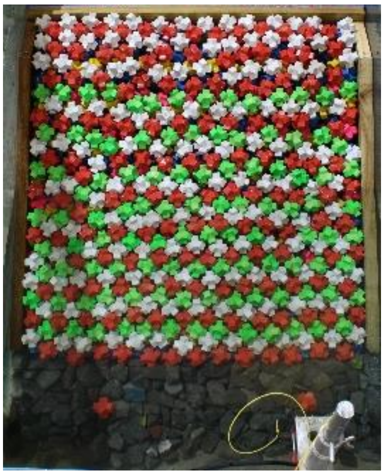

Test 2

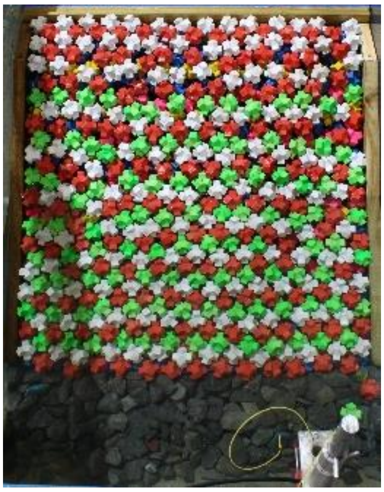

Test 3

Test 4

Test 5

TEST SERIES C2_2

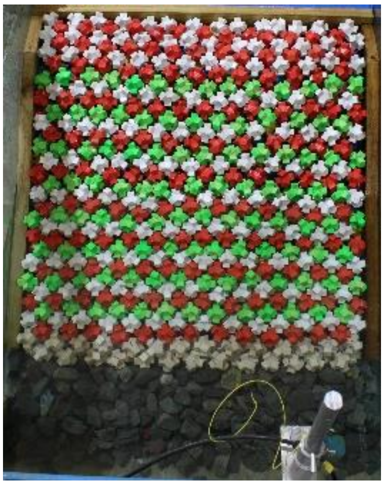

Settlement test

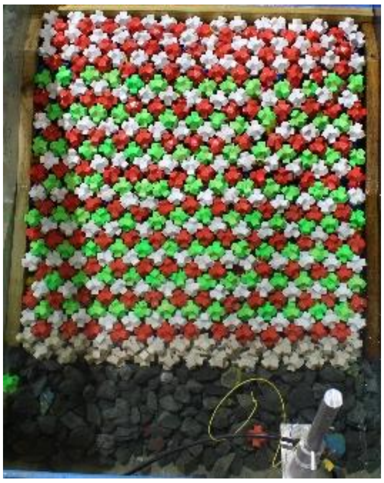

Test 1

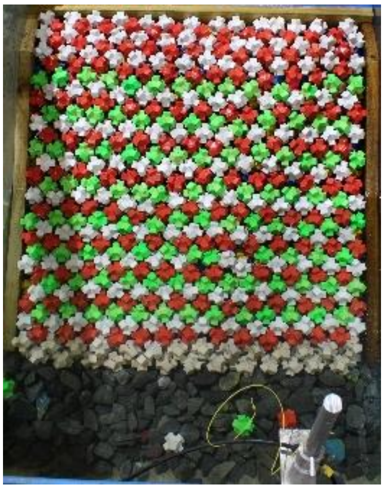

Test 2

Test 3

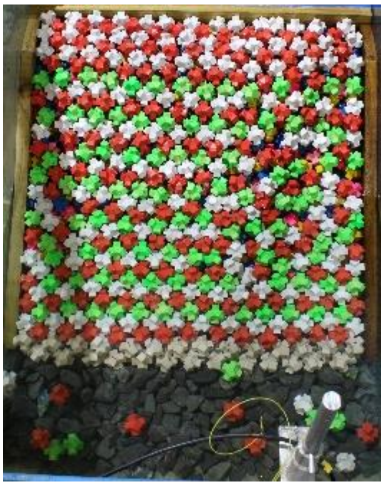

Test 4

Test 5

Test 6

TEST SERIES C2_3

Settlement test

Test 1

Test 2

Test 3

Test 4

Test 5

Test 6

APPENDIX K: TEST SERIES D PHOTOGRAPHS

TEST SERIES D3_1

Settlement test

Test 1

Test 2

Test 3

Test 4

Test 5

Test 6

TEST SERIES D3_2

Settlement test

Test 1

Test 2

Test 3

Test 4

Test 5

Test 6